สำนักหอสมุดกลาง พระจอมเกล้าลาดกระบัง

ANALYSIS OF RADIATION AND IMPEDANCE CHARACTERISTICS OF THE ANTENNA USING THE SLOT ON RECTANGULAR CAVITY

TITIPONG LERTWIRIYAPRAPA

King Mongkut's Institute of Technology Ladkrabang

เลขหมู่.....
เลขทะเบียน.....35746
วัน, เดือน, ปี.....8 ส.ค. 2543

A THESIS SUBMITTED IN PARTIAL FULFILLMENT
OF THE REQUIREMENT FOR THE DEGREE OF
MASTER OF ENGINEERING IN ELECTRICAL ENGINEERING
SCHOOL OF GRADUATE STUDIES
KING MONGKUT'S INSTITUTE OF TECHNOLOGY LADKRABANG
2000

ISBN 974-622-892-7

This material is reserved for educational use only, not allowed for commercial use.
Forbidden to modify the content, and cite the document when use.

COPYRIGHT 2000
SCHOOL OF GRADUATE STUDIES
KING MONGKUT'S INSTITUTE OF TECHNOLOGY LADKRABANG

This material is reserved for educational use only, not allowed for commercial use.
Forbidden to modify the content, and cite the document when use.

หัวข้อวิทยานิพนธ์	การวิเคราะห์คุณลักษณะการแพร่กระจายคลื่นและอิมพีแดนซ์ของสายอากาศชนิดร่องบนคาวิตี้ทรงสี่เหลี่ยมมุมฉาก
นักศึกษา	นายฐิติพงษ์ เลิศวิริยะประภา
รหัสประจำตัว	41061144
ปริญญา	วิศวกรรมศาสตรมหาบัณฑิต
สาขาวิชา	วิศวกรรมไฟฟ้า
พ.ศ.	2543
อาจารย์ผู้ควบคุมวิทยานิพนธ์	รศ. ดร. โมไนย ไกรฤกษ์

บทคัดย่อ

วิทยานิพนธ์ฉบับนี้เป็นการศึกษา พิสูจน์ คำนวณ วิเคราะห์ ออกแบบ สร้าง และทดสอบคุณลักษณะของสายอากาศแบบร่องบนคาวิตี้ตัวนำทรงสี่เหลี่ยมมุมฉาก ซึ่งสายอากาศชนิดนี้มีข้อดีตรงที่มีโครงสร้างไม่ซับซ้อน ไม่ต้านลม และยังสามารถสร้างได้ง่าย โครงสร้างของสายอากาศประกอบด้วยร่องที่ถูกเจาะลงบนผิวคาวิตี้ตัวนำและถูกป้อนด้วยโพรบไฟฟ้าเชิงเส้น การวิเคราะห์เริ่มจากการสร้างแบบจำลองของปัญหาแล้วแบ่งออกเป็นสองขอบเขตคือขอบเขตภายในและขอบเขตภายนอกของคาวิตี้ จากนั้นประยุกต์ใช้เงื่อนไขขอบเขตที่โพรบและร่องในทั้งสองบริเวณเพื่อช่วยในการตั้งสมการเชิงอินทิกรัล โดยที่ฟังก์ชันกรีนในรูปไดแอดิกมีบทบาทสำคัญในการสร้างสมการเชิงอินทิกรัลนั้น การแก้สมการเชิงอินทิกรัลได้ใช้วิธีโมเมนต์เพื่อคำนวณหาคุณลักษณะของสายอากาศอันได้แก่ การกระจายกระแสที่โพรบป้อนสัญญาณ แผ่นแม่เหล็กสมมูลย์บนปากร่อง แบบรูปการแพร่กระจายคลื่นของสายอากาศทั้งตัว ค่าการชี้ทิศทาง อิมพีแดนซ์ขาเข้าของสายอากาศ และอัตราส่วนคลื่นนิ่ง และได้แสดงผลการคำนวณเชิงเลขของคุณลักษณะดังกล่าวและยืนยันโดยเปรียบเทียบกับค่าที่ได้จากการทดสอบ สายอากาศชนิดนี้มีประโยชน์อย่างมากในการทำเป็นองค์ประกอบของสายอากาศชนิดแถวลำดับแบบร่องและสายอากาศชนิดแอกทีฟ

This material is reserved for educational use only, not allowed for commercial use.
Forbidden to modify the content, and cite the document when use.

Thesis Title	Analysis of Radiation and Impedance Characteristics of the Antenna Using the Slot on Rectangular Cavity
Student	Mr. Titipong Lertwiriyaprapa
Student ID.	41061144
Degree	Master of Engineering
Programme	Electrical Engineering
Year	2000
Thesis Advisor	Assoc. Prof. Dr. Monai Krairiksh

ABSTRACT

This thesis presents the study, derivation, calculation, analysis, design, fabrication and measurement of the characteristics of a rectangular cavity-backed slot antenna. The advantages of this antenna type are a simple and flush-mounted structure as well as easy for fabrication. The geometry of the problem is made up of the slot cut on the conducting rectangular cavity fed by a linear electric probe. The analysis model is subdivided into two canonical regions, internal and external cavity. The integral equations are established by enforcing the boundary conditions at the probe and the slot in both regions. The dyadic Green's function plays a vital role to fulfill the requirement of the integral equations. Method of Moments is applied to solve the integral equation to determine the antenna characteristics such as current distribution, radiation pattern, directivity, input impedance and standing wave ratio. The numerical results are illustrated and verified by the measurements. This antenna is very useful to apply as the array element of the linear slot array antenna and active antenna.

This material is reserved for educational use only, not allowed for commercial use.

Forbidden to modify the content, and cite the document when use.

ACKNOWLEDGEMENTS

Without the generous contributions from many individuals, this thesis would never have been accomplished. I would like to express my gratitude to Associate Professor Monai Krairiksh for his valuable recommendations, helpful guidance, kindly advises and forever stimulus throughout my graduate course. I am perpetually proud to have been his student. I am indebted to Associate Professor Jun-ichi Takada of Tokyo Institute of Technology for his useful lectures and comments relating to my works. His kindness to invite me to his laboratory at International Cooperation Center for Science and Technology under visiting research scholar is the most appreciated.

I am very grateful to Assistant Professor Sompol Kosulvit for his kindly discussions and experimental supports. Many comments of Associate Professor Narong Hemmakorn, Dr. Tongtod Vanisri and Associate Professor Suvepon Sittichivapak in examine the thesis are acknowledged.

I would like to sincerely appreciate to Associate Professor Jiro Hirokawa of Tokyo Institute of Technology for his valuable class at King Mongkut's Institute of Technology North Bangkok. Also, I would like to acknowledge Professor Toshio Wakabayashi of Tokai University who gave me useful comments.

I would like to thank to Mr. Chuwong Phongcharoenpanich for his limitless supports both analytical and technical aspects. I also deeply appreciate to him for giving me every material supports as possible as he can. Many thanks to Mr. Phaisan Ngamjanyaporn for his helps in experimental preparing this thesis. Mr. Anat Mearnchu, Miss Nitikarn Pasri and Mr. Chanchai Thongsopa for their aids in doing my experiments, Mr. Rangsan Wongsan and Mr. Wipoo Sriseubsai for their contributions to fabricate the prototype of the antenna, and Mr. Komsak Meksamoot, Mr. Duang-arthit Srimoon and Miss Wanlika Buasomboon for their useful discussions. Eventually, special thank to Miss Mingkwan Thanachaikan for her speedy typing the manuscripts.

I also extend my sincere appreciation to the Ministry of University Affairs for providing the graduate scholarship during my graduate study and to King Mongkut's Institute of Technology North Bangkok for supporting the grants for me to present the paper at United States.

Finally, I am substantially indebted to my parents and my younger brother for their encouragement, dedication and support.

Titipong Lertwiriyaprapa

This material is reserved for educational use only, not allowed for commercial use.

Forbidden to modify the content, and cite the document when use.

TABLE OF CONTENTS

page

Thai Abstract I

English Abstract.....II

Acknowledgements.....III

Table of Contents..... IV

List of Tables.....VII

List of Figures.....VIII

Chapter 1 Introduction.....1

1.1 History of slot antenna on rectangular waveguide and cavity.....1

1.2 Objective of the thesis.....2

1.3 Synopsis of subsequence chapters.....2

Chapter 2 Rectangular Cavity-Backed Slot Antenna.....4

2.1 Geometry of a rectangular cavity-backed slot antenna.....4

2.2 Division of analysis model into canonical regions.....5

2.3 Integral equation formulations.....7

2.4 Conclusions.....12

Chapter 3 Dyadic Green's Function Derivations.....13

3.1 Introduction.....13

3.2 Dyadic Green's functions in electromagnetic theory.....15

3.3 Dyadic Green's functions for internal region.....28

3.4 Dyadic Green's functions for external region.....30

3.5 Conclusions.....31

Chapter 4 Application of Method of Moments to Solve the Integral Equations.....32

4.1 Method of Moments.....32

4.2 Choice of basis and weighting functions.....39

4.3 System of linear equations.....41

4.4 Conclusions.....46

This material is reserved for educational use only, not allowed for commercial use.

Forbidden to modify the content and cite the document when use.

TABLE OF CONTENTS (to)

page

Chapter 5 Current Distribution and Radiation Characteristics of the Antenna.....47

5.1 Electric current distribution along the probe.....47

5.2 Magnetic current sheet on the slot.....48

5.3 Radiation pattern of a rectangular cavity-backed slot antenna fed by a linear electric probe.....48

5.4 Directivity estimations.....70

5.5 Numerical results.....71

5.6 Experimental results.....76

5.7 Application of the second kind Tschebyscheff array to synthesize linear slotted-waveguide array antenna.....79

5.8 Conclusions.....88

Chapter 6 Impedance Characteristics of the Antenna.....89

6.1 Input impedance characterizations.....89

6.2 Reflection coefficient and standing wave ratio evaluations.....90

6.3 Numerical results.....90

6.4 Experimental results.....110

6.5 Active antenna.....112

6.5 Conclusions.....114

Chapter 7 Discussions and Conclusions.....115

7.1 Summary of preceding chapters.....115

7.2 Remark for future researches in this field.....116

References.....117

Appendices.....121

Appendix A Trigonometric and Exponential Functions.....122

Appendix B Scalar, Vector and Dyadic Analyses.....125

This material is reserved for educational use only, not allowed for commercial use.
Forbidden to modify the content, and cite the document when use.

TABLE OF CONTENTS (to)

page

Appendix C Derivation of Dyadic Green's Function in Three-Based Directions.....128

Appendix D Some Orthogonal Relationships of the Vector Wave Functions.....131

Appendix E Integration of Reaction Expressions for External Region.....132

Author Biography 137

This material is reserved for educational use only, not allowed for commercial use.
Forbidden to modify the content and cite the document when use.

LIST OF TABLES

Table page

5.1 Dimension of cavity-backed slot with finite size ground plane in the model.....72

5.2 Dimension of cavity-backed slot with finite size ground plane in the experiment.....76

5.3 Slot length and slot offsets of the antenna.....85

6.1 Dimension of cavity-backed slot antenna: $a=0.75\lambda$ or *11.94* cm.....90

6.2 Dimension of cavity-backed slot antenna: $a=0.69\lambda$ or *10.89* cm.....91

This material is reserved for educational use only, not allowed for commercial use.

Forbidden to modify the content, and cite the document when use.

LIST OF FIGURES

Fig. page

2.1 Geometry of the rectangular cavity-backed slot antenna.....5

(a) excitation by probe in *x*-direction 5

(b) excitation by probe in *y*-direction.....5

2.2 Equivalent model for a slot model.....6

(a) covered by the PEC for probe in *x*-direction.....6

(b) covered by the PEC for probe in *y*-direction.....6

(c) assuming the magnetic current on the slot for the probe in *x*-direction.....6

(d) Assuming the magnetic current on the slot for the probe in *y*-direction.....6

2.3 Equivalent model for the slot and the linear probe.....7

(a) for excitation probe in *x*-direction.....7

(b) for excitation probe in *y*-direction.....7

3.1 Rectangular waveguide.....20

3.2 Rectangular cavity.....27

4.1 Piecewise constant or subdomain pulse function.....35

(a) Single function.....35

(b) Multiple function.....35

4.2 Piecewise linear or subdomain triangle function.....36

(a) Single function.....36

(b) Multiple function.....36

4.3 Piecewise sinusoidal or subdomain sinusoidal function.....37

(a) Single function.....37

(b) Multiple function.....37

4.4 Entire domain sinusoidal function.....37

4.5 Basis function on the slot aperture.....39

4.6 Basis function of the linear electric probe.....40

5.1 Electric current distribution on the linear probe.....47

5.2 Magnetic current on the slot.....48

This material is reserved for educational use only, not allowed for commercial use.

Forbidden to modify the content, and cite the document when use.

LIST OF FIGURES (to)

Fig. page

5.3 Slot on infinite ground plane.....49

(a) in z-direction.....49

(b) in y-direction.....49

5.4 Region separation of two dimensional conducting wedge.....58

5.5 Three dimensions of diffracted ray.....58

5.6 Two dimensions of diffracted ray.....62

5.7 Slot on finite-size ground plane.....63

(a) in *y* direction.....63

(b) in *z* direction.....63

5.8 *xz* plane diffracted ray in case of slot located along *y*-direction.....64

5.9 *yz* plane of diffracted ray in case of slot located along *y*-direction.....67

5.10 *xy* plane diffracted ray in case of slot located along *z*-direction.....68

5.11 *yz* plane diffracted ray in case of slot located along *z*-direction.....69

5.12 Radiation pattern of *y* direction slot with various size of ground plane and with infinite ground plane.....73

(a) ground plane 3λ.....73

(b) ground plane 10λ.....73

(c) ground plane 100λ.....73

(d) ground plane 1000λ.....73

5.13 Radiation pattern of *z* direction slot with various size of ground plane and with infinite ground plane.....74

(a) ground plane 3λ.....74

(b) ground plane 10λ.....74

(c) ground plane 100λ.....74

(d) ground plane 1000λ.....74

5.14 Directivity of slot on infinite ground plane.....75

5.15 Photograph of the cavity-backed slot antenna excited by probe with finite size ground plane (2.375λ).....77

This material is reserved for educational use only, not allowed for commercial use.

Forbidden to modify the content, and cite the document when use.

LIST OF FIGURES (to)

Fig. page

5.16 Radiation pattern of the cavity-backed slot antenna on finite size ground plane *2.375λ*.....78

(a) H plane.....78

(b) E plane.....78

5.17 How to form the major and the minor lobes.....82

5.18 A linear slotted-waveguide array antenna.....82

5.19 Element pattern of a slotted-waveguide antenna.....83

5.20 Amplitude current distribution and array pattern for the second kind Tschebyscheff array of *10* elements at SLL *20* dB with half guided wavelength spacing.....85

(a) Amplitude current distribution.....85

(b) Array factor.....85

5.21 Radiation pattern of a linear slotted-waveguide second kind Tschebycheff array antenna.....87

(a) Rectangular plot.....87

(b) Polar plot.....87

5.22 Photograph of the prototype fabricated antenna.....88

6.1 Input impedance of *x* direction probe for various cavity widths: *a*.....92

(a) Resistance.....92

(b) Reactance.....92

(c) SWR.....92

6.2 Input impedance of *y* direction probe for various cavity widths: *a*.....93

(a) Resistance.....93

(b) Reactance.....93

(c) SWR.....93

6.3 Input impedance for various *x* direction probe locations: y_p.....95

(a) Resistance.....95

(b) Reactance.....95

(c) SWR.....95

This material is reserved for educational use only, not allowed for commercial use.
Forbidden to modify the content, and cite the document when use.

LIST OF FIGURES (to)

Fig. page

6.4 Input impedance for various x direction probe locations: z_p 96

(a) Resistance 96

(b) Reactance 96

(c) SWR 96

6.5 Input impedance for various y direction probe locations: x_p 97

(a) Resistance 97

(b) Reactance 97

(c) SWR 97

6.6 Input impedance for various y direction probe locations: z_p 98

(a) Resistance 98

(b) Reactance 98

(c) SWR 98

6.7 Input impedance for various x direction probe for various probe length: l_p 100

(a) Resistance 100

(b) Reactance 100

(c) SWR 100

6.8 Input impedance for various y direction probe for various probe length: l_p 101

(a) Resistance 101

(b) Reactance 101

(c) SWR 101

6.9 Input impedance for various x direction probe for various slot offsets: x_s 103

(a) Resistance 103

(b) Reactance 103

(c) SWR 103

6.10 Input impedance for various x direction probe for various slot offsets: z_s 104

(a) Resistance 104

(b) Reactance 104

(c) SWR 104

This material is reserved for educational use only, not allowed for commercial use.

Forbidden to modify the content, and cite the document when use.

LIST OF FIGURES (to)

Fig. page

6.11 Input impedance for various y direction probe for various slot offsets: x_s.....105

(a) Resistance.....105

(b) Reactance.....105

(c) SWR.....105

6.12 Input impedance for various y direction probe for various slot offsets: z_s.....106

(a) Resistance.....106

(b) Reactance.....106

(c) SWR.....106

6.13 Input impedance of x direction probe for various slot length: l_s.....108

(a) Resistance.....108

(b) Reactance.....108

(c) SWR.....108

6.14 Input impedance of x direction probe for various slot length: l_s.....109

(a) Resistance.....109

(b) Reactance.....109

(c) SWR.....109

6.15 Photograph of prototype antenna cavity width 0.75λ.....110

(a) Without ground plane.....110

(b) Back view of antenna with ground plane 3λ.....110

(c) Front view of antenna with ground plane 3λ.....110

6.16 Impedance characteristics if antenna for probe in x direction and 0.75λ cavity width..111

(a) Reflection (dB).....111

(b) SWR.....111

6.17 Diagram of active antenna.....112

6.18 Equivalent circuit of active antenna.....112

6.19 Experiment of active antenna.....113

6.20 Experimental result from spectrum analyzer.....114

This material is reserved for educational use only, not allowed for commercial use.

Forbidden to modify the content, and cite the document when use.

CHAPTER 1
INTRODUCTION

The literature review of the works relating with this thesis as well as the objective of the thesis and synopsis of the materials in the thesis are introduced in this chapter.

1.1 History of Slot Antenna on Rectangular Waveguide and Cavity

Over a half of century, the slot cut on the conductor; both on flat plate and curved surface have been widely and continuously investigated. The slot backed by the conducting flat plate such as, rectangular waveguide [1], rectangular cavity [2], radial line waveguide [3] and many others [4]-[9] are very attractive since they belong to the flush-mounted structure that make them low profile. Historically, in 1948 Stevenson published a classical paper [1]. He used boundary value problem to analyze the scattering of a longitudinal slot excited by an incident wave TE_{10} mode. In view of a slot cut on the rectangular cavity, it was first published by Galejs in 1963 [2]. His model was rectangular cavity-backed slot excited by a current source connected across its center and later [5] was published. At the advent of the high-performance computer, several researches launched solving their electromagnetic field problem by numerical methods such as a subsection and point-matching method and Galerkin's method, so-called Method of Moments (coined by R. F. Harrington) [10]. Up till now, this procedure has come into widespread applications in practical electromagnetic computations, especially in slot antenna [6]-[9], [11]-[16] and [44]. The researches on the rectangular slotted-waveguide antennas have been extensively conducted because they are very useful to model as the array element of the very large aperture antennas such as planar slot array antenna [15]-[16] and radial line slot antenna [17] with the large number of elements. When the ends of the waveguide are shorted by the conductor, it becomes the cavity. Therefore, the effect at the shorted ends must be taken into account. The cavity-backed slot antenna is suitable for utilizing in the investigation of the characteristics of the slot on the bounded region particularly for the small aperture antennas at which the slotted-waveguide model cannot be accurately applied. To excite the cavity-backed slot antenna, there are several techniques such as microstrip feed and coaxial feed at the center of the slot aperture. It

This material is reserved for educational use only, not allowed for commercial use.
Forbidden to modify the content, and cite the document when use.

equations are formulated. The integral equations are expressed in terms of the integration of product of unknown current and dyadic Green's function.

Chapter 3 expresses the dyadic Green's functions derived by using the eigenfunction expansion method along with the scattering superposition method. Various kinds of both internal and external dyadic Green's functions for rectangular cavity are illustrated.

Chapter 4 describes the application of Method of Moments to solve the integral equations of the unknown electric and magnetic currents. The entire domain sinusoidal basis function as well as the Galerkin's method is chosen to determine the unknown functions.

Chapter 5 illustrates the current distribution and radiation characteristics of the antenna. The uniform geometrical theory of diffraction is combined with the Method of Moments to realize the pattern for the finite size ground plane at the top of the cavity in place of the infinite ground plane assumption. The application of the slot on the waveguide to synthesize the array antenna using the second kind Tschebyscheff polynomial is also proposed.

Chapter 6 characterizes the input impedance of the antenna for various parameters to perform the resonance and optimum conditions. These aforementioned results can be applied in practice for further applications. The active antenna is used to be an application of input impedance.

Chapter 7 summarizes the materials presented in the preceding chapters and included the remark for further studies.

Finally, the mathematical relations for the trigonometric and the exponential functions are reported in Appendix A. In addition, the scalar, vector and dyadic analyses are included in Appendix B for convenient in derivations. The final results of the dyadic Green's functions in three-based directions are shown in Appendix C. Some orthogonal relationships of the vector wave functions are illustrated in Appendix D. Integration of reaction expressions for external region in the integral equation are derived in Appendix E.

This material is reserved for educational use only, not allowed for commercial use.
Forbidden to modify the content, and cite the document when use.

CHAPTER 2
RECTANGULAR CAVITY-BACKED SLOT ANTENNA

This chapter shows the configuration of a rectangular cavity-backed slot antenna. It is excited by a linear electric probe oriented along either y direction or x direction. Based on Field Equivalent Principle, this antenna is analyzed. The integral equations in terms of dyadic Green's functions and delta gap source model are established by enforcing the boundary conditions at the slot aperture and at the linear electric probe.

2.1 Geometry of a Rectangular Cavity-Backed Slot Antenna

Geometry of a rectangular cavity-backed slot antenna is composed of a slot of the length l_s and the width w_s cut on the top surface of a rectangular cavity with the width a, the height b and the length c. The slot is aligned along z direction where its center is located at (x_s,z_s,b). The excitation is arranged into two cases, i.e. the linear electric probe of the length l_p is located along x-direction at the position $(0,y_p,z_p)$ and is located along y-direction at position $(x_p,0,z_p)$ as shown in Figs.2.1(a) and (b), respectively. At the top of the cavity surface, the slot is surrounded by the infinite ground plane.

In order to investigate the antenna characteristics, the following assumption are specified:

- The infinite ground plane is assumed on the top of cavity.
- The cavity wall and probe are made of perfect electric conductor (PEC).
- The thickness of cavity wall is negligible.
- The probe is very thin in order to disregard its diameter.

This material is reserved for educational use only, not allowed for commercial use.
Forbidden to modify the content, and cite the document when use.

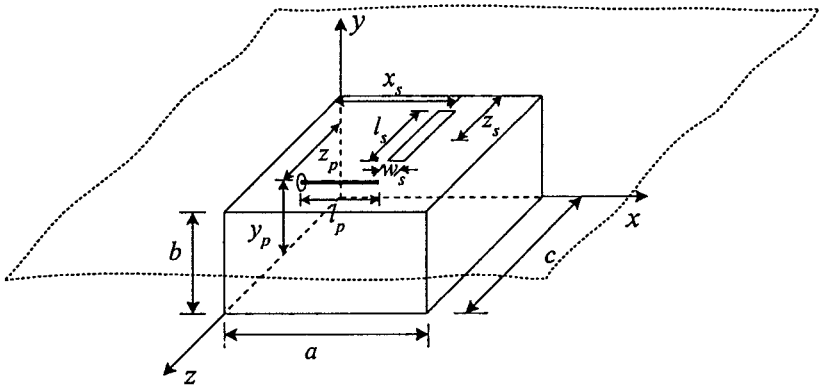

(a)

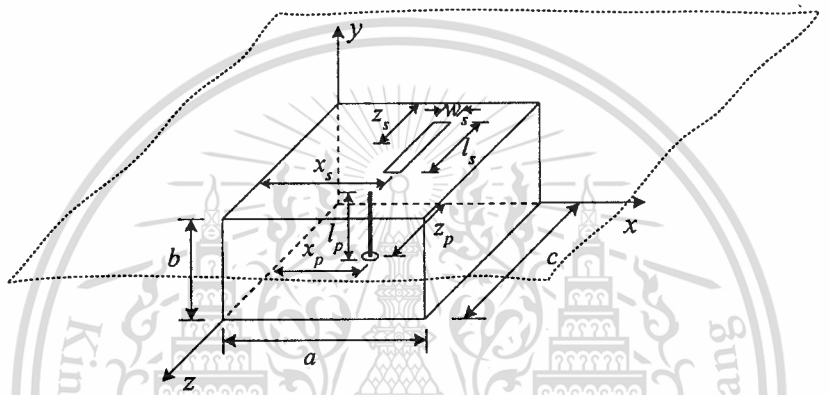

(b)

Fig. 2.1 Geometry of the rectangular cavity-backed slot antenna
(a) excitation by probe in x-direction
(b) excitation by probe in y-direction

2.2 Division of Analysis Model into Canonical Regions

From the analysis model in Figs. 2.1(a) and (b), it consists of a slot aperture and a linear electric probe inside the cavity. It is evident that this structure possesses the discontinuities in structure at the slot and probe. In order to dispose these discontinuities, the Field Equivalent Principle [19] is applied by following these conditions:

- For the slot aperture
  - Assuming the PEC surface encloses the original problem as dash lines shown in Figs. 2.2(a) and (b)

This material is reserved for educational use only, not allowed for commercial use.
Forbidden to modify the content, and cite the document when use.

- The magnetic current $\overline{M}$ is assumed at the slot aperture in both sides of the cavity. They have opposite direction to each other i.e., outside the cavity $\overline{M} = \overline{E} \times \hat{n}$ and inside the cavity $\overline{M} = \overline{E} \times (-\hat{n})$, as illustrated in Figs. 2.2(c) and (d), where $\hat{n}$ denotes the unit normal outward vector.

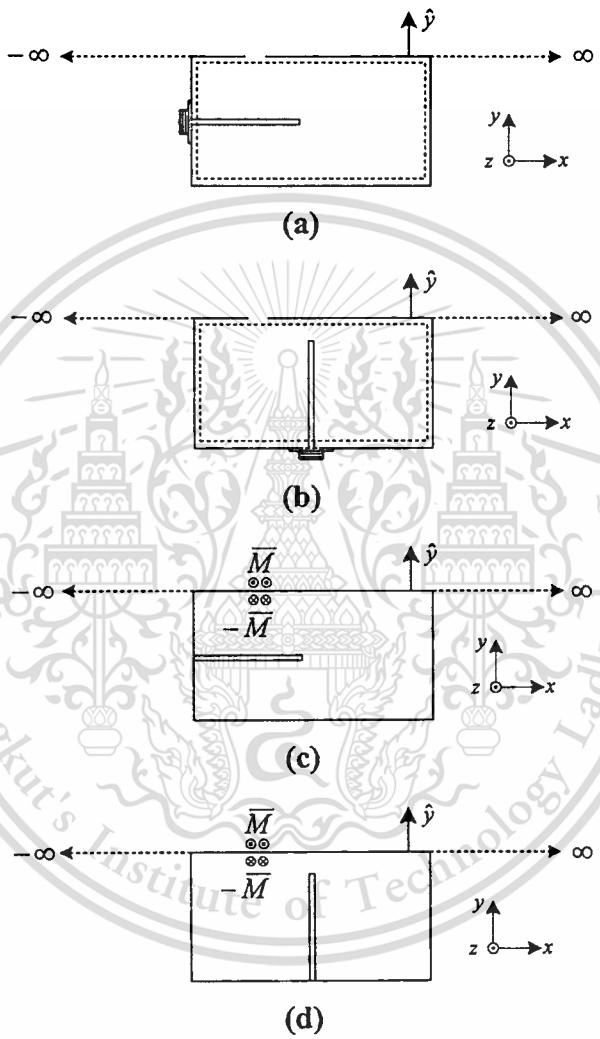

Fig. 2.2 Equivalent model for the slot aperture

(a) covered by the PEC for the probe in x-direction

(b) covered by the PEC for the probe in y-direction

(c) assuming the magnetic current on the slot for the probe in x-direction

(d) assuming the magnetic current on the slot for the probe in y-direction

This material is reserved for educational use only, not allowed for commercial use.
Forbidden to modify the content, and cite the document when use.

- For the linear electric probe.
  - Removing the linear electric probe
  - The electric current $\bar{J}$ is assumed along the linear electric probe.

In addition, the Field Equivalent Principle is used to divide this analysis model into two canonical regions, external region (*ext*) and internal region (*int*). By following all of above conditions, the equivalent model is established as displayed in Figs. 2.3(a) and (b).

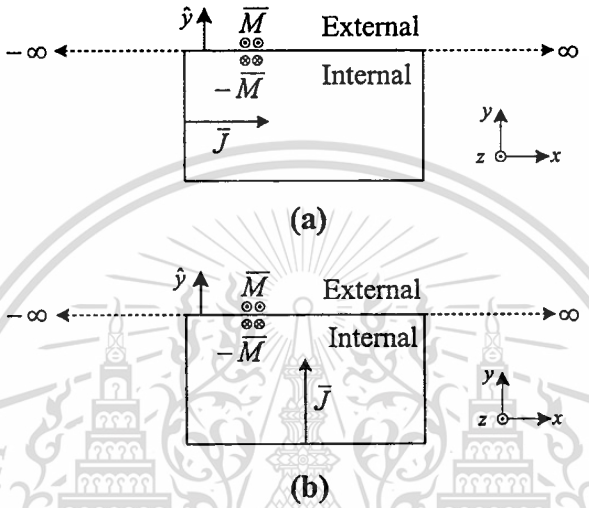

Fig. 2.3 Equivalent model for the slot and the linear probe
(a) for excitation probe in x-direction
(b) for excitation probe in y-direction

2.3 Integral Equation Formulations

From these equivalent models, since the discontinuities in the structure were eliminated, the continuity conditions of the tangential magnetic fields are automatically satisfied at the slot aperture.

$$\bar{H}_{tan}^{ext} = \bar{H}_{tan}^{int} \tag{2.1a}$$

$$\bar{H}_{tan}^{ext} = \bar{H}_{s}^{ext} \times \hat{y} \tag{2.1b}$$

$$\bar{H}_{tan}^{int} = \left(\bar{H}_{s}^{int} + \bar{H}_{p}^{int}\right) \times \hat{y} \tag{2.1c}$$

$$\bar{H}_{s}^{ext} = \bar{H}_{s}^{int} + \bar{H}_{p}^{int} \tag{2.1d}$$

This material is reserved for educational use only, not allowed for commercial use.
Forbidden to modify the content, and cite the document when use.

where $\overline{H}_{tan}^{ext}$ and $\overline{H}_{tan}^{int}$ represent the external and internal tangential magnetic fields, respectively. $\overline{H}_{p}^{int}$ and $\overline{H}_{s}^{int}$ are the internally radiated magnetic field from the linear electric probe and the slot aperture, respectively. $\overline{H}_{s}^{ext}$ denotes the external magnetic field radiated from the slot aperture. $\hat{y}$ is the unit normal vector to *xz* surface.

With the aid of the dyadic Green's function [20], it is feasible to immediately calculate the magnetic field of each term, namely

$$\overline{H}_{s}^{ext}(\overline{R}) = j\omega\varepsilon_0 \iint_{S_a} \overline{\overline{G}}_{HM}^{ext}(\overline{R},\overline{R}') \cdot (\overline{E}(\overline{R}') \times \hat{y}) dS'$$

$$= j\omega\varepsilon_0 \iint_{S_a} \overline{\overline{G}}_{HM}^{ext}(\overline{R},\overline{R}') \cdot \overline{M}(\overline{R}') dS' \tag{2.2}$$

and

$$\overline{H}_{s}^{int}(\overline{R}) = j\omega\varepsilon_0 \iint_{S_a} \overline{\overline{G}}_{HM}^{int}(\overline{R},\overline{R}') \cdot (\overline{E}(\overline{R}') \times -\hat{y}) dS'$$

$$= -j\omega\varepsilon_0 \iint_{S_a} \overline{\overline{G}}_{HM}^{int}(\overline{R},\overline{R}') \cdot \overline{M}(\overline{R}') dS', \tag{2.3}$$

$$\overline{H}_{p}^{int}(\overline{R}) = \iint_{S_f} \overline{\overline{G}}_{HJ}^{int}(\overline{R},\overline{R}') \cdot \overline{J}(\overline{R}') dS' \tag{2.4}$$

where $\overline{\overline{G}}_{HM}^{ext,int}(\overline{R},\overline{R}')$ and $\overline{\overline{G}}_{HJ}^{int}(\overline{R},\overline{R}')$ denote the magnetic dyadic Green's function produced by a magnetic current sheet and electric current density, respectively. S_a and S_f are limit of integration on the surface of slot aperture and on the length of probe, respectively. $\overline{R}$ and $\overline{R}'$ are the location coordinates of field and source point, respectively. In this thesis, the time function $e^{j\omega t}$ is used. Substituting (2.2) (2.3) and (2.4) into (2.1d) the simultaneous equation across the slot can be obtained as:

This material is reserved for educational use only, not allowed for commercial use.
Forbidden to modify the content, and cite the document when use.

$$j\omega\varepsilon_0 \iint_{S_a} \left\{ \overline{\overline{G}}_{HM}^{ext}(\bar{R},\bar{R}') + \overline{\overline{G}}_{HM}^{int}(\bar{R},\bar{R}') \right\} \cdot \bar{M}(\bar{R}')dS' - \iint_{S_f} \overline{\overline{G}}_{HJ}^{int}(\bar{R},\bar{R}') \cdot \bar{J}(\bar{R}')dS' = 0 \tag{2.5}$$

Alternatively, not only the boundary condition on the tangential electric field along the probe is considered, but the delta gap electric field at the bottom of the probe is also considered as the excitation. Therefore,

$$E_{tan}^{int} = 0 \tag{2.6a}$$

For the excitation by probe in x-direction, E_{tan}^{int} can be written as

$$E_{tan}^{int} = \left(\bar{E}^{int} \cdot \hat{x}\right) + E_a \tag{2.6b}$$

In case of the probe excited in y-direction, E_{tan}^{int} is

$$E_{tan}^{int} = \left(\bar{E}^{int} \cdot \hat{y}\right) + E_a \tag{2.6c}$$

where E_a is applied field, defined by delta gap modeling as

$$E_a = \delta(\bar{R} - \bar{R}')$$

and $\bar{E}^{int}$ denotes internal scattering field, given as

$$\bar{E}^{int} = \bar{E}_s^{int} + \bar{E}_p^{int}$$

Following (2.6a) and using delta gap model, (2.6b) and (2.6c) can be rearranged as

$$\bar{E}^{int} \cdot \hat{x} = -E_a \tag{2.7a}$$

and

$$\bar{E}^{int} \cdot \hat{y} = -E_a \tag{2.7b}$$

This material is reserved for educational purposes. Not allowed for commercial use.
Forbidden to modify the content, and cite the document when use.

The complete condition can be stated as:

$$\left(\overline{E}_s^{int} + \overline{E}_p^{int}\right)\cdot \hat{x} = -\delta\left(\overline{R}'\right), \tag{2.8a}$$

and

$$\left(\overline{E}_s^{int} + \overline{E}_p^{int}\right)\cdot \hat{y} = -\delta\left(\overline{R}'\right) \tag{2.8b}$$

where $\overline{E}_s^{int}$ and $\overline{E}_p^{int}$ are the internally electric field from the slot aperture and the probe, respectively. $-\delta\left(\overline{R}'\right)$ is the assumed voltage source from the delta gap source model.

$$\overline{E}_s^{int}(\overline{R}) = \iint_{S_a} \overline{\overline{G}}_{EM}^{int}\left(\overline{R},\overline{R}'\right)\cdot\left(\overline{E}\left(\overline{R}'\right)\times -\hat{y}\right)dS'$$

$$= -\iint_{S_a} \overline{\overline{G}}_{EM}^{int}\left(\overline{R},\overline{R}'\right)\cdot \overline{M}\left(\overline{R}'\right)dS' \tag{2.9}$$

$$\overline{E}_p^{int}(\overline{R}) = -j\omega\mu_0 \iint_{S_f} \overline{\overline{G}}_{EJ}^{int}\left(\overline{R},\overline{R}'\right)\cdot \overline{J}\left(\overline{R}'\right)dS', \tag{2.10}$$

where $\overline{\overline{G}}_{EM}^{int}\left(\overline{R},\overline{R}'\right)$ and $\overline{\overline{G}}_{EJ}^{int}\left(\overline{R},\overline{R}'\right)$ denote the electric dyadic Green's functions produced by magnetic current sheet and electric current density, respectively. Substituting (2.9) and (2.10) into (2.8), the simultaneous integral equation on the probe can be obtained as:

$$-\iint_{S_a} \overline{\overline{G}}_{EM}^{in}\left(\overline{R},\overline{R}'\right)\cdot \overline{M}\left(\overline{R}'\right)dS' - j\omega\mu_0 \iint_{S_f} \overline{\overline{G}}_{EJ}^{in}\left(\overline{R},\overline{R}'\right)\cdot \overline{J}\left(\overline{R}'\right)dS' = -\delta\left(\overline{R}'\right) \tag{2.11}$$

Now the integral equations have been obtained as shown in (2.5) and (2.11). The next step is evaluation of the unknown of magnetic current sheet and electric current density. This can be accomplished by using Method of Moments.

This material is reserved for educational use only, not allowed for commercial use.
Forbidden to modify the content, and cite the document when use.

2.4 Conclusions

This chapter shows the geometry of the slot on the rectangular cavity excited by the linear electric probe. The analysis model is divided into canonical regions according to the discontinuity of structure. The continuous in this structure can be achieved by applying the Field Equivalent Principle and enforcing the boundary conditions at the probe and the slot aperture. The delta gap is chosen to be source model at the bottom of the probe. The integral equations of the unknown currents are established in terms of the dyadic Green's functions. These integral equations can be solved by using Method of Moments as described in Chapter 4 after the dyadic Green's functions are derived in Chapter 3.

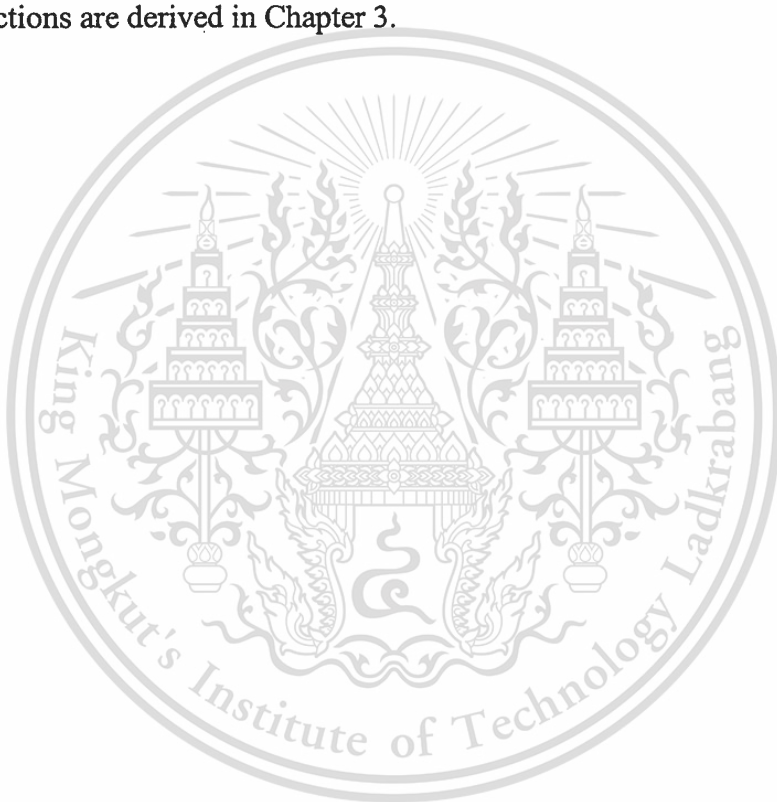

This material is reserved for educational use only, not allowed for commercial use.
Forbidden to modify the content, and cite the document when use.

CHAPTER 3
DYADIC GREEN'S FUNCTION DERIVATIONS

Dyadic Green's functions play a vital role in calculation the electromagnetic field in any regions. They are categorized into four kinds according to the electric and magnetic fields due to electric and magnetic sources. They can be originally derived from Maxwell's equations. Starting with the rectangular waveguide, the method of G_m is used to derive the vector wave equations in conjunction with the dyadic Green's functions. The scattering superposition is used for determining various kinds of dyadic Green's functions for rectangular cavity in the desired direction.

3.1 Introduction

Generally, the sets of Maxwell's equations, established by James Clerk Maxwell in 1873, are substantially used to explain the electromagnetic phenomena both theoretical and applied concepts. As a well-established discipline, they serve as the fundamental rules of nature and vital links to other scientific fields. In fact, these equations can be addressed either in differential or in integral form. The former one is more suitable to use and is applied in this thesis. Therefore, only the differential equations of Maxwell's equations are expressed here:

$$\nabla \times \overline{E} = -\overline{M}_i - \frac{\partial \overline{B}}{\partial t} \tag{3.1a}$$

$$\nabla \times \overline{H} = \overline{J}_i + \overline{J}_c + \frac{\partial \overline{D}}{\partial t} \tag{3.1b}$$

$$\nabla \cdot \overline{J} = -\frac{\partial q_{ev}}{\partial t} \tag{3.1c}$$

$$\nabla \cdot \overline{D} = q_{ev} \tag{3.1d}$$

$$\nabla \cdot \overline{B} = q_{mv} \tag{3.1e}$$

This material is reserved for educational use only, not allowed for commercial use.
Forbidden to modify the content, and cite the document when use.

where

$\overline{E}$: electric field intensity (volts/meter),

$\overline{H}$: magnetic field intensity (amperes/meter),

$\overline{D}$: electric flux density (coulombs/square meter),

$\overline{B}$: magnetic flux density (webers/square meter),

$\overline{J}_i$: impressed (source) electric current density (amperes/square meter),

$\overline{J}_c$: conduction electric current density (amperes/square meter),

$\overline{M}_i$: impressed (source) magnetic current density (volts/square meter),

q_{ev} : electric charge density (coulombs/cubic meter),

q_{mv} : magnetic charge density (webers/cubic meter).

In any situation, these constitutive relations between the field quantities are needed. They can be expressed as follows:

$$\overline{D} = \varepsilon \overline{E} \tag{3.2a}$$

$$\overline{B} = \mu \overline{H} \tag{3.2b}$$

$$\overline{J} = \sigma \overline{E} \tag{3.2c}$$

where ε, μ, σ denote, respectively, the permittivity, the permeability and the conductivity of the medium.

$$\varepsilon = \varepsilon_o \varepsilon_r$$

$$\mu = \mu_o \mu_r.$$

where ε_r, μ_r are the relative permittivity and permeability which depend on the electrical properties of the materials. ε_o is the free space permittivity and is equal to 8.854×10^{-12} or about $10^{-9}/36\pi$ farads per meter. In the same manner, μ_o is the free space permeability which equals $4\pi\times10^{-7}$ henries per meter. For free space the conductivity vanishes.

This thesis is provided for educational use only, not allowed for commercial use.
Forbidden to modify the content, and cite the document when use.

Usually, Maxwell's equations are presented either in time varying electromagnetic or in time-harmonic. In such time-harmonic, the system of equations can be simplified considerably. They are represented by the complex time function form, $e^{j\omega t}$. Hence, the time conventional throughout this thesis is $e^{j\omega t}$. Therefore, Maxwell's equations can be expressed as

$$\nabla \times \bar{E} = -\bar{M}_i - j\omega\bar{B} \tag{3.3a}$$

$$\nabla \times \bar{H} = \bar{J}_i + \bar{J}_c + j\omega\bar{D} \tag{3.3b}$$

$$\nabla \cdot \bar{J} = -j\omega q_{ev} \tag{3.3c}$$

$$\nabla \cdot \bar{D} = q_{ev} \tag{3.3d}$$

$$\nabla \cdot \bar{B} = q_{mv}. \tag{3.3e}$$

where ω is the operating angular frequency which equals 2π times the frequency.

3.2 Dyadic Green's Functions in Electromagnetic Theory

In view of dyadic form, Maxwell's equations can be written as [20] by juxtaposing a unit vector $\hat{x}_j$ at the posterior position and summing the three sets of equations with respect to j. Then, three infinitesimal electric dipoles are considered to be the source term, $\bar{J}$. The expression of various dyadic functions can be shown as

$$\nabla \times \bar{\bar{G}}_e = \bar{\bar{G}}_m \tag{3.4a}$$

$$\nabla \times \bar{\bar{G}}_m = \bar{\bar{I}}\delta(\bar{R} - \bar{R}') + k^2 \bar{\bar{G}}_e \tag{3.4b}$$

$$\nabla \cdot \bar{\bar{G}}_e = \frac{1}{k^2}\nabla\delta(\bar{R} - \bar{R}') \tag{3.4c}$$

$$\nabla \cdot \bar{\bar{G}}_m = 0. \tag{3.4d}$$

This material is reserved for educational use only, not allowed for commercial use.
Forbidden to modify the content, and cite the document when use.

From the vector wave equations, the dyadic wave equations can be derived as

$$\nabla\times\nabla\times\overline{\overline{G}}_e - k^2\overline{\overline{G}}_e = \overline{\overline{I}}\delta(\overline{R}-\overline{R}') \tag{3.5a}$$

and

$$\nabla\times\nabla\times\overline{\overline{G}}_m - k^2\overline{\overline{G}}_m = \nabla\times[\overline{\overline{I}}\delta(\overline{R}-\overline{R}')]. \tag{3.5b}$$

where $\overline{\overline{I}}$ denotes the idem factor and k is a propagation constant.

$$\overline{\overline{I}} = \hat{x}\hat{x} + \hat{y}\hat{y} + \hat{z}\hat{z}$$

The classification of various dyadic Green's functions depends upon the type of dyadic conditions, Dirichlet and Neumann. In free space media there are two types of electric and magnetic dyadic Green's functions. The electric and magnetic types satisfy (3.5a) and (3.5b), respectively. Both of them are also categorized into two kinds, first and second kind. The first kind electric and magnetic dyadic Green's function, denoted, respectively, by $\overline{\overline{G}}_{e1}(\overline{R},\overline{R}')$ and $\overline{\overline{G}}_{m1}(\overline{R},\overline{R}')$, are required to satisfy the dyadic Dirichlet boundary condition, namely,

$$\hat{n}\times\overline{\overline{G}}_{e1}(\overline{R},\overline{R}')=0 \tag{3.6a}$$

and

$$\hat{n}\times\overline{\overline{G}}_{m1}(\overline{R},\overline{R}')=0\,. \tag{3.6b}$$

Knowing $\overline{\overline{G}}_{e1}$ and $\overline{\overline{G}}_{m1}$, the electric field can be found, respectively, as

$$\overline{E}(\overline{R}) = -j\omega\mu_o \iiint_V \overline{\overline{G}}_{e1}(\overline{R},\overline{R}')\cdot\overline{J}(\overline{R}')dV' \tag{3.7a}$$

$$\overline{E}(\overline{R}) = -\iint_{S_a}\overline{\overline{G}}_{m1}(\overline{R},\overline{R}')\cdot\overline{M}(\overline{R}')dS' \tag{3.7b}$$

This material is reserved for educational use only, not allowed for commercial use.
Forbidden to modify the content, and cite the document when use.

Alternatively, the dyadic Neumann boundary condition is satisfied for the second kind of electric and magnetic dyadic Green's function, denoted, respectively, by $\overline{\overline{G}}_{e2}(\overline{R},\overline{R}')$ and $\overline{\overline{G}}_{m2}(\overline{R},\overline{R}')$, namely,

$$\hat{n}\times\nabla\times\overline{\overline{G}}_{e2}(\overline{R},\overline{R}')=0 \tag{3.8a}$$

$$\hat{n}\times\nabla\times\overline{\overline{G}}_{m2}(\overline{R},\overline{R}')=0 \tag{3.8b}$$

Also, they can be used to calculate the magnetic field, given as

$$\overline{H}(\overline{R})=\iiint_{V}\overline{\overline{G}}_{m2}(\overline{R},\overline{R}')\cdot\overline{J}(\overline{R}')dV' \tag{3.9a}$$

$$\overline{H}(\overline{R})=-j\omega\varepsilon_{o}\iint_{S_a}\overline{\overline{G}}_{e2}(\overline{R},\overline{R}')\cdot\overline{M}(\overline{R}')dS' \tag{3.9b}$$

From the expression of dyadic functions (3.4a), the relationship between $\overline{\overline{G}}_{e2}$ and $\overline{\overline{G}}_{m1}$ can be found corresponding to the Neumann condition. It yields

$$\nabla\times\overline{\overline{G}}_{e2}=\overline{\overline{G}}_{m1} \tag{3.10}$$

To complete the relationship between $\overline{\overline{G}}_{e1}$ and $\overline{\overline{G}}_{m2}$, they will be derived by using the symmetrical relations of vector wave functions, and can be shown as

$$\nabla\times\overline{\overline{G}}_{e1}=\overline{\overline{G}}_{m2} \tag{3.11}$$

In view of (3.4b), under the Dirichlet condition the $\overline{\overline{G}}_{e1}$ can be expressed as

$$\nabla\times\overline{\overline{G}}_{m2}=\overline{\overline{I}}\delta(\overline{R}-\overline{R}')+k^2\overline{\overline{G}}_{e1} \tag{3.12}$$

35746
This material is reserved for educational use only, not allowed for commercial use.
Forbidden to modify the content, and cite the document when use.

and under the Neumann condition $\overline{\overline{G}}_{e2}$ can be denoted as

$$\nabla \times \overline{\overline{G}}_{m1} = \overline{\overline{I}}\delta(\overline{R} - \overline{R}') + k^2 \overline{\overline{G}}_{e2} \tag{3.13}$$

From the expression of Maxwell's equation, it is evident that the $\overline{\overline{G}}_{m2}$ is a solenoidal dyadic function, that is

$$\nabla \cdot \overline{\overline{G}}_{m2} = 0, \tag{3.14}$$

but $\overline{\overline{G}}_{e2}$ is nonsolenoidal.

3.2.1 Rectangular Vector Wave Function

To derive the various kinds of dyadic Green's functions, the vector wave functions are needed. Following Stratton's work [21], there are three kinds of vector wave functions, i.e. $\overline{L}$, $\overline{M}$ and $\overline{N}$. All of them are the solutions of the homogeneous vector Helmholtz equation. $\overline{M}$ and $\overline{N}$ are solenoidal function but $\overline{L}$ is not. Thus, from (3.14), in the previous section, only $\overline{M}$ and $\overline{N}$ are needed to derive the magnetic dyadic Green's functions. Subsequently, the other types of dyadic are derived by using some relationships in the previous section.

First, by taking curl of (3.3a) and (3.3b) with homogeneous medium and source free conditions, they are written as

$$\nabla \times \nabla \times \overline{E} - k^2 \overline{E} = 0 \tag{3.15a}$$

$$\nabla \times \nabla \times \overline{H} - k^2 \overline{H} = 0 \tag{3.16b}$$

By imposing $\overline{F}$ as any vector and κ is considered to be the arbitrary constant, then

$$\nabla \times \nabla \times \overline{F} - \kappa^2 \overline{F} = 0 \tag{3.17}$$

This material is reserved for educational use only, not allowed for commercial use.
Forbidden to modify the content, and cite the document when use.

There are two kinds of vector wave functions, which are

$$\overline{M} = \nabla \times (\psi \hat{a}) \tag{3.18a}$$

$$\overline{N} = \frac{1}{\kappa} \nabla \times \nabla \times (\psi \hat{a}) \tag{3.18b}$$

where ψ denotes a characteristic function which satisfies the scalar wave equation

$$\nabla^2 \psi + \kappa^2 \psi = 0 \tag{3.19}$$

In case of an identical generating function ψ is used for both $\overline{M}$ and $\overline{N}$, we have the following symmetrical relations

$$\overline{N} = \frac{1}{\kappa} \nabla \times \overline{M} \tag{3.20a}$$

$$\overline{M} = \frac{1}{\kappa} \nabla \times \overline{N} \tag{3.20b}$$

To derive the vector wave functions, there are two steps, the expression of the scalar function and choice of the piloting vector $\hat{a}$. To deal with the configuration of the rectangular waveguide as shown in Fig.3.1, the unit vector $\hat{z}$ is the most appropriate because it would provide the transverse electric (*TE*) and transverse magnetic (*TM*) modes, which are usually desired in the theory of rectangular waveguide.

By using separation of variables [22], the scalar wave equation (3.19) can be solved as follow:

$$\psi = f(x)g(y)h(z) \tag{3.21}$$

This material is reserved for educational use only, not allowed for commercial use.
Forbidden to modify the content, and cite the document when use.

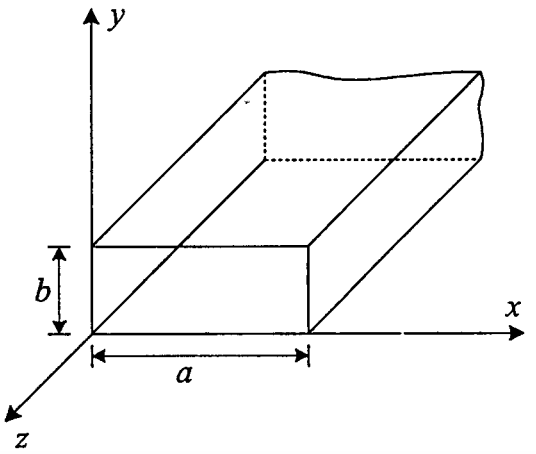

Fig. 3.1 Rectangular waveguide

Both of the functions, *f(x)* and *g(y)* must be chosen to represent standing waves function because the waveguide is bounded in x and y direction. The appropriate functions are

$$f(x) = A\cos(k_x x) + B\sin(k_x x) \tag{3.22a}$$

$$g(y) = C\cos(k_y y) + D\sin(k_y y) \tag{3.22b}$$

Since the waveguide is infinite extent in length, *h(z)* has to represent the traveling waves as :

$$h(z) = Ee^{-jhz} + Fe^{jhz} \tag{3.23}$$

Considering only $+z$ direction, thus $F = 0$

$$h(z) = Ee^{-jhz} \tag{3.24}$$

By substituting (3.22a), (3.22b) and (3.24) into (3.21), the solution of the scalar wave equation becomes

$$\psi = \{A\cos(k_x x) + B\sin(k_x x)\}\{C\cos(k_y y) + D\sin(k_y y)\}Ee^{-jhz} \tag{3.25}$$

This material is reserved for educational use only, not allowed for commercial use.
Forbidden to modify the content, and cite the document when use.

where $k_x^2 + k_y^2 + h^2 = \kappa^2$

$$k_x = \frac{m\pi}{a} \quad , m=0,1,2,...$$

$$k_y = \frac{n\pi}{b} \quad , n=0,1,2,...$$

For *TE* mode, applying the boundary condition that tangential electric field vanishes at the wall, $x=0$ and a as well as $y=0$ and b, the solution of scalar wave equation becomes

$$\psi_{emn}(h) = A_{mn}\cos(k_x x)\cos(k_y y)e^{-jhz} \tag{3.26}$$

where A_{mn} denotes the arbitrary constant. The subscript "e " is an abbreviation of even.

Similarly, for *TM* mode the solution is

$$\psi_{omn}(h) = B_{mn}\sin(k_x x)\sin(k_y y)e^{-jhz} \tag{3.27}$$

where B_{mn} denotes the arbitrary constant. The subscript "o " is an abbreviation of odd.

In view of electric field in a waveguide, the vector wave functions with normalizing modal coefficients ($A_{mn} = B_{mn} = 1$) $\overline{M}_{emn}$ and $\overline{N}_{omn}$ are defined to satisfy the vector Dirichlet boundary condition at the wall of the waveguide,

$$\hat{n} \times \overline{M}_{emn} = 0 \tag{3.28a}$$

and

$$\hat{n} \times \overline{N}_{omn} = 0 \tag{3.28b}$$

as

$$\begin{aligned} \overline{M}_{emn}(h) &= \nabla \times [\psi_{emn}(h)\hat{z}] \\ &= (-k_y C_x S_y \hat{x} + k_x S_x C_y \hat{y})e^{-jhz} \end{aligned} \tag{3.29}$$

This material is reserved for educational use only, not allowed for commercial use.
Forbidden to modify the content, and cite the document when use.

where $\overline{M}_{emn}(h)$ represents the electric field of TE_{mn} and $\overline{N}_{omn}$ are that of TM_{mn} mode. and

$$S_x = \sin(k_x x) \qquad C_x = \cos(k_x x)$$

$$S_y = \sin(k_y y) \qquad C_y = \cos(k_y y)$$

$$\kappa^2 = k_x^2 + k_y^2 + h^2 = k_c^2 + h^2$$

$$k_c^2 = k_x^2 + k_y^2$$

Similarly, $\overline{N}_{omn}$ are given by

$$\overline{N}_{omn}(h) = \frac{1}{\kappa}\nabla\times\nabla\times[\psi_{omn}(h)\hat{z}]$$

$$= \frac{1}{\kappa}(-jk_x C_x S_y \hat{x} - jk_y S_x C_y \hat{y} + k_c^2 S_x S_y \hat{z})e^{-jhz} \qquad (3.30)$$

From the symmetrical relations in (3.20a) and (3.20b), the proper vector functions to represent the magnetic field in a rectangular waveguide are

$$\overline{M}_{omn}(h) = \frac{1}{\kappa}\nabla\times\overline{N}_{omn}(h) = \nabla\times[\psi_{omn}(h)\hat{z}]$$

$$= (k_y S_x C_y \hat{x} - k_x C_x S_y \hat{y})e^{-jhz} \qquad (3.31)$$

$$\overline{N}_{emn}(h) = \frac{1}{\kappa}\nabla\times\overline{M}_{emn}(h) = \frac{1}{\kappa}\nabla\times\nabla\times[\psi_{emn}(h)\hat{z}]$$

$$= \frac{1}{\kappa}(jhk_x S_x C_y \hat{x} + jhk_y C_x S_y \hat{y} + k_c^2 C_x C_y \hat{z})e^{-jhz} \qquad (3.32)$$

$\overline{M}_{omn}$ and $\overline{N}_{emn}$ satisfy the vector Neumann condition on the boundary, namely

$$\hat{n}\times\nabla\times\overline{M}_{omn}(h) = 0 \qquad (3.33a)$$

$$\hat{n}\times\nabla\times\overline{N}_{emn}(h) = 0 \qquad (3.33b)$$

This material is reserved for educational use only; not allowed for commercial use.
Forbidden to modify the content, and cite the document when use.

In summary, the complete sets of vector wave functions can be written as

$$\overline{M}_{\substack{e\\o}mn}(h) = \nabla \times \left[\psi_{\substack{e\\o}mn}(h)\hat{z} \right] \tag{3.34a}$$

$$\overline{N}_{\substack{e\\o}mn}(h) = \frac{1}{\kappa} \nabla \times \nabla \times \left[\psi_{\substack{e\\o}mn}(h)\hat{z} \right] \tag{3.34b}$$

where $\psi_{\substack{e\\o}mn}(h) = \begin{pmatrix} \cos\frac{m\pi x}{a} & \cos\frac{n\pi y}{b} \\ \sin\frac{m\pi x}{a} & \sin\frac{n\pi y}{b} \end{pmatrix} e^{-jhz} = \begin{pmatrix} C_x & C_y \\ S_x & S_y \end{pmatrix} e^{-jhz}$

$$\kappa^2 = \left(\frac{m\pi}{a}\right)^2 + \left(\frac{n\pi}{b}\right)^2 + h^2 = k_c^2 + h^2$$

3.2.2 Dyadic Green's Functions of a Rectangular Cavity

According to the method of $\overline{\overline{G}}_m$ [20], the dyadic Green's functions for rectangular waveguide are first obtained. Subsequently, the dyadic Green's functions for rectangular cavity can be derived. By using the Ohm-Rayleigh method, the second kind magnetic dyadic Green's function of the rectangular waveguide satisfies the equation

$$\nabla \times \nabla \times \overline{\overline{G}}_{m2}(\overline{R}, \overline{R}') - k^2 \overline{\overline{G}}_{m2}(\overline{R}, \overline{R}') = \nabla \times [\overline{\overline{I}}\delta(\overline{R} - \overline{R}')] \tag{3.35}$$

This equation is valid in the domain $0 \le x \le a$, $0 \le y \le b$, $-\infty < z < \infty$ in Fig. 3.1, and the Neumann boundary condition

$$\hat{n} \times \nabla \times \overline{\overline{G}}_{m2}(\overline{R}, \overline{R}') = 0$$

at $x=0$ and a, $y=0$ and b, and where $k = \omega\sqrt{\mu_o \varepsilon_o}$

From the Ohm-Rayleigh method, the eigenfunction expansion for source function $\nabla \times [\overline{\overline{I}}\delta(\overline{R} - \overline{R}')]$ is

This material is reserved for educational use only, not allowed for commercial use.
Forbidden to modify the content, and cite the document when use.

$$\nabla\times[\overline{\overline{I}}\delta(\overline{R}-\overline{R}')]=\int_{-\infty}^{\infty}\sum_{m=0}^{\infty}\sum_{n=0}^{\infty}[\overline{N}_{emn}(h)\overline{A}_{emn}(h)+\overline{M}_{omn}(h)\overline{B}_{omn}(h)]dh \quad (3.36)$$

By taking the anterior scalar product of source term of (3.36) with $\overline{N}_{em'n'}(-h')$ and $\overline{M}_{om'n'}(-h')$, integrating the resultant equation throughout the entire configuration domain and then using the dyadic Gauss theorem in conjunction with the orthogonal relationships between the vector wave functions described in Appendix D, one obtains

$$\overline{A}_{emn}(h)=\frac{(2-\delta_o)\kappa}{\pi abk_c^2}\overline{M}'_{emn}(-h) \quad (3.37)$$

and

$$\overline{B}_{omn}(h)=\frac{(2-\delta_o)\kappa}{\pi abk_c^2}\overline{N}'_{omn}(-h) \quad (3.38)$$

where δ_o denotes the Kronecker delta function defined as

$$\delta_o=\begin{cases}1, & m \text{ or } n=0\\ 0, & m \text{ and } n\neq 0\end{cases}$$

Substituting (3.37) and (3.38) into (3.36), the eigenfunction expansion of $\nabla\times[\overline{\overline{I}}\delta(\overline{R}-\overline{R}')]$ is given by

$$\nabla\times[\overline{\overline{I}}\delta(\overline{R}-\overline{R}')]=\int_{-\infty}\sum_{m,n}^{\infty}\frac{(2-\delta_o)\kappa}{\pi abk_c^2}[\overline{N}_{emn}(h)\overline{M}'_{emn}(-h)+\overline{M}_{omn}(h)\overline{N}'_{omn}(-h)]dh \quad (3.39)$$

To find $\overline{\overline{G}}_{m2}$, the same expansion of source function as shown in (3.39) can be used. The additional unknown coefficients *a(h)* and *b(h)* are appeared as

This material is reserved for educational use only, not allowed for commercial use.
Forbidden to modify the content, and cite the document when use.

$$\overline{\overline{G}}_{m2}(\overline{R},\overline{R}') = \int_{-\infty}^{\infty}\sum_{m,n} \frac{(2-\delta_o)\kappa}{\pi abk_c^2} \cdot[a(h)\overline{N}_{emn}(h)\overline{M}'_{emn}(-h) + b(h)\overline{M}_{omn}(h)\overline{N}'_{omn}(-h)]dh \tag{3.40}$$

substituting (3.39) and (3.40) into (3.35) and using

$$\nabla\times\nabla\times\begin{bmatrix}\overline{N}_{emn}\\ \overline{M}_{omn}\end{bmatrix} = \kappa^2\begin{bmatrix}\overline{N}_{emn}\\ \overline{M}_{omn}\end{bmatrix}$$

then the coefficients of (3.40) are

$$a(h) = b(h) = \frac{1}{\kappa^2 - k^2}.$$

Therefore, $\overline{\overline{G}}_{m2}(\overline{R},\overline{R}')$ is given by

$$\overline{\overline{G}}_{m2}(\overline{R},\overline{R}') = \int_{-\infty}^{\infty}\sum_{m,n} \frac{(2-\delta_o)\kappa}{\pi abk_c^2(\kappa^2 - k^2)} \cdot[\overline{N}_{emn}(h)\overline{M}'_{emn}(-h) + \overline{M}_{omn}(h)\overline{N}'_{omn}(-h)]dh \tag{3.41}$$

By applying the method of contour integration, $\overline{\overline{G}}_{m2}$ can be obtained as

$$\overline{\overline{G}}_{m2}(\overline{R},\overline{R}') = \frac{-jk}{ab}\sum_{m,n}\frac{2-\delta_o}{k_c^2 k_g} \cdot[\overline{N}_{emn}(\pm k_g)\overline{M}'_{emn}(\mp k_g) + \overline{M}_{omn}(\pm k_g)\overline{N}'_{omn}(\mp k_g)], \quad z \gtrless z' \tag{3.42}$$

where $k_g = (k^2 - k_c^2)^{\frac{1}{2}}$ for real $k > k_c$ and imagine $k < k_c$

This material is reserved for educational use only, not allowed for commercial use.
Forbidden to modify the content, and cite the document when use.

From Maxwell's equation in dyadic form

$$\nabla \times \overline{\overline{G}}_{m2}(\overline{R},\overline{R}') = \overline{\overline{I}}\delta(\overline{R}-\overline{R}') + k^2 \overline{\overline{G}}_{e1}(\overline{R},\overline{R}')$$

in conjunction with aiding of Heaviside unit step functions that satisfy the dyadic Dirichlet condition, namely

$$\hat{n} \times \overline{\overline{G}}_{e1}(\overline{R},\overline{R}') = 0 .$$

$\overline{\overline{G}}_{e1}$ can be derived as

$$\overline{\overline{G}}_{e1}(\overline{R},\overline{R}') = -\frac{1}{k^2}\hat{z}\hat{z}\delta(\overline{R}-\overline{R}') - \frac{j}{ab}\sum_{m,n}\frac{2-\delta_o}{k_c^2 k_g}[\overline{M}_{emn}(\pm k_g)\overline{M}'_{emn}(\mp k_g) + \overline{N}_{omn}(\pm k_g)\overline{N}'_{omn}(\mp k_g)], \quad \begin{matrix} z > z' \\ z < z' \end{matrix} \tag{3.43}$$

where $\delta(\overline{R}-\overline{R}')$ is Dirac delta function.

In order to avoid a possible confusion of field type and source type of various kinds of dyadic Green's functions, another representation form of them is

$$\overline{\overline{G}}_{e1} = \overline{\overline{G}}_{EJ}$$

$$\overline{\overline{G}}_{m1} = \overline{\overline{G}}_{EM}$$

$$\overline{\overline{G}}_{e2} = \overline{\overline{G}}_{HM}$$

$$\overline{\overline{G}}_{m2} = \overline{\overline{G}}_{HJ}$$

where $\overline{\overline{G}}_{EJ}(\overline{R},\overline{R}')$ denotes the electric dyadic Green's function produced by electric current density. $\overline{\overline{G}}_{EM}(\overline{R},\overline{R}')$ is the electric dyadic Green's function produced by

This material is reserved for educational use only, not allowed for commercial use.
Forbidden to modify the content, and cite the document when use.

magnetic current sheet. $\overline{\overline{G}}_{HM}(\overline{R},\overline{R}')$ is the magnetic dyadic Green's function produced by a magnetic current sheet. $\overline{\overline{G}}_{HJ}(\overline{R},\overline{R}')$ represents the magnetic dyadic Green's function produced by electric current density. Therefore, these nomenclatures will be used from the following subsection.

Next, the dyadic Green's functions for rectangular cavity can be derived by using the dyadic Green's functions for rectangular waveguide together with the method of scattering superposition. There are two steps to accomplish. First, the waveguide is assumed to be terminated at $z = 0$. The functions for a semi-infinite waveguide $0 \le z < \infty$ are determined from the summation of the functions for waveguide and scattered term. In the functions for scattered term, two unknown coefficients are occurred. By using the Dirichlet boundary condition at $z = 0$ for *TE* and *TM* modes, these coefficients can be determined. The semi-infinite waveguide is again terminated at $z = c$. Therefore, it now becomes a rectangular cavity, $0 \le z \le c$ as illustrated in Fig. 3.2.

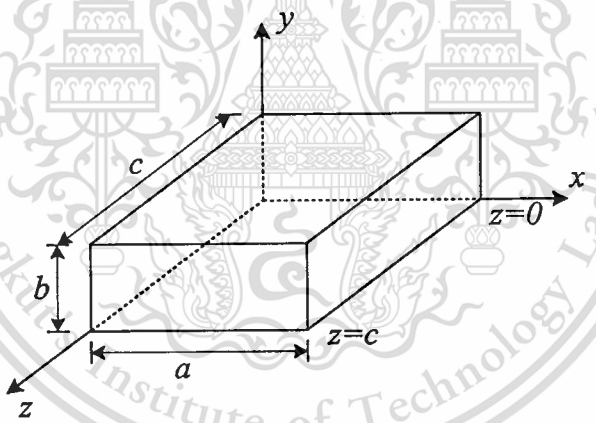

Fig. 3.2 Rectangular cavity

In the same manner, the first kind dyadic Green's function for rectangular cavity can be derived [23]

$$\overline{\overline{G}}_{EJ}^{in}(\overline{R},\overline{R}') = -\frac{1}{k^2}\hat{z}\hat{z}\delta(\overline{R}-\overline{R}') + \frac{2}{ab}\sum_{m,n}\frac{(2-\delta_o)}{k_g k_c^2 \sin k_g c}\begin{cases} \overline{M}_{eo}^{z}(c-z)\overline{M}_{eo}^{\prime z}(z') - \overline{N}_{oe}^{z}(c-z)\overline{N}_{oe}^{\prime z}(z'), z > z' \\ \overline{M}_{eo}^{z}(z)\overline{M}_{eo}^{\prime z}(c-z') - \overline{N}_{oe}^{z}(z)\overline{N}_{oe}^{\prime z}(c-z'), z < z' \end{cases} \quad (3.44)$$

This material is reserved for educational use only, not allowed for commercial use.
Forbidden to modify the content, and cite the document when use.

The prime vector wave function $\overline{M}'$ and $\overline{N}'$ are the excitation functions and the unprime function $\overline{M}$ and $\overline{N}$ are the field functions. From symmetrical relationships in (3.11), the second kind magnetic dyadic Green's function for rectangular cavity can straightforwardly be shown as

$$\overline{\overline{G}}_{HJ}(\overline{R},\overline{R}') = \frac{2k}{ab}\sum_{m,n}\frac{(2-\delta_o)}{k_{gz}k_{cz}^2\sin k_{gz}c}\begin{Bmatrix}\overline{N}_{eo}^{z}(c-z)\overline{M}_{eo}^{'z}(z') - \overline{M}_{oe}^{z}(c-z)\overline{N}_{oe}^{'z}(z'), z>z'\\ \overline{N}_{eo}^{z}(z)\overline{M}_{eo}^{'z}(c-z') - \overline{M}_{oe}^{z}(z)\overline{N}_{oe}^{'z}(c-z'), z<z'\end{Bmatrix} \tag{3.45}$$

Similarly, by applying the same procedure used in deriving $\overline{\overline{G}}_{EJ}$, we can obtain

$$\overline{\overline{G}}_{HM}(\overline{R},\overline{R}') = -\frac{1}{k^2}\hat{z}\hat{z}\delta(\overline{R}-\overline{R}') + \frac{2}{ab}\sum_{m,n}\frac{(2-\delta_o)}{k_{gz}k_{cz}^2\sin k_{gz}c}\begin{Bmatrix}\overline{N}_{eo}^{z}(c-z)\overline{N}_{eo}^{'z}(z') - \overline{M}_{oe}^{z}(c-z)\overline{M}_{oe}^{'z}(z'), z>z'\\ \overline{N}_{eo}^{z}(z)\overline{N}_{eo}^{'z}(c-z') - \overline{M}_{oe}^{z}(z)\overline{M}_{oe}^{'z}(c-z'), z<z'\end{Bmatrix} \tag{3.46}$$

then,

$$\overline{\overline{G}}_{EM}(\overline{R},\overline{R}') = \frac{2k}{ab}\sum_{m,n}\frac{(2-\delta_o)}{k_{gz}k_{cz}^2\sin k_{gz}c}\begin{Bmatrix}\overline{M}_{eo}^{z}(c-z)\overline{N}_{eo}^{'z}(z') - \overline{N}_{oe}^{z}(c-z)\overline{M}_{oe}^{'z}(z'), z>z'\\ \overline{M}_{eo}^{z}(z)\overline{N}_{eo}^{'z}(c-z') - \overline{N}_{oe}^{z}(z)\overline{M}_{oe}^{'z}(c-z'), z<z'\end{Bmatrix} \tag{3.47}$$

where $\overline{M}_{eo}^{z}(z)$, $\overline{M}_{oe}^{z}(z)$, $\overline{N}_{eo}^{z}(z)$ and $\overline{N}_{oe}^{z}(z)$ are defined in Appendix C.

3.3 Dyadic Green's Functions for Internal Region

From chapter 2, the dyadic Green's functions for rectangular cavity are linear operator, which should be known functions. Therefore, they have to be considered. All of them were formed exclusively in z-direction but in fact, the dyadic Green's functions must be constructed with respect to direction of source function. For instance, on the y-direction probe the dyadic Green's functions have to be formulated in y-direction, similarly in x-direction probe, and on the z-direction slot aperture they have to be also derived in z-direction. In this section, various kinds of internal dyadic Green's functions are shown in term of source directions. Since the magnetic current

This material is reserved for educational use only, not allowed for commercial use.
Forbidden to modify the content, and cite the document when use.

sheet is assumed to be source on the slot in z-direction, the dyadic Green's function $\overline{\overline{G}}_{HM}^{int}(\bar{R},\bar{R}')$, in z-direction is used. It was rigorously derived in previous section and can be rewritten as

$$\overline{\overline{G}}_{HM}^{int}(\bar{R},\bar{R}') = -\frac{1}{k^2}\hat{z}\hat{z}\delta(\bar{R}-\bar{R}') + \frac{2}{ab}\sum_{m,n}\frac{(2-\delta_o)}{k_{gz}k_{cz}^2\sin k_{gz}c}\begin{cases}\bar{N}_{eo}^{z}(c-z)\bar{N}_{eo}^{\prime z}(z') - \bar{M}_{oe}^{z}(c-z)\bar{M}_{oe}^{\prime z}(z'), z>z'\\ \bar{N}_{eo}^{z}(z)\bar{N}_{eo}^{\prime z}(c-z') - \bar{M}_{oe}^{z}(z)\bar{M}_{oe}^{\prime z}(c-z'), z<z'\end{cases} \tag{3.48}$$

For the electric current along the linear electric probe, the dyadic Green's functions $\overline{\overline{G}}_{EJ}^{int}(\bar{R},\bar{R}')$, in y-direction and in x-direction are required. They can be obtained by rotating the coordinating system [24] then is given in desired direction as follows:

$$\overline{\overline{G}}_{EJ}^{int}(\bar{R},\bar{R}') = -\frac{1}{k^2}\hat{y}\hat{y}\delta(\bar{R}-\bar{R}') + \frac{2}{ac}\sum_{m,n}\frac{(2-\delta_o)}{k_{gy}k_{cy}^2\sin k_{gy}b}\begin{cases}\bar{M}_{eo}^{y}(b-y)\bar{M}_{eo}^{\prime y}(y') - \bar{N}_{oe}^{y}(b-y)\bar{N}_{oe}^{\prime y}(y'), y>y'\\ \bar{M}_{eo}^{y}(y)\bar{M}_{eo}^{\prime y}(b-y') - \bar{N}_{oe}^{y}(y)\bar{N}_{oe}^{\prime y}(b-y'), y<y'\end{cases} \tag{3.49}$$

$$\overline{\overline{G}}_{EJ}^{int}(\bar{R},\bar{R}') = -\frac{1}{k^2}\hat{x}\hat{x}\delta(\bar{R}-\bar{R}') + \frac{2}{bc}\sum_{m,n}\frac{(2-\delta_o)}{k_{gx}k_{cx}^2\sin k_{gx}a}\begin{cases}\bar{M}_{eo}^{x}(a-x)\bar{M}_{eo}^{\prime x}(x') - \bar{N}_{oe}^{x}(a-x)\bar{N}_{oe}^{\prime x}(x'), x>x'\\ \bar{M}_{eo}^{x}(x)\bar{M}_{eo}^{\prime x}(a-x') - \bar{N}_{oe}^{x}(x)\bar{N}_{oe}^{\prime x}(a-x'), x<x'\end{cases} \tag{3.50}$$

where $\bar{M}_{eo}^{y}(y)$, $\bar{M}_{oe}^{y}(y)$, $\bar{N}_{eo}^{y}(y)$, $\bar{N}_{oe}^{y}(y)$, $\bar{M}_{eo}^{x}(x)$, $\bar{M}_{oe}^{x}(x)$, $\bar{N}_{eo}^{x}(x)$ and $\bar{N}_{oe}^{x}(x)$ are defined in Appendix C

Next, the dyadic Green's functions for mutual term between slot and probe and vice versa are $\overline{\overline{G}}_{HJ}^{int}$ and $\overline{\overline{G}}_{EM}^{int}$.

This material is reserved for educational use only, not allowed for commercial use.
Forbidden to modify the content, and cite the document when use.

$$\overline{\overline{G}}^{int}_{HJ}(\bar{R},\bar{R}') = \frac{2k}{bc}\sum_{m,n}\frac{(2-\delta_o)}{k_{gy}k_{cy}^2\sin k_{gy}b}\begin{Bmatrix}\bar{N}^y_{eo}(b-y)\bar{M}'^y_{eo}(y') - \bar{M}^y_{oe}(b-y)\bar{N}'^y_{oe}(y'), y>y'\\ \bar{N}^y_{eo}(y)\bar{M}'^y_{eo}(b-y') - \bar{M}^y_{oe}(y)\bar{N}'^y_{oe}(b-y'), y<y'\end{Bmatrix} \tag{3.51}$$

$$\overline{\overline{G}}^{int}_{EM}(\bar{R},\bar{R}') = \frac{2k}{bc}\sum_{m,n}\frac{(2-\delta_o)}{k_{gy}k_{cy}^2\sin k_{gy}b}\begin{Bmatrix}\bar{M}^y_{eo}(c-y)\bar{N}'^y_{eo}(y') - \bar{N}^y_{oe}(c-y)\bar{M}'^y_{oe}(y'), y>y'\\ \bar{M}^y_{eo}(y)\bar{N}'^y_{eo}(c-y') - \bar{N}^y_{oe}(y)\bar{M}'^y_{oe}(c-y'), y<y'\end{Bmatrix} \tag{3.52}$$

3.4 Dyadic Green's Function for External Region

Let us consider the dyadic Green's function in free space condition $\overline{\overline{G}}_{Ho}$,

$$\nabla\times\nabla\times\overline{\overline{G}}_{Ho} - k^2\overline{\overline{G}}_{Ho} = \overline{\overline{I}}\delta(\bar{R}-\bar{R}') \tag{3.53}$$

By using the dyadic identity (B.19)

$$\nabla\times\left(\nabla\times\overline{\overline{a}}\right) = \nabla\left(\nabla\cdot\overline{\overline{a}}\right) - \nabla^2\overline{\overline{a}}$$

(3.53) can be converted into the form

$$\nabla\left(\nabla\cdot\overline{\overline{G}}_{Ho}\right) - \nabla^2\overline{\overline{G}}_{Ho} - k^2\overline{\overline{G}}_{Ho} = \overline{\overline{I}}\delta(\bar{R}-\bar{R}') \tag{3.54}$$

by taking the divergence of (3.53), we obtain

$$\nabla\cdot\overline{\overline{G}}_{Ho} = -\frac{1}{k^2}\nabla\cdot\delta(\bar{R}-\bar{R}') \qquad ;\nabla\cdot\left(\nabla\times\nabla\times\overline{\overline{G}}_{Ho}\right) = 0$$

Substituting into (3.54), thus (3.54) can be written in the form

$$\left(\nabla^2+k^2\right)\overline{\overline{G}}_{Ho} = -\left(\overline{\overline{I}} + \frac{1}{k^2}\nabla\nabla\right)\delta(\bar{R}-\bar{R}') \tag{3.55}$$

This material is reserved for educational use only, not allowed for commercial use.
Forbidden to modify the content, and cite the document when use.

To fine $\overline{\overline{G}}_{Ho}$, from free-space scalar Green's function

$$\left(\nabla^2 + k^2\right)G_o = -\delta(\overline{R} - \overline{R}') \qquad ;G_o = j\omega\varepsilon_o \frac{e^{jk|\overline{R}-\overline{R}'|}}{4\pi|\overline{R} - \overline{R}'|}$$

$$\left(\nabla^2 + k^2\right)\overline{\overline{G}}_{Ho} = \left(\overline{\overline{I}} + \frac{1}{k^2}\nabla\nabla\right)\left(\nabla^2 + k^2\right)G_o$$

$$\overline{\overline{G}}_{Ho} = j\omega\varepsilon_o\left(\overline{\overline{I}} + \frac{1}{k^2}\nabla\nabla\right)\frac{e^{jk|\overline{R}-\overline{R}'|}}{4\pi|\overline{R} - \overline{R}'|} \tag{3.56}$$

where $|\overline{R} - \overline{R}'| = \sqrt{(x-x')^2 + (y-y')^2 + (z-z')^2}$

In half free-space, we obtain

$$\overline{\overline{G}}^{ext}_{HM} = j\omega\varepsilon_o\left(\overline{\overline{I}} + \frac{1}{k^2}\nabla\nabla\right)\frac{e^{jk|\overline{R}-\overline{R}'|}}{2\pi|\overline{R} - \overline{R}'|} \tag{3.57}$$

3.5 Conclusions

The dyadic Green's functions are derived in this chapter by using the eigenfunction expansion method. The scalar functions were constructed by considering the solution of the scalar wave equation in case of free from the source. After that the vector functions were derived by using the scalar functions. Only the solenoidal vector wave functions are necessary for deriving the dyadic Green's function of the magnetic type dyadic Green's function method. The dyadic Green's functions can be constructed by juxtaposing those vector wave functions. The unknown coefficients of the dyadic Green's functions were determined by applying the Dirichlet and Neumann boundary conditions. The complete expression of the dyadic Green's function for the rectangular cavity can be accomplished by applying the scattering superposition techniques from the case of the rectangular wavguide. The dyadic Green's functions both electric and magnetic type produced by the electric and magnetic sources are reported in this chapter. From the results of the dyadic Green's function obtained in this chapter, they will be used to fulfill in the integral equations derived in the previous chapter.

This material is reserved for educational use only, not allowed for commercial use.
Forbidden to modify the content, and cite the document when use.

CHAPTER 4
APPLICATION OF METHOD OF MOMENTS TO SOLVE THE INTEGRAL EQUATIONS

Method of Moments is the powerful tool to solve the linear equation by transforming it to the system of simultaneous algebraic equations. Many kinds of basis and weighting function are investigated. The accuracy and ease of numerical calculations are heavily relied on the choice of basis and weighting functions. Both of them are discussed in this chapter. By following the appropriate selections of basis and weighting functions, the system of equations is also presented both linear equation and matrix form.

4.1 Method of Moments

Before the advent of the high-speed computer, the computations of electromagnetic field by numerical methods were unpopular because the required computation was considerably tedious. The analytical methods were extensively used instead. During World War II, the large-scale attempt to solve the practical electromagnetic engineering problems was undertaken. Many researchers used the variational methods to fulfill their requirement. In mid 1960s, with the development of computers the numerical techniques were started to solve the electromagnetic field equations. In 1967, Roger Harrington first introduced the novel numerical method so-called Method of Moments [10] and [25]. Within a few year from 1966 till now, Method of Moments have been widely used for solving linear operator equations in many electromagnetic problems and especially applying to various practical antenna problems [26].

Method of Moments is a numerical procedure for solving a linear equation by transforming it to a system of simultaneous algebraic equation [27]-[28]. The basic idea of transforming is rather old. Galerkin, a Russian mechanical engineer, developed the method, bearing his name, around 1920s. It was the specialization of the more general Method of Moments.

This material is reserved for educational use only, not allowed for commercial use.
Forbidden to modify the content, and cite the document when use.

Consider the linear equation [25]

$$Lf = g \tag{4.1}$$

where L is a linear operator, g is a known function (excitation), f is an unknown function. As the first step of this approach, the approximation of unknown function f by a finite sum is expressed in terms of basis or expansion function as

$$f = \sum_{i=1}^{N} a_i f_i \tag{4.2}$$

where a_i are unknown coefficients to be determined, f_i are known expansion functions or basis functions. More details of basis function can be found in next section. Substituting (4.2) into (4.1) one obtains

$$\sum_{i=1}^{N} a_i L f_i = g \tag{4.3}$$

For exact solution, the limit of summation is infinite; for approximate solution it is usually finite. Theoretically, the exact solution is desired but practically, the approximate solution is usually obtained. Therefore, due to the approximate way the residual is formed. The next step of Method of Moments is that the residual is weighted to be zero with respect to the suitable weighting function w_{n_j}, $j=1,...,N_j$ by taking inner product and use the linearity of the inner product. Then, (4.3) can be expressed in form of a matrix equation as

$$\sum_{i=1}^{N_j} a_i < w_{n_j}, Lf_i > = < w_{n_j}, g > \tag{4.4}$$

where $< >$ represents the inner product.

The unknown coefficient (a_i) can be calculated from solution of (4.4). In this way, the problem has been reduced to that of a set of linear algebraic equations, which can be written in matrix form as

This material is reserved for educational use only, not allowed for commercial use.
Forbidden to modify the content, and cite the document when use.

$$[L][a]=[g] \tag{4.5}$$

where

$$L=\begin{bmatrix} <w_1,Lf_1> & <w_1,Lf_2> & \cdots \\ <w_2,Lf_1> & <w_2,Lf_2> & \cdots \\ \vdots & \vdots & \end{bmatrix}$$

$$a=\begin{bmatrix} a_1 \\ a_2 \\ \vdots \end{bmatrix} \qquad g=\begin{bmatrix} <w_1,g> \\ <w_2,g> \\ \vdots \end{bmatrix}$$

4.1.1 Basis Functions

The basis functions chosen for a particular problem have to satisfy the following criteria:

1) They must satisfy the boundary and differentiability conditions of problem at least in some distributional manner.
2) They should be linearly independent.
3) They have to be a set of complete functions in the domain of the operator.

Usually, there are two kinds of function such as subdomain and entire domain functions.

4.1.1.1 Subdomain Functions

The subdomain approach can be considered by subdividing the structure into N segments. Each of basis function exists only over subsections of the domain of f. The unknown coefficient of basis function affects the approximation of f only over subsection of interested region.

There are various kinds of subdomain basis functions. The most common of these basis functions is the pulse function (piecewise constant) shown in Fig. 4.1(a). It is defined by

$$P_n(x)=\begin{cases} 1 & x_{n-1} \le x \le x_n \\ 0 & \text{elsewhere} \end{cases} \tag{4.6}$$

This material is reserved for educational use only, not allowed for commercial use.
Forbidden to modify the content, and cite the document when use.

When the unknown coefficients are determined, this function is shown in the form of staircase, shown in Fig. 4.1(b)

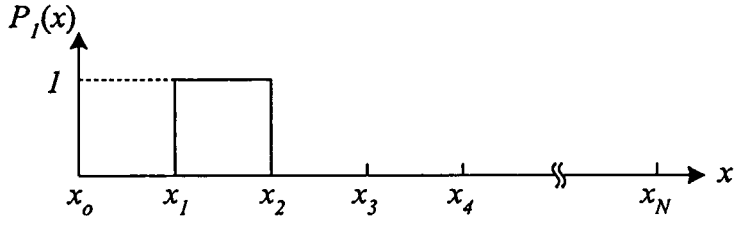

(a)

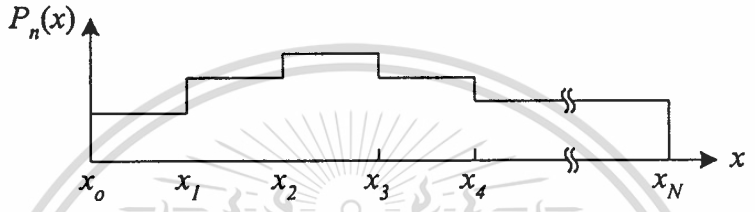

(b)

Fig. 4.1 Piecewise constant or subdomain pulse function
(a) Single function
(b) Multiple function

The triangle function or piecewise linear is another basis function, defined as

$$T_n(x) = \begin{cases} \dfrac{x - x_{n-1}}{x_n - x_{n-1}}, & x_{n-1} \le x \le x_n \\ \dfrac{x_{n+1} - x}{x_{n+1} - x_n}, & x_n \le x \le x_{n+1} \\ 0, & \text{elsewhere} \end{cases} \tag{4.7}$$

A combination of triangle functions provides a piecewise linear approximation to basis function, as represented by Fig. 4.2.

This material is reserved for educational use only, not allowed for commercial use.
Forbidden to modify the content, and cite the document when use.

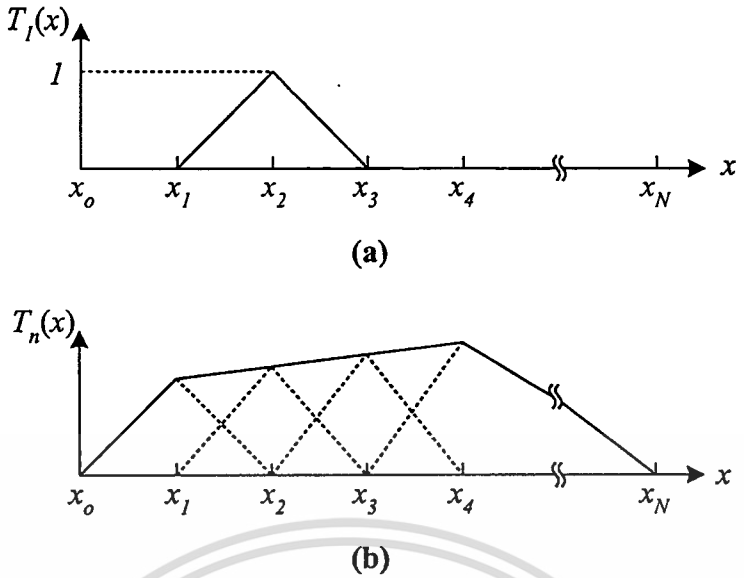

Fig. 4.2 Piecewise linear or subdomain triangle function
(a) Single function
(b) Multiple function

The more sophisticated subdomain basis function is the sinusoidal function (piecewise sinusoidal). Though increasing the complicated function may not be warranted that the improvement of accuracy is achieved. However, in some situations, the specialized functions are very useful. The sinusoidal function is shown in Fig.4.3.

$$S_n(x) = \begin{cases} \dfrac{\sin k(x - x_{n-1})}{\sin k(x_n - x_{n-1})}, & x_{n-1} \le x \le x_n \\ \dfrac{\sin k(x_{n+1} - x)}{\sin k(x_{n+1} - x_n)}, & x_n \le x \le x_{n+1} \end{cases} \tag{4.8}$$

This material is reserved for educational use only, not allowed for commercial use.
Forbidden to modify the content, and cite the document when use.

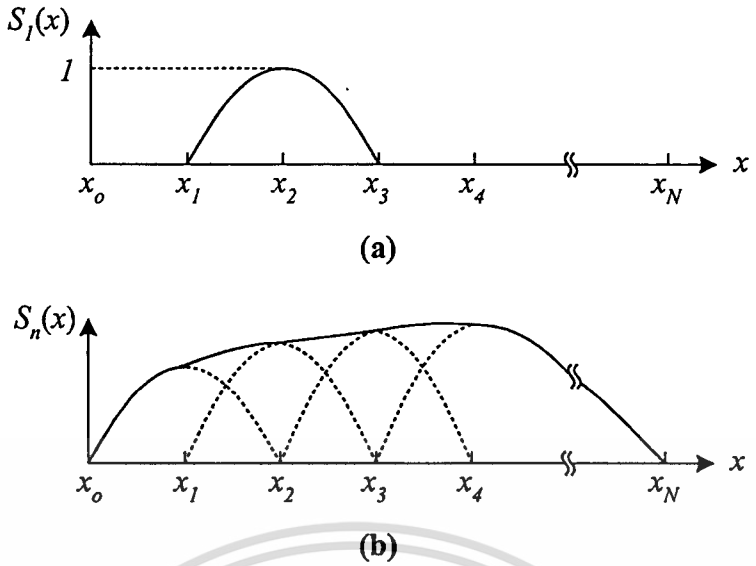

Fig. 4.3 Piecewise sinusoidal or subdomain sinusoidal function
(a) Single function
(b) Multiple function

4.1.1.2 Entire-Domain Functions

Entire-domain basis functions are defined to be nonzero over the entire structure. Thus the subsections are not appearing. In addition, it has the continuous form over the structure. Therefore, the numerical convergence is enhanced. The entire-domain basis function is defined as

$$S(x) = \sin\frac{i\pi}{l_s}\left(x_i + \frac{l_s}{2}\right) \;;\; i = 1...N \tag{4.9}$$

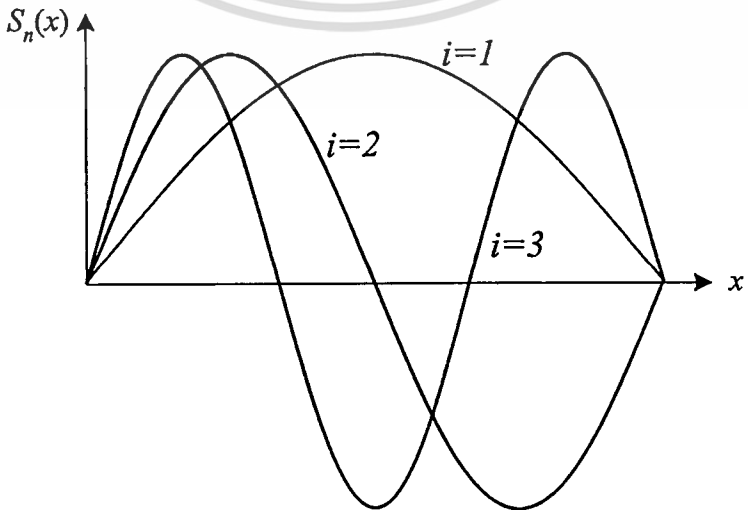

Fig. 4.4 Entire domain sinusoidal function

This material is reserved for educational use only, not allowed for commercial use.
Forbidden to modify the content, and cite the document when use.

4.1.2 Weighting function

To extinguish the residuals from the approximate solutions, the weighting functions are used to weight the residual across the entire domain L. In fact, there are many procedures to weight [29]; namely

- Point-Matching Method
- Galerkin's method
- Method of least squares

The point-matching method is the simple and straightforward way to obtain the approximate solutions. In view of Method of Moments, it is equivalent to using Dirac delta functions as the weighting functions. Usually, this method is used, when a large number of basis functions are required to approximate the unknown functions.

For Galerkin's method, the weighting functions are not delta functions but they can be selected as

$$w_j = f_i \tag{4.10}$$

The Galerkin's method has been extensively used in electromagnetic problems [30]. This method has been found to yield accurate results with rapid convergence, in case of low-order solutions, i.e., when few basis functions are needed.

Finally, for the weighting functions of least squares method they are defined as

$$w_j = Lx_i \tag{4.11}$$

This method is more sensitive to the proper choice of expansion functions than the other two techniques. However, it always leads to a monotonic convergence of the residual [31].

In any particular problem, one of the main tasks is to choose the appropriated basis and weighting functions to the problem. There are considerably possible sets of basis and weighting functions. Some sets may yield faster convergence than other, easier matrix to determine or desired accuracy solutions.

This material is reserved for educational use only, not allowed for commercial use.
Forbidden to modify the content, and cite the document when use.

4.2 Choice of Basis and Weighting Functions

4.2.1 Basis Function

As described in section 4.1, there are two kinds of functions, subdomain or piecewise sinusoidal and entire domain functions. From the choice of basis functions, the suitable function should be physically meaningful bases. Therefore, the natures of electric field on a slot aperture are considered.

- The behavior of aperture electric field distribution is cosinusoidal with respect to the direction of slot length.[9]
- The effect from the width of slot is reasonably uniform.

In order to deal with the natures of a slot aperture, the sinusoidal entire domain is appropriate because it is continuous and smooth function throughout a slot aperture. It is easy to include the higher order mode functions into the analysis. Only a few expansion terms are usually adequate to obtain the required accuracy. Accordingly, the expansion of magnetic current can be expressed as following

$$\overline{M}_s(\overline{R}') = \sum_{i=1}^{N_1} A_i \overline{m}_i(\overline{R}') \tag{4.12}$$

where

$$\overline{m}_i(\overline{R}') = \frac{1}{w_s} \sin \frac{i\pi}{l_s}\left(z' + \frac{l_s}{2}\right)\hat{z}$$

where $\overline{m}_i(\overline{R}')$ is a basis function. z' is the source point on the slot coordinate system. A_i is the unknown coefficients.

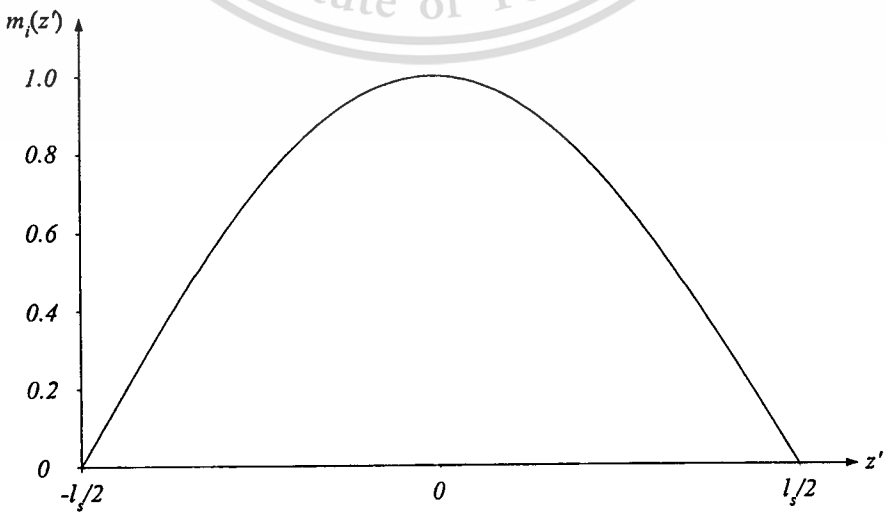

Fig. 4.5 Basis function on the slot aperture

This material is reserved for educational use only, not allowed for commercial use.
Forbidden to modify the content, and cite the document when use.

The above basis function will be used in this thesis and shown in Fig. 4.5. In view of a linear probe, there are two types, open and shorted end. For the shorted one, the uniform current is assumed as

$$\bar{J}_p(\bar{R}') = \hat{z} \tag{4.13}$$

On the other hand, for open ended structure, the space between cavity wall and the end of wire probe is optimized for suppressing reflection [17] Thus, the current on the linear probe is approximated by

$$\bar{J}_p(\bar{R}') = \sum_{g=1}^{N_g} B_g \bar{j}_g(\bar{R}') \tag{4.14}$$

$$\bar{j}_g(\bar{R}') = \frac{1}{2}\left(1 + \sin\frac{g\pi}{2l_p}\left(y' + l_p\right)\right)\hat{y}$$

where $\bar{j}_g(\bar{R}')$ denotes the basis and weighting function. y' represents the source point.

Since the excitation of this model is the open-ended probe, the later one is chosen as the basis function of linear probe excitation and can be shown as Fig. 4.6.

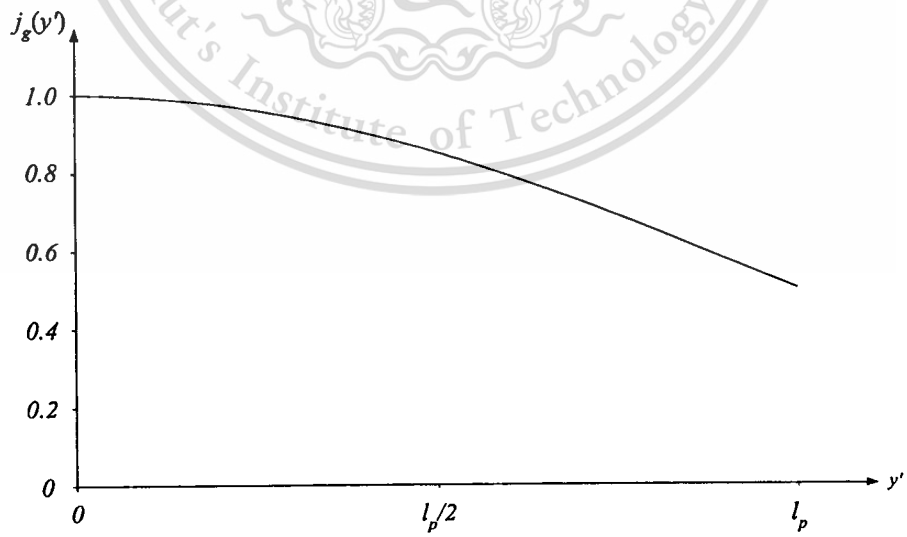

Fig. 4.6 Basis function of the linear electric probe

This material is reserved for educational use only, not allowed for commercial use.
Forbidden to modify the content, and cite the document when use.

4.2.2 Weighting Function

The selection of appropriate weighting function plays an important role to obtain the high accuracy result, ease of evaluation of matrix elements and analytically solution. There are many ways to choose the weighting function. However, the Galerkin's method can be responsible for these requirements. This procedure is to select the weighting function to be the same as the basis functions. Accordingly, the weighting function of the slot aperture is represented as

$$\overline{m}_{n_j}(\overline{R}) = \frac{1}{w_s}\sin\frac{n_j\pi}{l_s}\left(z+\frac{l_s}{2}\right)\hat{z} \quad ; n_j = 1,2,3,\ldots,N_j \tag{4.15}$$

and the weighting function of the linear electric probe is

$$\bar{j}_{n_q}(\overline{R}) = \frac{1}{2}\left(1+\sin\frac{n_q\pi}{2l_p}\left(y+l_p\right)\right)\hat{y} \quad ; n_q = 1,2,3,\ldots,N_q \tag{4.16}$$

where $\overline{m}_{n_j}(\overline{R}')$ and $\bar{j}_{n_q}(\overline{R})$ are weighting function. z and y is the field point on the slot and along the probe coordinate system, respectively.

4.3 System of Linear Equations

Substituting (4.12) and (4.15) into (2.5) and (4.13) and (4.16) into (2.11), the inner product with the integral over the field point of weighting function is taken as following

$$j\omega\varepsilon_0\sum_{i=1}^{N_i}A_i\iint_{S_a}\iint_{S_a}\overline{m}_{n_j}(\overline{R})\cdot\left\{\overline{\overline{G}}_{HM}^{ext}(\overline{R},\overline{R}')+\overline{\overline{G}}_{HM}^{int}(\overline{R},\overline{R}')\right\}\cdot\overline{m}_i(\overline{R}')dS'dS$$

$$-\sum_{g=1}^{N_g}B_g\iint_{S_f}\iint_{S_a}\overline{m}_{n_j}(\overline{R})\cdot\overline{\overline{G}}_{HJ}^{int}(\overline{R},\overline{R}')\cdot\bar{j}_g(\overline{R}')dS'dS = 0 \tag{4.17a}$$

and

This material is reserved for educational use only, not allowed for commercial use.
Forbidden to modify the content, and cite the document when use.

$$-\sum_{i=1}^{N_i} A_i \iint_{S_a}\iint_{S_f} \bar{j}_{n_q}(\bar{R})\cdot \bar{\bar{G}}_{EM}^{int}(\bar{R},\bar{R}')\cdot \bar{m}_i(\bar{R}')dS'dS$$

$$-j\omega\mu_0\sum_{g=1}^{N_g} B_g \iint_{S_f}\iint_{S_f} \bar{j}_{n_q}(\bar{R})\cdot \bar{\bar{G}}_{EJ}^{int}(\bar{R},\bar{R}')\cdot \bar{j}_g(\bar{R}')dS'dS = -\delta(\bar{R}') \qquad (4.17b)$$

By assuming the delta gap source function $\delta(\bar{R}')$ equals unity at the excitation point. (4.17a) and (4.17b), in case of y-direction probe, can be rewritten as

$$j\omega\varepsilon_0\sum_{i=1}^{N_i} A_i \int_{-\frac{l_s}{2}}^{\frac{l_s}{2}}\int_{-\frac{w_s}{2}}^{\frac{w_s}{2}}\int_{-\frac{l_s}{2}}^{\frac{l_s}{2}}\int_{-\frac{w_s}{2}}^{\frac{w_s}{2}} m_{n_j}(z)\left\{G_{HM,zz}^{ext}+G_{HM,zz}^{int}\right\}m_i(z')dx'dz'dxdz$$

$$-\sum_{g=1}^{N_g} B_g \int_{-\frac{l_s}{2}}^{\frac{l_s}{2}}\int_{-\frac{w_s}{2}}^{\frac{w_s}{2}}\int_{0}^{l_p} m_{n_j}(z)G_{HJ,zy}^{int}j_g(y')dy'dxdz = 0 \qquad (4.18a)$$

$$-\sum_{i=1}^{N_i} A_i \int_{0}^{l_p}\int_{-\frac{l_s}{2}}^{\frac{l_s}{2}}\int_{-\frac{w_s}{2}}^{\frac{w_s}{2}} j_{n_q}(y)G_{EM,yz}^{int}m_i(z')dx'dz'dy$$

$$-j\omega\mu_0\sum_{g=1}^{N_g} B_g \int_{0}^{l_p}\int_{0}^{l_p} j_{n_q}(y)G_{EJ,yy}^{int}j_g(y')dy'dy = -1 \qquad (4.18b)$$

where

$$G_{HM,zz}^{ext} = j\omega\varepsilon_0\left(1+\frac{1}{k^2}\frac{\partial^2}{\partial z^2}\right)\frac{e^{-jk\sqrt{(x-x')^2+(z-z')^2}}}{\sqrt{(x-x')^2+(z-z')^2}}$$

$$G_{HM,zz}^{int} = -\frac{1}{k^2}\delta(x-x',y-y',z-z')+\frac{2}{ab}\sum_{m=0}^{\infty}\sum_{n=0}^{\infty}\frac{(2-\delta_0)k_{c,zz}^2}{k^2\sin k_{g,zz}c}$$

$$\cdot C_x' C_y C_{x'} C_{y'}\begin{cases}\sin k_{g,zz}(c-z-z_o)\sin k_{g,zz}(z'+z_o), z>z'\\ \sin k_{g,zz}(z+z_o)\sin k_{g,zz}(c-z'-z_o), z<z'\end{cases}$$

This material is reserved for educational use only, not allowed for commercial use.
Forbidden to modify the content, and cite the document when use.

$$G_{EJ,yy}^{int} = -\frac{1}{k^2}\delta(x-x',y-y',z-z') - \frac{2}{ac}\sum_{m=0}^{\infty}\sum_{n=0}^{\infty}\frac{(2-\delta_0)k_{c,yy}^2}{k^2\sin k_{g,yy}b}$$

$$\cdot S_x S_z S_{x'} S_{z'} \begin{Bmatrix} \cos k_{g,yy}(b-y)\cos k_{g,yy}y', y > y' \\ \cos k_{g,yy}y\cos k_{g,yy}(b-y'), y < y' \end{Bmatrix}$$

$$G_{HJ,zy}^{int} = -\frac{2\pi}{a^2 c}\sum_{m=0}^{\infty}\sum_{n=0}^{\infty}\frac{(2-\delta_0)m}{k_{g,zy}\sin k_{g,zy}b} C_x' S_z' S_{x'} S_{z'} \left\{\cos k_{g,zy}(b-y)\cos k_{g,zy}y', y > y'\right\}$$

$$G_{EM,yz}^{int} = -\frac{2\pi}{a^2 c}\sum_{m=0}^{\infty}\sum_{n=0}^{\infty}\frac{(2-\delta_0)m}{k_{g,yz}\sin k_{g,yz}b} S_x S_z C_{x'}' S_{z'}' \left\{\cos k_{g,yz}y\cos k_{g,yz}(b-y'), y < y'\right\}$$

$$k_{c,yy}^2 = k_{c,zy}^2 = k_{c,yz}^2 = \left(\frac{m\pi}{a}\right)^2 + \left(\frac{n\pi}{c}\right)^2,\ k_{c,zz}^2 = \left(\frac{m\pi}{a}\right)^2 + \left(\frac{n\pi}{b}\right)^2,$$

$$k_{g,zz}^2 = k^2 - k_{c,zz}^2,\ k_{g,yy}^2 = k_{g,yz}^2 = k_{g,zy}^2 = k^2 - k_{c,yy}^2,$$

$$C_y = \cos\left(\frac{n\pi}{b}y\right),\ S_z = \sin\left(\frac{n\pi}{c}z\right),\ C_x = \cos\left(\frac{m\pi}{a}x\right),\ S_x = \sin\left(\frac{m\pi}{a}x\right),$$

$$S_x' = \sin\left(\frac{m\pi}{a}(x+x_o)\right),\ C_x' = \cos\left(\frac{m\pi}{a}(x+x_o)\right) \text{ and } S_z' = \sin\left(\frac{n\pi}{c}(z+z_o)\right)$$

and in case of x-direction probe, they are expressed as

$$j\omega\varepsilon_0\sum_{i=1}^{N_i}A_i\int_{-\frac{l_s}{2}}^{\frac{l_s}{2}}\int_{-\frac{w_s}{2}}^{\frac{w_s}{2}}\int_{-\frac{l_s}{2}}^{\frac{l_s}{2}}\int_{-\frac{w_s}{2}}^{\frac{w_s}{2}} m_{n_j}(z)\left\{G_{HM,zz}^{ext} + G_{HM,zz}^{int}\right\}m_i(z')dx'dz'dxdz$$

$$-\sum_{g=1}^{N_g}B_g\int_{-\frac{l_s}{2}}^{\frac{l_s}{2}}\int_{-\frac{w_s}{2}}^{\frac{w_s}{2}}\int_{0}^{l_p} m_{n_j}(z)G_{HJ,zx}^{int}j_g(x')dx'dxdz = 0 \qquad (4.19a)$$

$$-\sum_{i=1}^{N_i}A_i\int_{0}^{l_p}\int_{-\frac{l_s}{2}}^{\frac{l_s}{2}}\int_{-\frac{w_s}{2}}^{\frac{w_s}{2}} j_{n_q}(x)G_{EM,yz}^{int}m_i(z')dx'dz'dx$$

$$-j\omega\mu_0\sum_{g=1}^{N_g}B_g\int_{0}^{l_p}\int_{0}^{l_p} j_{n_q}(x)G_{EJ,xx}^{int}j_g(x')dx'dx = -1 \qquad (4.19b)$$

This material is reserved for educational use only, not allowed for commercial use.
Forbidden to modify the content, and cite the document when use.

where

$$G_{EJ,xx}^{int} = -\frac{1}{k^2}\delta(x-x',y-y',z-z') - \frac{2}{bc}\sum_{m=0}^{\infty}\sum_{n=0}^{\infty}\frac{(2-\delta_0)k_{c,xx}^2}{k^2\sin k_{g,xx}a}$$

$$\cdot S_z''S_yS_{z'}'S_{y'}\begin{Bmatrix}\cos k_{g,xx}(a-x-x_o)\cos k_{g,xx}x', x>x' \\ \cos k_{g,xx}(x+x_o)\cos k_{g,xx}(a-x'), x<x'\end{Bmatrix}$$

$$G_{HJ,zx}^{int} = -\frac{2k}{ac}\sum_{m=0}^{\infty}\sum_{n=0}^{\infty}\frac{(2-\delta_0)}{\sin k_{g,zx}b}C_x'S_z'C_xS_{z'}\left\{\cos k_{g,zx}(b-y)\sin k_{g,zx}y', y>y'\right\}$$

$$G_{EM,xz}^{int} = -\frac{2k}{ac}\sum_{m=0}^{\infty}\sum_{n=0}^{\infty}\frac{(2-\delta_0)}{\sin k_{g,xz}b}C_xS_zC_{x'}S_{z'}\left\{\sin k_{g,xz}y\cos k_{g,xz}(b-y'), y<y'\right.$$

$$k_{c,xx}^2 = \left(\frac{m\pi}{c}\right)^2 + \left(\frac{n\pi}{b}\right)^2,\ k_{c,xz}^2 = k_{c,zx}^2 = \left(\frac{m\pi}{a}\right)^2 + \left(\frac{n\pi}{c}\right)^2,\ k_{g,xx}^2 = k^2 - k_{c,xx}^2,$$

$$k_{g,xz}^2 = k_{g,zx}^2 = k^2 - k_{c,xz}^2,\ S_z'' = \sin\left(\frac{m\pi}{c}(z+z_o)\right)\ S_{z'}' = \sin\left(\frac{m\pi}{c}z'\right) \text{ and } S_y = \sin\left(\frac{n\pi}{b}y\right).$$

These systems of linear equations can be written in view of reaction as

$$\sum_{i=1}^{N_I} A_i\left[Y_{n_ji}^{in} + Y_{n_ji}^{ext}\right] - \sum_{g=1}^{N_g} B_g\alpha_{n_jg}^{in} = 0 \qquad (4.20a)$$

$$\sum_{i=1}^{N_I} A_i\beta_{n_qi}^{in} + \sum_{g=1}^{N_g} B_gZ_{n_qg}^{in} = -1. \qquad (4.20b)$$

They can be expressed in terms of matrix form as

This material is reserved for educational use only, not allowed for commercial use.
Forbidden to modify the content, and cite the document when use.

$$
\begin{bmatrix}
\left\langle \overline{m}_1 \middle| \left\{ \overline{\overline{G}}^{ext}_{HM}(\overline{R},\overline{R}') + \overline{\overline{G}}^{int}_{HM}(\overline{R},\overline{R}') \right\} \middle| \overline{m}_1 \right\rangle & \cdots & \left\langle \overline{m}_1 \middle| \left\{ \overline{\overline{G}}^{ext}_{HM}(\overline{R},\overline{R}') + \overline{\overline{G}}^{int}_{HM}(\overline{R},\overline{R}') \right\} \middle| \overline{m}_i \right\rangle \\
\vdots & & \vdots \\
\left\langle \overline{m}_{n_j} \middle| \left\{ \overline{\overline{G}}^{ext}_{HM}(\overline{R},\overline{R}') + \overline{\overline{G}}^{int}_{HM}(\overline{R},\overline{R}') \right\} \middle| \overline{m}_1 \right\rangle & \cdots & \left\langle \overline{m}_{n_j} \middle| \left\{ \overline{\overline{G}}^{ext}_{HM}(\overline{R},\overline{R}') + \overline{\overline{G}}^{int}_{HM}(\overline{R},\overline{R}') \right\} \middle| \overline{m}_i \right\rangle \\
-\left\langle \overline{j}_1 \middle| \overline{\overline{G}}^{int}_{EM}(\overline{R},\overline{R}') \middle| \overline{m}_1 \right\rangle & \cdots & -\left\langle \overline{j}_1 \middle| \overline{\overline{G}}^{int}_{EM}(\overline{R},\overline{R}') \middle| \overline{m}_i \right\rangle \\
\vdots & & \vdots \\
-\left\langle \overline{j}_{n_q} \middle| \overline{\overline{G}}^{int}_{EM}(\overline{R},\overline{R}') \middle| \overline{m}_1 \right\rangle & \cdots & -\left\langle \overline{j}_{n_q} \middle| \overline{\overline{G}}^{int}_{EM}(\overline{R},\overline{R}') \middle| \overline{m}_i \right\rangle
\end{bmatrix}
$$

$$
\begin{bmatrix}
-\left\langle \overline{m}_1 \middle| \overline{\overline{G}}^{int}_{HJ}(\overline{R},\overline{R}') \middle| \overline{j}_1 \right\rangle & \cdots & -\left\langle \overline{m}_1 \middle| \overline{\overline{G}}^{int}_{HJ}(\overline{R},\overline{R}') \middle| \overline{j}_g \right\rangle \\
\vdots & & \vdots \\
-\left\langle \overline{m}_{n_j} \middle| \overline{\overline{G}}^{int}_{HJ}(\overline{R},\overline{R}') \middle| \overline{j}_1 \right\rangle & \cdots & -\left\langle \overline{m}_{n_j} \middle| \overline{\overline{G}}^{int}_{HJ}(\overline{R},\overline{R}') \middle| \overline{j}_g \right\rangle \\
-\left\langle \overline{j}_1 \middle| \overline{\overline{G}}^{int}_{EJ}(\overline{R},\overline{R}') \middle| \overline{j}_1 \right\rangle & \cdots & -\left\langle \overline{j}_1 \middle| \overline{\overline{G}}^{int}_{EJ}(\overline{R},\overline{R}') \middle| \overline{j}_g \right\rangle \\
\vdots & & \vdots \\
-\left\langle \overline{j}_{n_q} \middle| \overline{\overline{G}}^{int}_{EJ}(\overline{R},\overline{R}') \middle| \overline{j}_1 \right\rangle & \cdots & -\left\langle \overline{j}_{n_q} \middle| \overline{\overline{G}}^{int}_{EJ}(\overline{R},\overline{R}') \middle| \overline{j}_g \right\rangle
\end{bmatrix}
\cdot
\begin{bmatrix} A_1 \\ \vdots \\ A_i \\ B_1 \\ \vdots \\ B_g \end{bmatrix}
=
\begin{bmatrix} 0 \\ \vdots \\ 0 \\ -1 \\ \vdots \\ -1 \end{bmatrix}
\tag{4.21}
$$

Using inverse matrix, the unknown coefficients can be solved

$$[X]\cdot[Y]=[Z] \tag{4.22a}$$

$$[Y]=[X]^{-1}\cdot[Z] \tag{4.22b}$$

Then the unknown coefficients, A_i and B_g, can be calculated by means of Gauss elimination [32] or other methods. In view of numerical integration, the Romberg Integration is used [33]. Finally, the desired characteristics will be analyzed.

This material is reserved for educational use only, not allowed for commercial use.
Forbidden to modify the content, and cite the document when use.

4.4 Conclusions

In this chapter, Methods of Moments is applied to solve the integral equations in which it was derived in the previous chapter. The choice of the basis function that is the most important in determining the unknown functions is considered. Subsequently, the entire domain sinusoidal basis function as well as the Galerkin method is utilized to achieve the compromise between more simple and high accuracy. The numerical results are demonstrated in the subsequent chapter, Chapter 5 and Chapter 6.

This material is reserved for educational use only, not allowed for commercial use.
Forbidden to modify the content, and cite the document when use.

CHAPTER 5
CURRENT DISTRIBUTION AND RADIATION CHARACTERISTICS OF THE ANTENNA

The unknown coefficients of electric current on the linear electric probe and magnetic current on the slot aperture are calculated and discussed in this chapter. These currents are employed to investigate radiation pattern and directivity, subsequently. In this investigation, the ideal case in which the slot is on an infinite ground plane is firstly derived. Then the practical situation which the finite size ground plane is considered by using the uniform theory of diffraction (UTD). Numerical results of these cases are illustrated and compared with the experimental ones.

5.1 Electric Current Distribution along the Linear Electric Probe

From solutions of a system of integral equations, the numerical result of unknown electric current on the probe and magnetic current sheet over the slots are carried out. The electric current distribution on the probe is shown in Fig.5.1

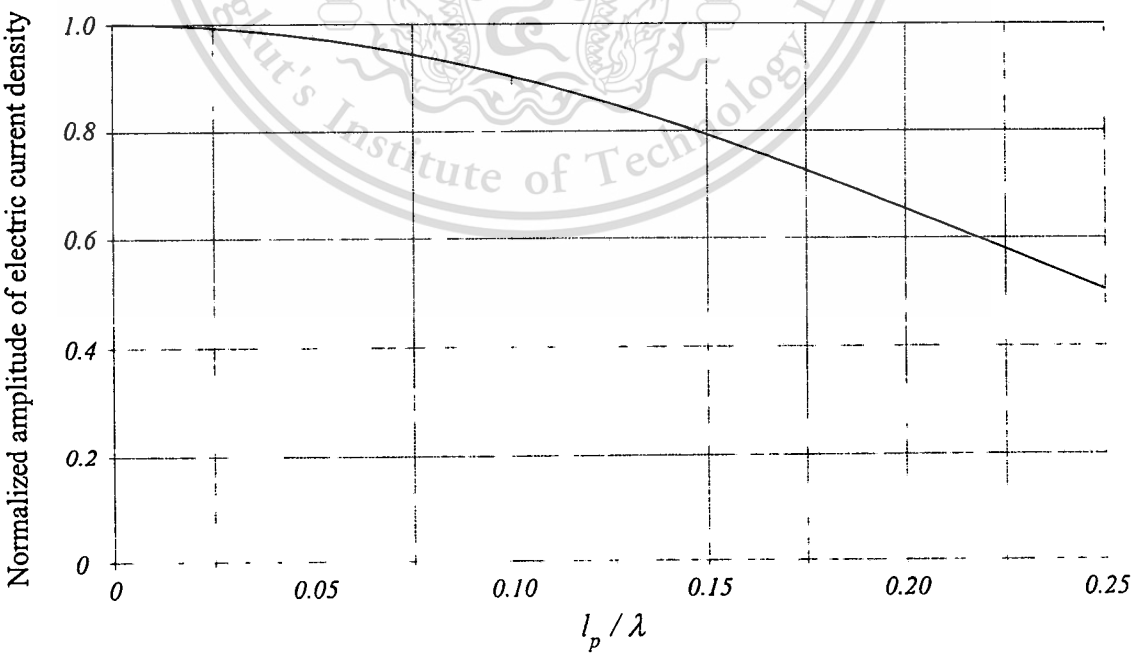

Fig. 5.1 Electric current distribution on the linear probe

This material is reserved for educational use only, not allowed for commercial use.
Forbidden to modify the content, and cite the document when use.

It is obvious that the peak of the electric current on the probe occurred at the feed point as expected.

5.2 Magnetic Current Sheet on the Slot

The magnetic current sheet over the slot aperture is shown in Fig.5.2

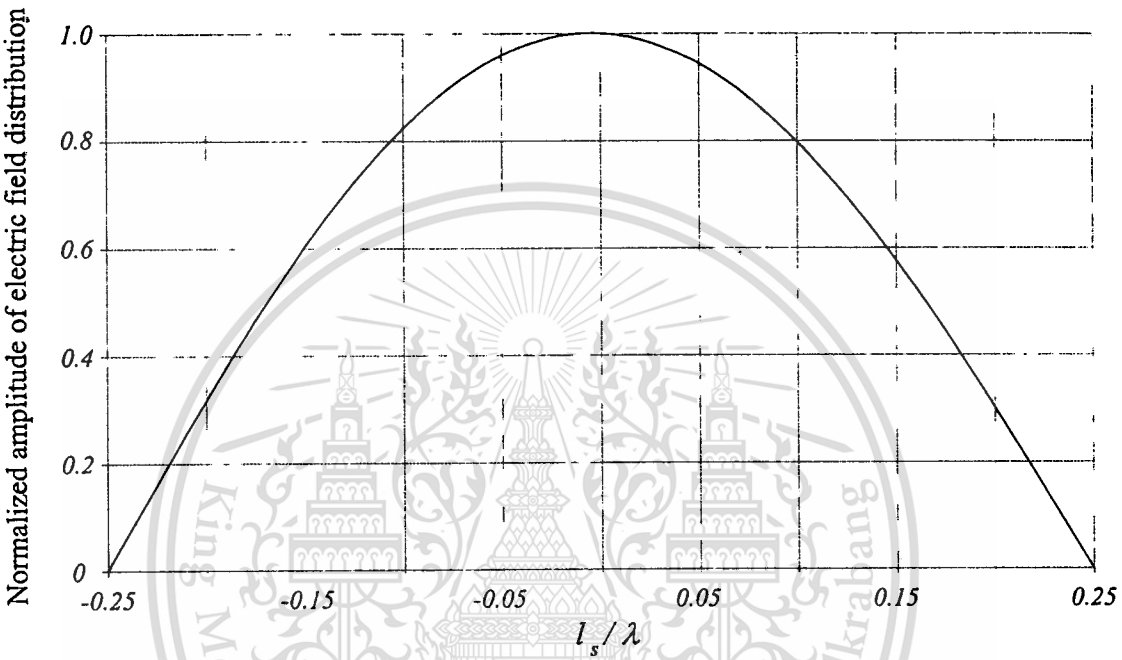

Fig. 5.2 Magnetic current on the slot

Apparently, the maximum magnetic current of the slot is at the center and decreased as the sinusoidal distribution until became zero at the ends of the slot.

5.3 Radiation Pattern of a Rectangular Cavity-Backed Slot Antenna Fed by a Linear Electric Probe

5.3.1 Radiation Pattern of Slot on Infinite Ground Plane

Physically, there are three regions surrounding the antenna, i.e.; near field region, intermediate field region (Fresnel region) and far field region (Fraunhofer region). The last-two regions are characterized by the type of approximations. Since the far-field region is used to describe the radiation pattern of antenna, it is considered in this thesis. The far-field region is formed under the conditions that the distance of the field

This material is reserved for educational use only, not allowed for commercial use.
Forbidden to modify the content, and cite the document when use.

point (r) is much greater than the maximum value of the distance of source point (r') and also substantially more than the free-space wavelength λ_0, that is

$$kr >> 1$$

In this subsection, two directions of slot on infinite ground plane are considered. They are in y-direction and z-direction as shown in Figs. 5.3(a) and (b), respectively.

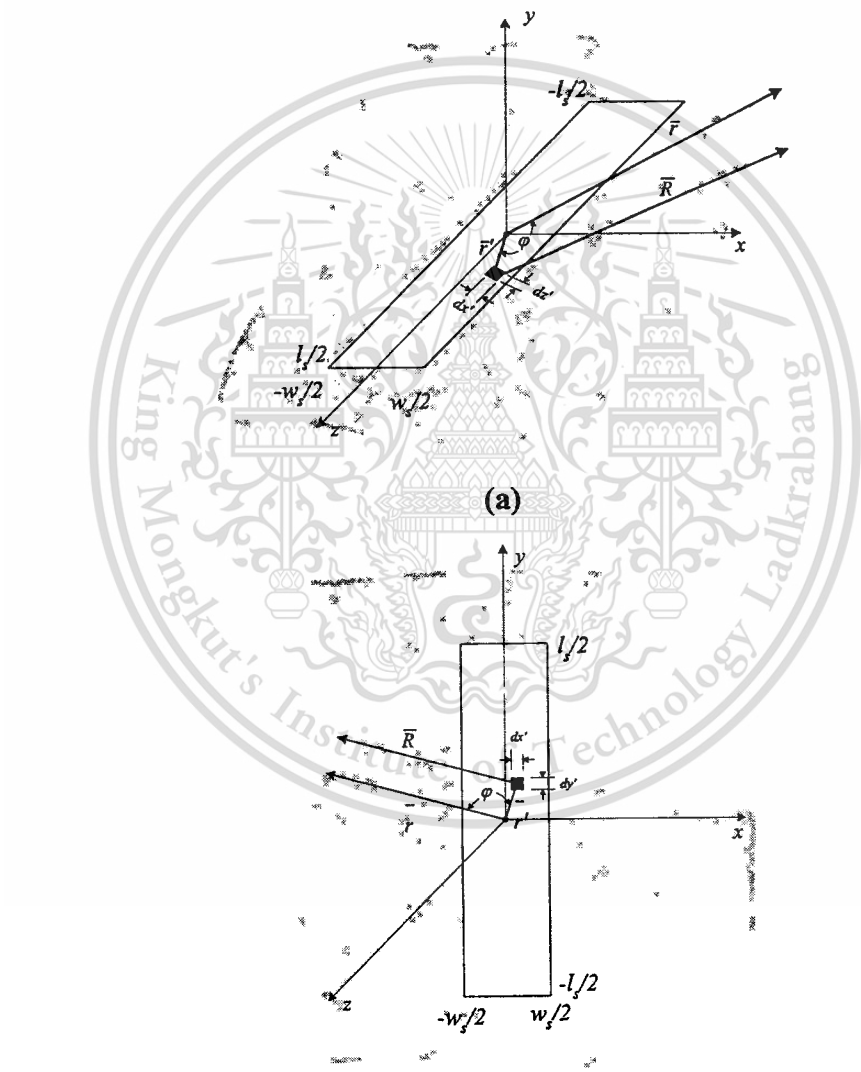

Fig. 5.3 Slot on infinite ground plane

(a) in z-direction

(b) in y-direction

This material is reserved for educational use only, not allowed for commercial use.
Forbidden to modify the content, and cite the document when use.

From the slot on a ground plane as Figs.5.3 (a) and (b), the far-field observation R can most commonly be approximated by

$$R \approx r - r' \cos\varphi \qquad \text{for phase variations} \tag{5.1a}$$

and

$$R \approx r \qquad \text{for amplitude variations} \tag{5.1b}$$

Generally, the various kind of vector potentials can be expressed in terms of far-field condition as

$$\overline{A} \approx \frac{\mu_o}{4\pi} \iint_s \overline{J}_s \frac{e^{-jk(r-r'\cos\varphi)}}{r} dS' \tag{5.2a}$$

and

$$\overline{F} \approx \frac{\varepsilon_o}{4\pi} \iint_s \overline{M}_s \frac{e^{-jk(r-r'\cos\varphi)}}{r} dS' \tag{5.2b}$$

Referring to chapter 2, only the magnetic current are induced and there is not any electric current on the slot aperture. Therefore, the vector potential $\overline{F}$ can be given as

$$\overline{F} \approx \frac{\varepsilon_o}{4\pi r} e^{-jkr} \overline{L} \tag{5.3a}$$

where

$$\overline{L} = \iint_s \overline{M} e^{jkr'\cos\psi} dS' \tag{5.3b}$$

In far-field region, only the θ and ϕ components of the electric field and magnetic field are dominant. Although the radial components (r) are not necessarily zero, they

This material is reserved for educational use only, not allowed for commercial use.
Forbidden to modify the content, and cite the document when use.

are negligible compared to the θ and ϕ components. Accordingly, the electric and magnetic fields in θ and ϕ components are written in form of vector potential ($\overline{F}$) as

$$E_r \approx 0 \tag{5.4a}$$

$$E_\theta \approx \frac{-jke^{-jkr}}{4\pi r} L_\phi \tag{5.4b}$$

$$E_\phi \approx \frac{jke^{-jkr}}{4\pi r} L_\theta \tag{5.4c}$$

$$H_\theta \approx \frac{-jke^{-jkr}}{4\pi r\eta} L_\theta \tag{5.4d}$$

$$H_\phi \approx \frac{-jke^{-jkr}}{4\pi r\eta} L_\phi \tag{5.4e}$$

From (5.3b), the magnetic current can be expanded and written in spherical coordinate as

$$\overline{L} = \iint_s (M_x \hat{x} + M_y \hat{y} + M_z \hat{z}) e^{jkr' \cos\varphi} dS' \tag{5.5}$$

$$\overline{L} = \iint_s (L_\theta + L_\phi) e^{jkr' \cos\varphi} dS' \tag{5.6}$$

where

$$L_\theta = M_x \cos\theta \cos\phi + M_y \cos\theta \sin\phi - M_z \sin\theta$$

$$L_\phi = -M_x \sin\phi + M_y \cos\phi$$

According to Fig. 5.3(a), the phase term $r'\cos\varphi$ in (5.1a) can be expressed in rectangular terms of source variables as

This material is reserved for educational use only, not allowed for commercial use.
Forbidden to modify the content, and cite the document when use.

$$r'\cos\varphi = r'\cdot\hat{r} = (x'\hat{x} + z'\hat{z})(\sin\theta\cos\phi\hat{x} + \sin\theta\sin\phi\hat{y} + \cos\theta\hat{z})$$

$$= x'\sin\theta\cos\phi + z'\cos\theta \tag{5.7}$$

By inserting $r'\cos\varphi$ into L_θ and L_ϕ, these equations are given as

$$L_\theta = \iint_s \left[M_x\cos\theta\cos\phi + M_y\cos\theta\sin\phi - M_z\sin\theta\right] e^{jk(x'\sin\theta\cos\phi + z'\cos\theta)}\,dS' \tag{5.8a}$$

$$L_\phi = \iint_s \left[-M_x\sin\phi + M_y\cos\phi\right] e^{jk(x'\sin\theta\cos\phi + z'\cos\theta)}\,dS' \tag{5.8b}$$

In fact, only the z component appears in the magnetic current term. Hence, L_θ and L_ϕ can be rewritten as

$$L_\theta = \iint_s \left[-M_z\sin\theta\right] e^{jk(x'\sin\theta\cos\phi + z'\cos\theta)}\,dS' \tag{5.9a}$$

$$L_\phi = 0 \tag{5.9b}$$

Substituting the magnetic current function from (4.12) chapter 4 into (5.9a) and using the image theory, it yields

$$L_\theta = \frac{-2}{w_s}\sum_{i=1}^{N_i} A_i \int_{-\frac{l_s}{2}}^{\frac{l_s}{2}}\int_{-\frac{w_s}{2}}^{\frac{w_s}{2}} \sin\frac{i\pi}{l_s}(z' + \frac{l_s}{2})\sin\theta e^{jk(x'\sin\theta\cos\phi + z'\cos\theta)}\,dx'dz' \tag{5.10}$$

Then, using exponential relations from (A.28)

$$\sin\alpha = \frac{e^{j\alpha} - e^{-j\alpha}}{2j}$$

and the integral

This material is reserved for educational use only, not allowed for commercial use.
Forbidden to modify the content, and cite the document when use.

$$\int_{-\frac{c}{2}}^{\frac{c}{2}} e^{j\alpha z} dz = c\left[\frac{\sin(\frac{\alpha}{2}c)}{\frac{\alpha}{2}c}\right]$$

L_{θ_i} can be integrated as

$$L_\theta = l_s \sin\theta \sum_{i=1}^{N_i} A_i \left\{ j\cos\frac{i\pi}{2}\left[\frac{\sin\left(\frac{kl_s}{2}\cos\theta+\frac{i\pi}{2}\right)}{\frac{kl}{2}\cos\theta+\frac{i\pi}{2}} - \frac{\sin\left(\frac{kl_s}{2}\cos\theta-\frac{i\pi}{2}\right)}{\frac{kl}{2}\cos\theta-\frac{i\pi}{2}}\right]\right.$$

$$\left. -\sin\frac{i\pi}{2}\left[\frac{\sin\left(\frac{kl_s}{2}\cos\theta+\frac{i\pi}{2}\right)}{\frac{kl_s}{2}\cos\theta+\frac{i\pi}{2}} - \frac{\sin\left(\frac{kl_s}{2}\cos\theta-\frac{i\pi}{2}\right)}{\frac{kl_s}{2}\cos\theta-\frac{i\pi}{2}}\right]\right\} \frac{\sin\left(\frac{kw_s}{2}\sin\theta\cos\phi\right)}{\frac{kw_s}{2}\sin\theta\cos\phi} \tag{5.11}$$

Substituting (5.9a) and (5.9b) into (5.4a), (5.4b), (5.4c), (5.4d) and (5.4e), the fields radiated by the z-direction slot on infinite ground plane can be written as

$$E_r = 0 \tag{5.12a}$$

$$E_\theta = 0 \tag{5.12b}$$

$$E_\phi = \frac{jkl_s}{4\pi}\sum_{i=1}^{N_i} A_i \sin\theta \left\{ j\cos\frac{i\pi}{2}\left[\frac{\sin\left(\frac{kl_s}{2}\cos\theta+\frac{i\pi}{2}\right)}{\frac{kl_s}{2}\cos\theta+\frac{i\pi}{2}} - \frac{\sin\left(\frac{kl_s}{2}\cos\theta-\frac{i\pi}{2}\right)}{\frac{kl_s}{2}\cos\theta-\frac{i\pi}{2}}\right]\right.$$

$$\left. -\sin\frac{\pi}{2}\left[\frac{\sin\left(\frac{kl_s}{2}\cos\theta+\frac{i\pi}{2}\right)}{\frac{kl_s}{2}\cos\theta+\frac{i\pi}{2}} + \frac{\sin\left(\frac{kl_s}{2}\cos\theta-\frac{i\pi}{2}\right)}{\frac{kl_s}{2}\cos\theta-\frac{i\pi}{2}}\right]\right\} \frac{\sin\left(\frac{kw_s}{2}\sin\theta\cos\phi\right)}{\frac{kw_s}{2}\sin\theta\cos\phi} \tag{5.12c}$$

This material is reserved for educational use only, not allowed for commercial use.
Forbidden to modify the content, and cite the document when use.

$$H_r = 0 \tag{5.12d}$$

$$H_\theta = \frac{-E_\phi}{\eta} \tag{5.12e}$$

$$H_\phi = 0 \tag{5.12f}$$

Alternatively, the y-direction slot on infinite ground plane can be shown as Fig. 5.3 (b). The magnetic current in the same orientation of slot is given as

$$\overline{M} = M_y \hat{y} \tag{5.13a}$$

$$M_y = \sum_{i=1}^{N_i} A_i \frac{1}{w_s} \sin\frac{i\pi}{l_s}\left(y' + \frac{l_s}{2}\right) \tag{5.13b}$$

From (5.8a) and (5.8b), L_θ and L_ϕ are

$$L_\theta = \iint_s M_y \cos\theta \sin\phi e^{jkr'\cos\varphi} dS' \tag{5.14a}$$

$$L_\phi = \iint_s M_y \cos\phi e^{jkr'\cos\varphi} dS' \tag{5.14b}$$

where

$$r'\cos\varphi = r'\hat{r} = (x'\hat{x} + y'\hat{y}) \cdot (\sin\theta\cos\phi\hat{x} + \sin\theta\sin\phi\hat{y} + \cos\theta\hat{z})$$
$$= x'\sin\theta\cos\phi + y'\sin\theta\sin\phi$$

Similarly in z-direction slot, L_θ and L_ϕ can be derived as

This material is reserved for educational use only, not allowed for commercial use.
Forbidden to modify the content, and cite the document when use.

$$L_\theta = jl_s \cos\theta \sin\phi \sum_{i=1}^{N_l} A_i \left\{ \frac{\sin\left(\frac{kl_s}{2}\sin\theta\sin\phi + \frac{i\pi}{2}\right)}{\frac{kl_s}{2}\sin\theta\sin\phi + \frac{i\pi}{2}} e^{j\frac{i\pi}{2}} \right.$$

$$\left. - \frac{\sin\left(\frac{kl_s}{2}\sin\theta\sin\phi - \frac{i\pi}{2}\right)}{\frac{kl_s}{2}\sin\theta\sin\phi - \frac{i\pi}{2}} e^{-j\frac{i\pi}{2}} \right\} \frac{\sin\left(\frac{kw_s}{2}\sin\theta\cos\phi\right)}{\frac{kw_s}{2}\sin\theta\cos\phi} \tag{5.15a}$$

$$L_\phi = jl_s \cos\phi \sum_{i=1}^{N_l} A_i \left\{ \frac{\sin\left(\frac{kl_s}{2}\sin\theta\sin\phi + \frac{i\pi}{2}\right)}{\frac{kl_s}{2}\sin\theta\sin\phi + \frac{i\pi}{2}} e^{j\frac{i\pi}{2}} \right.$$

$$\left. - \frac{\sin\left(\frac{kl_s}{2}\sin\theta\sin\phi - \frac{i\pi}{2}\right)}{\frac{kl_s}{2}\sin\theta\sin\phi - \frac{i\pi}{2}} e^{-j\frac{i\pi}{2}} \right\} \frac{\sin\left(\frac{kw_s}{2}\sin\theta\cos\phi\right)}{\frac{kw_s}{2}\sin\theta\cos\phi} \tag{5.15b}$$

Finally, the radiated fields can be expressed as

$$E_r = 0 \tag{5.16a}$$

$$E_\theta = \frac{kl_s}{4\pi r} e^{-jkr} \sum_{i=1}^{N_l} A_i \cos\phi \left\{ \frac{\sin\left(\frac{kl_s}{2}\sin\theta\sin\phi + \frac{i\pi}{2}\right)}{\frac{kl_s}{2}\sin\theta\sin\phi + \frac{i\pi}{2}} e^{j\frac{i\pi}{2}} \right.$$

$$\left. - \frac{\sin\left(\frac{kl_s}{2}\sin\theta\sin\phi - \frac{i\pi}{2}\right)}{\frac{kl_s}{2}\sin\theta\sin\phi - \frac{i\pi}{2}} e^{-j\frac{i\pi}{2}} \right\} \frac{\sin\left(\frac{kw_s}{2}\sin\theta\cos\phi\right)}{\frac{kw_s}{2}\sin\theta\cos\phi} \tag{5.16b}$$

This material is reserved for educational use only, not allowed for commercial use.
Forbidden to modify the content, and cite the document when use.

$$E_\phi = \frac{-kl_s}{4\pi r} e^{-jkr} \sum_{i=1}^{N_1} A_i \cos\theta \sin\phi \left\{ \frac{\sin\left(\frac{kl_s}{2}\sin\theta\sin\phi + \frac{i\pi}{2}\right)}{\frac{kl_s}{2}\sin\theta\sin\phi + \frac{i\pi}{2}} e^{j\frac{i\pi}{2}} \right.$$

$$\left. - \frac{\sin\left(\frac{kl_s}{2}\sin\theta\sin\phi - \frac{i\pi}{2}\right)}{\frac{kl_s}{2}\sin\theta\sin\phi - \frac{i\pi}{2}} e^{-j\frac{i\pi}{2}} \right\} \frac{\sin\left(\frac{kw_s}{2}\sin\theta\cos\phi\right)}{\frac{kw_s}{2}\sin\theta\cos\phi} \tag{5.16c}$$

$$H_r = 0 \tag{5.16d}$$

$$H_\theta = \frac{-E_\phi}{\eta} \tag{5.16e}$$

$$H_\phi = \frac{E_\theta}{\eta} \tag{5.16f}$$

In practical case, the number of basis is sufficient to be unity. Therefore, in case of infinite ground plane and under the far-field condition, the fields are given in two forms:

In *y*-direction

$$E_\theta = -\cos\phi \frac{\cos\left(\frac{kl_s}{2}\sin\theta\sin\phi\right)}{\left(\frac{kl_s}{2}\sin\theta\sin\phi\right)^2 - \left(\frac{\pi}{2}\right)^2} \frac{\sin\left(\frac{kw_s}{2}\sin\theta\cos\phi\right)}{\frac{kw_s}{2}\sin\theta\cos\phi} \frac{e^{-jkr}}{r} \tag{5.17a}$$

$$E_\phi = -\cos\theta\sin\phi \frac{\cos\left(\frac{kl_s}{2}\sin\theta\sin\phi\right)}{\left(\frac{kl_s}{2}\sin\theta\sin\phi\right)^2 - \left(\frac{\pi}{2}\right)^2} \frac{\sin\left(\frac{kw_s}{2}\sin\theta\cos\phi\right)}{\frac{kw_s}{2}\sin\theta\cos\phi} \frac{e^{-jkr}}{r} \tag{5.17b}$$

In *z*-direction

$$E_\phi = \sin\theta \frac{\cos\left(\frac{kl_s}{2}\cos\theta\right)}{\left(\frac{kl_s}{2}\cos\theta\right)^2 - \left(\frac{\pi}{2}\right)^2} \frac{\sin\left(\frac{kw_s}{2}\sin\theta\cos\phi\right)}{\frac{kw_s}{2}\sin\theta\cos\phi} \frac{e^{-jkr}}{r} \tag{5.18}$$

This material is reserved for educational use only, not allowed for commercial use.
Forbidden to modify the content, and cite the document when use.

5.3.2 Uniform Theory of Diffraction

In 1844, the classical geometrical optics was first introduced for solving high-frequency electromagnetic problems but it is confined because there is no mention of the concept of phase, polarization and diffraction [34]. It deals solely with geometrical curves. After light had been shown to be an electromagnetic wave governed by Maxwell's equations, the diffraction scheme was studied continuously by Lord Rayleigh, Lord Kelvin, Sir George Stokes, Kirchoff, Helmholtz, Mei, Sommerfeld and many other famous physicists. Then to be able to account for phase, polarization and to obtain quantitative results for the field amplitudes, the classical geometrical optics has been extended to the modern geometrical optics (GO). It is the oldest and most widely used theory of light propagation. This method is an approximate high-frequency method for determining wave propagation for incident reflected and refracted fields. The shortcoming of GO is that it fails to predict fields in the shadow regions, caused by diffraction was from the edges [35]. To handle this defect the geometrical theory of diffraction was developed by Keller in 1950s [36]-[37] as an extension to GO. However, the Geometrical Theory of Diffraction (GTD) still has some serious drawbacks namely, it can foretell the diffracted fields in regions away from the shadow boundaries but become singular in the transition regions surroundings such boundaries in Fig.5.4. In 1974, Kouyomajian and Pathak [38] presented the uniform theory of diffraction (UTD). They had performed an asymptotic analysis [39]. Even so, the UTD still suffers from some of shortcoming like GTD but they can be compensated. For instance, equivalent current can be used to calculate fields at caustics, slope diffraction is used in cased where the incident field has a rapid spatial variation and higher-order diffraction term is included to solve a discontinuity across a shadow boundary [40].

In this chapter the uniform theory of diffraction is introduced to compensate the shortcomings of GO. By aiding of Fresnel integrals and the asymptotic analysis, the edge diffraction is treated.

This material is reserved for educational use only, not allowed for commercial use.
Forbidden to modify the content, and cite the document when use.

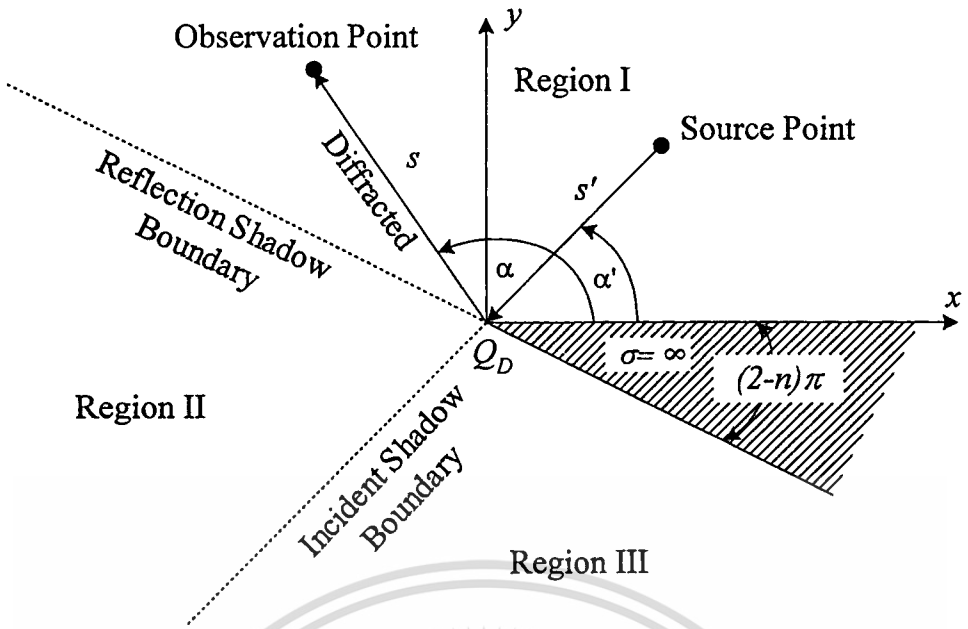

Fig.5.4 Region separation of two dimensional conducting wedge

5.3.2 Straight Edge Diffraction

When the edge is straight, the source is located at distance s' from the point of diffraction and the observations are at distance s far from it, as shown in Fig.5.5.

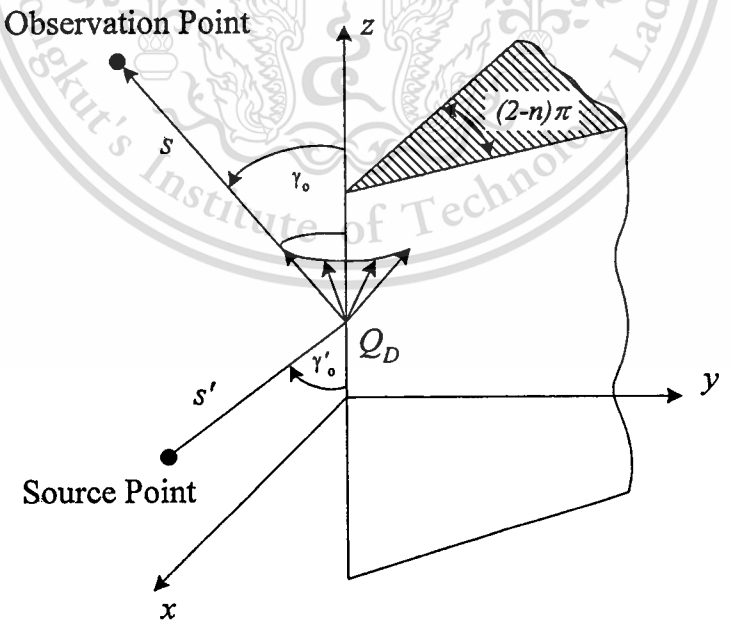

Fig.5.5 Three dimensions of diffracted ray

This material is reserved for educational use only, not allowed for commercial use.
Forbidden to modify the content, and cite the document when use.

Following the analogy of GO reflected rays, the diffracted field can be written as [38]

$$\overline{E}^d(s) = \overline{E}^j(Q_D) \cdot \overline{D} A(s',s) e^{-jks} \tag{5.19}$$

where $\overline{E}^j(Q_D)$ is the field incident on the point of diffraction (Q_D) on an edge, $\overline{D}$ is a dyadic diffraction coefficient, $A(s',s)$ is a spreading factor;

$$A(s',s) = \begin{cases} \dfrac{1}{\sqrt{s}} & \text{for plane and conical wave incidence} \\ \dfrac{1}{\sqrt{s \sin\beta_0}} & \text{for cylindrical wave incidences} \\ \sqrt{\dfrac{s'}{s(s+s')}} & \text{for spherical wave incidences} \end{cases} \tag{5.20}$$

As GTD solution, if the field point is not close to the shadow or reflection boundary, the scalar diffraction coefficient can be expressed as [39]

$$D_{s,h}(\alpha,\alpha';\beta_0) = \frac{e^{-j\frac{\pi}{4}} \sin\frac{\pi}{n}}{n\sqrt{2\pi k}\sin\beta_0} \left[\frac{1}{\cos\frac{\pi}{n} - \cos\left(\frac{\alpha-\alpha'}{n}\right)} \mp \frac{1}{\cos\frac{\pi}{n} - \cos\left(\frac{\alpha+\alpha'}{n}\right)} \right] \tag{5.21}$$

where D_s is referred to as the soft (Dirichlet) scalar diffraction coefficient and D_h is the hard (Neumann) scalar diffraction coefficient. α' and α are the angles of the incident and diffracted rays, respectively, as indicated in Fig.5.4. This expression becomes singular as shadow or reflection boundaries are approached. Both of them are referred to as transition regions. In order to obtain the continuity in these regions, an expression for the dyadic coefficient is exhibited

This material is reserved for educational use only, not allowed for commercial use.
Forbidden to modify the content, and cite the document when use.

$$D_{s\atop h}(d_{\xi\zeta},\alpha,\alpha',n)=\frac{-e^{-j\frac{\pi}{4}}}{2n\sqrt{2\pi k}}\Bigg[\cot\left(\frac{\pi+\alpha-\alpha'}{2n}\right)F\left[kd_{\xi\zeta}a^{+}(\alpha-\alpha')\right]$$

$$+\cot\left(\frac{\pi-\alpha+\alpha'}{2n}\right)F\left[kd_{\xi\zeta}a^{-}(\alpha-\alpha')\right]$$

$$\mp\Bigg\{\cot\left(\frac{\pi+\alpha+\alpha'}{2n}\right)F\left[kd_{\xi\zeta}a^{+}(\alpha+\alpha')\right]$$

$$+\cot\left(\frac{\pi-\alpha-\alpha'}{2n}\right)F\left[kd_{\xi\zeta}a^{-}(\alpha+\alpha')\right]\Bigg\}\Bigg] \tag{5.22}$$

where ξ is either x or y and ζ is either 1 or 2 ,and $F(\nu)=2j\left|\sqrt{\nu}\right|e^{j\nu}\int_{|\sqrt{\nu}|}^{\infty}e^{-j\tau^2}d\tau$

and

$$a^{\pm}(\alpha\pm\alpha')=2\cos^2\left(\frac{2n\pi N^{\pm}-(\alpha\pm\alpha')}{2}\right)$$

in which $N^{\pm}$ are the integers, which most satisfy

$$2\pi nN^{+}-(\alpha\pm\alpha')=\pi$$

and

$$2\pi nN^{-}-(\alpha\pm\alpha')=-\pi\,.$$

The definitions of parameters are as follows :

α' = the incident angle

α = the diffraction angle

L = distance parameter, determined for several types of illumination. It is found that

This material is reserved for educational use only, not allowed for commercial use.
Forbidden to modify the content, and cite the document when use.

$$L=\begin{cases} s\sin^2\gamma_0 & \text{for plane wave incidence} \\ \dfrac{\rho'\rho}{\rho+\rho'} & \text{for cylindrical wave incidence} \\ \dfrac{s's\sin^2\gamma_0}{s+s'} & \text{for conical and spherical wave incidence} \end{cases} \tag{5.23}$$

Now that all the necessary relationships to calculate D_s and D_h are obtained above. For plane wave incidence in the ray-fixed system, (5.19) can be written generally as

$$\begin{bmatrix} E_s^d(s) \\ E_h^d(s) \end{bmatrix} = \begin{bmatrix} -D_s & 0 \\ 0 & -D_h \end{bmatrix} \begin{bmatrix} E_s^i(Q) \\ E_h^i(Q) \end{bmatrix} A(s)e^{-jks} \tag{5.24}$$

5.3.3 Slope Diffraction

As expressed in previous section, (5.19) and (5.24) are generally called the first order-diffracted fields from a diffraction point Q_D on an edge. In some problems, there is a discontinuity across a shadow boundary. To implement this problem, a higher-order diffraction term is taken into account. The second-order diffraction term is the field, emanated from the specific point Q_D due to diffraction field from the other points.

In general, the UTD diffracted field from a point Q_D on an edge consists not only of the first and second-order diffracted fields considered so far, but also of the so-called slope-diffracted fields. While the first and second-order diffracted fields are proportional to the incident field at Q_D, the slope-diffracted field is proportional to the derivative of the incident one. It can express in the general manner of slope-diffracted field as

$$E_{sd}(s) = \frac{1}{jk\sin\beta_0'} \frac{\partial E^i(Q_D)}{\partial n} \frac{\partial D_{s,h}}{\partial \phi'} A(s)e^{-jks} \tag{5.25}$$

where $\dfrac{\partial E^i}{\partial n}$ is the directional derivative of the field in the direction $\hat{n}$, perpendicular to direction of $\hat{s}'$ as shown in Fig.5.6.

This material is reserved for educational use only, not allowed for commercial use.
Forbidden to modify the content, and cite the document when use.

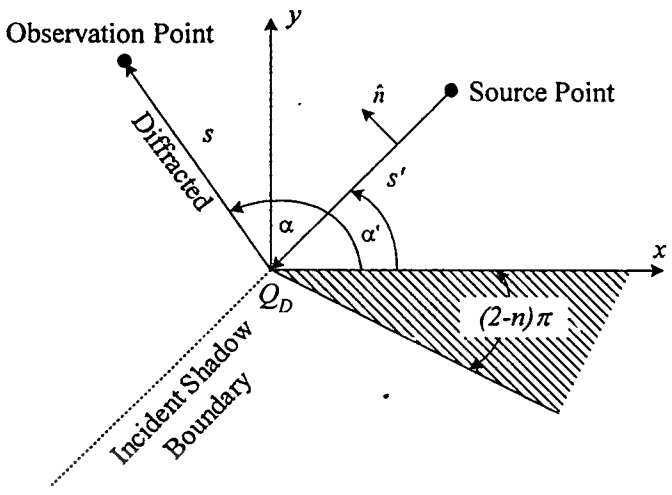

Fig. 5.6 Two dimensions of diffracted ray

The slope diffraction coefficients can be obtained by

$$\frac{\partial D_h^s}{\partial \phi'}(L,\alpha,\alpha',n)=\frac{-e^{-j\frac{\pi}{4}}}{4n^2\sqrt{2\pi k}\sin\beta_0'}\left[\csc^2\left(\frac{\pi+(\alpha-\alpha')}{2n}\right)F_s\left[kLa^+(\alpha-\alpha')\right]\right.$$
$$-\csc^2\left(\frac{\pi-(\alpha-\alpha')}{2n}\right)F_s\left[kLa^-(\alpha-\alpha')\right]$$
$$\pm\left\{\csc^2\left(\frac{\pi+(\alpha+\alpha')}{2n}\right)F_s\left[kLa^+(\alpha+\alpha')\right]\right.$$
$$\left.\left.-\csc^2\left(\frac{\pi-(\alpha+\alpha')}{2n}\right)F_s\left[kLa^-(\alpha-\alpha')\right]\right\}\right] \tag{5.26}$$

The total diffracted field in particular point on an edge can be expressed as

$$E^d(s)=\left[E^i(Q_D)D_{s,h}+\frac{1}{jk\sin\beta_0}\frac{\partial D_h^s}{\partial\phi'}\frac{\partial E^i(Q_D)}{\partial n}\right]A(s)e^{-jks} \tag{5.27}$$

For the finite-size ground plane condition, the edge effects of the finite ground plane are taken into account. In case of slot located along *y* direction, the edge of the ground

This material is reserved for educational use only, not allowed for commercial use.
Forbidden to modify the content, and cite the document when use.

plane is apart from the slot in the negative and positive x direction at the distance d_{x1} and d_{x2}, and the negative and positive y direction at the distance d_{y1} and d_{y2}, respectively as shown in Fig.5.7(a). Alternatively, for slot located on z direction the edge of the ground plane is far from the slot in the x direction at the distance d_{x1} and d_{x2}, and the z direction at the distance d_{z1} and d_{z2}, respectively as shown in Fig.5.7(b).

From the uniform theory of diffraction, the far field geometrical optic is first considered as the field incident on a specific diffracted point. Then, the spatial attenuation factor $A(s)$ is chosen. The spherical wave incidence is suitable candidate in this condition. In far field condition ($s>>s'$), the distance parameter L and $A(s)$ reduce, respectively, to

$$L = s' \sin^2 \beta_0' \tag{5.28}$$

$$A(s) = \frac{\sqrt{s'}}{s} \tag{5.29}$$

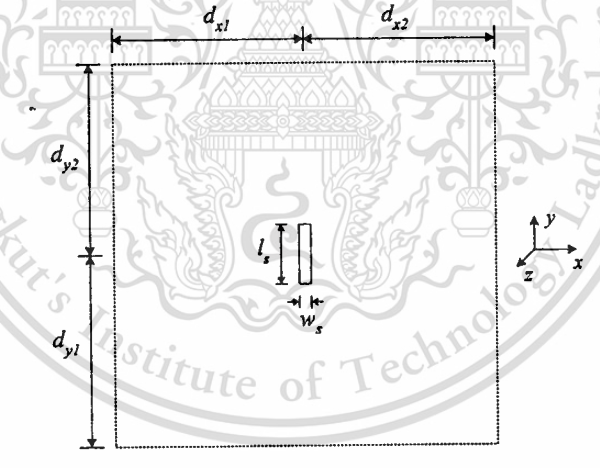

(a)

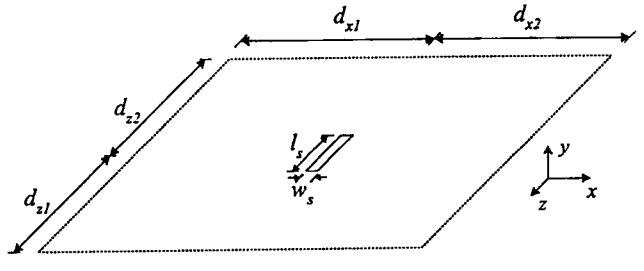

(b)

Fig. 5.7 Slot on finite-size ground plane

(a) in y direction

(b) in z direction

This material is reserved for educational purposes. Not allowed for commercial use.
Forbidden to modify the content, and cite the document when use.

Due to the two directions of slot, y and z direction, are now interested. The y-direction one is illustrated first. In xz plane, the incident ray from the narrow slot at observation point $P(r, \theta, \phi=0)$ is

$$E_{\theta}^{i}(Q_{D1}) = \frac{\sin\left(\frac{kw_s}{2}\sin\theta\right)}{\frac{kw_s}{2}\sin\theta}\frac{e^{-jkd_{x1}}}{d_{x1}} \tag{5.30}$$

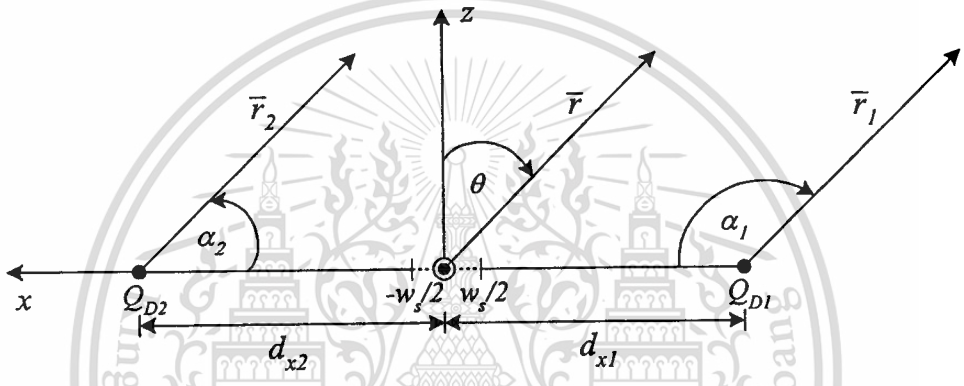

Fig. 5.8 xz plane diffracted ray in case of slot located along y-direction

Following the above conditions, $A(s)$, L and β_o' are obtained by

$$A(s) = \frac{\sqrt{d_{x1}}}{r_1} \tag{5.31a}$$

and

$$L = d_{x1} \tag{5.31b}$$

$$\beta_0' = \frac{\pi}{2} \tag{5.31c}$$

Since the angle of incidence from the main source toward the point of diffraction is zero degrees ($\alpha' = 0$), then

This material is reserved for educational use only, not allowed for commercial use.
Forbidden to modify the content, and cite the document when use.

$$\alpha - \alpha' = \alpha + \alpha' = \theta + \frac{\pi}{2} \tag{5.32}$$

In case of half plane, the wedge factor is equal to 2 (see Fig.5.6). Substituting (5.30), (5.31a), (5.31b), (5.31c) and (5.32) into (5.22), the diffraction coefficients are given by

$$D_h(L,\alpha) = \frac{-e^{-j\frac{\pi}{4}}}{\sqrt{2\pi k}} \frac{F[kLa(\alpha)]}{\cos\frac{\alpha}{2}} \tag{5.33}$$

where $L = d_{x1}$ and $\alpha = \theta + \frac{\pi}{2}$

$$D_s = 0$$

In case of $\alpha' = 0$ so-called grazing incidence, all diffraction coefficients are divided by two [40]. Therefore, the diffracted field can now be written as

$$E^d_{Q_{D1}}(\theta) = E^i_\theta(Q_{D1}) \frac{D_h}{2} A(s) e^{-jkr_1} \tag{5.34}$$

In similar procedure, the edge-diffracted ray from Q_{D2} at $P(r, \theta, \phi = 0)$ yields

$$E^d_{Q_{D2}}(\theta) = E^i_\theta(Q_{D2}) \frac{D_h}{2} A(s) e^{-jkr_2} \tag{5.35}$$

where

$$E^i_\theta(Q_{D2}) = \frac{\sin\left(\frac{kw_s}{2}\sin\theta\right)}{\frac{kw_s}{2}\sin\theta} \frac{e^{-jkd_{x2}}}{d_{x2}}$$

$$\alpha \pm \alpha' = \begin{cases} \frac{\pi}{2} - \theta & , 0 \le \theta \le \frac{\pi}{2} \\ \frac{5\pi}{2} - \theta & , \frac{\pi}{2} < \theta \le \pi \end{cases}$$

This material is reserved for educational use only, not allowed for commercial use.
Forbidden to modify the content, and cite the document when use.

$$A(s) = \frac{\sqrt{d_{x2}}}{r_2} \qquad \text{and} \qquad L = d_{x2}$$

According to far field observations

$$\left.\begin{aligned} r_1 &\approx r - d_{x1}\sin\theta \\ r_2 &\approx r + d_{x2}\sin\theta \end{aligned}\right\} \quad \text{for phase term}$$

$$r_1 \approx r_2 \approx r \qquad \text{for amplitude term}$$

The total field at an observation point $P(r, \theta, \phi=0)$ then becomes

$$E^t(\theta) = E^i(\theta) + E^d_{Q_{D1}}(\theta) + E^d_{Q_{D2}}(\theta) \tag{5.36}$$

In fact, there is a discontinuity in the pattern at $\theta = \pi/2$, the transition at the shadow boundary. This indicates that a scattering algorithm has not been considered. To solve this circumstance, high-order diffraction terms are included. To identify this high-order term, the examination of the continuity of $E^i(\theta)$, $E^d_{Q_{D1}}$ and $E^d_{Q_{D2}}$. It is found that function $E^d_{Q_{D1}}$ is discontinuous across that boundary. Therefore, the second order diffracted term is necessary to solve this problem. This second-order-diffracted term is field, radiated from Q_{D1}, due to the diffracted field from Q_{D2}. Using a similar procedure, it can be expressed as

$$E^d_{Q_{D12}}(\theta) = E^d_{Q_{D2}}(Q_{D1})\frac{D_h}{2}A(s)e^{-jkr_1} \tag{5.37}$$

Additionally, the total pattern is given by

$$E^t(\theta) = \begin{cases} E^i(\theta) + E^d_{Q_{D1}}(\theta) + E^d_{Q_{D2}}(\theta) + E^d_{Q_{D12}}(\theta) & , \ 0 \le \theta \le \dfrac{\pi}{2} \\ E^d_{Q_{D1}}(\theta) + E^d_{Q_{D2}}(\theta) + E^d_{Q_{D12}}(\theta) & , \ \dfrac{\pi}{2} \le \theta \le \pi \end{cases} \tag{5.38}$$

For yz plane $P(r, \theta, \phi = \frac{\pi}{2})$ as depicted in Fig.5.9, the incident rays are

This material is reserved for educational use only, not allowed for commercial use.
Forbidden to modify the content, and cite the document when use.

$$E_{\phi}^{i}(Q_{D3}) = \cos\theta \frac{\cos\left(\frac{kl_s}{2}\sin\theta\right)}{\left(\frac{kl_s}{2}\sin\theta\right)^2 - \left(\frac{\pi}{2}\right)^2} \frac{e^{-jkd_{y3}}}{d_{y3}} \tag{5.39a}$$

$$E_{\phi}^{i}(Q_{D4}) = \cos\theta \frac{\cos\left(\frac{kl_s}{2}\sin\theta\right)}{\left(\frac{kl_s}{2}\sin\theta\right)^2 - \left(\frac{\pi}{2}\right)^2} \frac{e^{-jkd_{y4}}}{d_{y4}} \tag{5.39b}$$

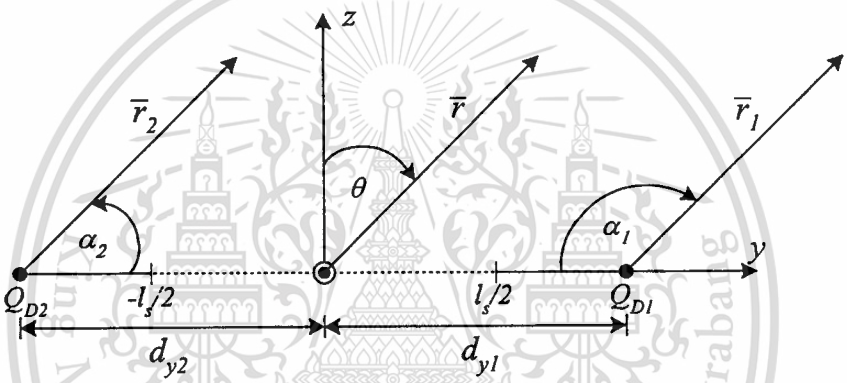

Fig. 5.9 *yz* plane of diffracted ray in case of slot located along *y*-direction

In this case, these incident rays are zero at the point of diffraction, $\theta = \pi/2$. This caused the diffracted field to be vanished. Thus, the additional term so-called slope diffraction is considered. It is rather on the slope of the incident field at the point of diffraction. For this problem, there are two points of diffraction in this *yz* plane. Hence, the slope diffraction of these points are defined as

$$E_{Q_{D3}}^{sd}(\theta) = \frac{1}{jk} \frac{\partial E_{\phi}^{i}(Q_{D3})}{\partial n} \frac{\partial D_h(Q_{D3})}{\partial \alpha'} A(s) e^{-jkr_3} \tag{5.40a}$$

$$E_{Q_{D4}}^{sd}(\theta) = \frac{1}{jk} \frac{\partial E_{\phi}^{i}(Q_{D4})}{\partial n} \frac{\partial D_h(Q_{D4})}{\partial \alpha'} A(s) e^{-jkr_4} \tag{5.40b}$$

This material is reserved for educational use only, not allowed for commercial use.
Forbidden to modify the content, and cite the document when use.

The derivatives of the incident rays are shown as

$$\frac{\partial E^i}{\partial n} = \frac{1}{s'}\frac{\partial E^i}{\partial \phi'} = \frac{1}{s'}\frac{\partial E^i}{\partial \theta} \tag{5.41}$$

$$\frac{\partial E_\phi^i(Q_{D3})}{\partial n} = \frac{-\cos\left(\frac{kl_s}{2}\right)}{\left(\frac{kl_s}{2}\right)^2 - \left(\frac{\pi}{2}\right)^2}\frac{e^{-jkd_{y3}}}{d_{y3}} \quad ; \ \theta = \frac{\pi}{2} \tag{5.42a}$$

$$\frac{\partial E_\phi^i(Q_{D4})}{\partial n} = \frac{-\cos\left(\frac{kl_s}{2}\right)}{\left(\frac{kl_s}{2}\right)^2 - \left(\frac{\pi}{2}\right)^2}\frac{e^{-jkd_{y4}}}{d_{y4}} \quad ; \ \theta = \frac{\pi}{2} \tag{5.42b}$$

By substituting the specified parameters into (5.42a) and (5.42b), the derivative of diffraction coefficient can be determined. In similar procedure of normal diffracted field, we can calculate the slope diffraction field straightforwardly. The total field in this plane becomes

$$E^t(\theta) = \begin{cases} E^t(\theta) + E_{Q_{D3}}^{sd} + E_{Q_{D4}}^{sd} & , \ 0 \le \theta \le \frac{\pi}{2} \\ E_{Q_{D3}}^{sd} + E_{Q_{D4}}^{sd} & , \ \frac{\pi}{2} < \theta \le \pi \end{cases} \tag{5.43}$$

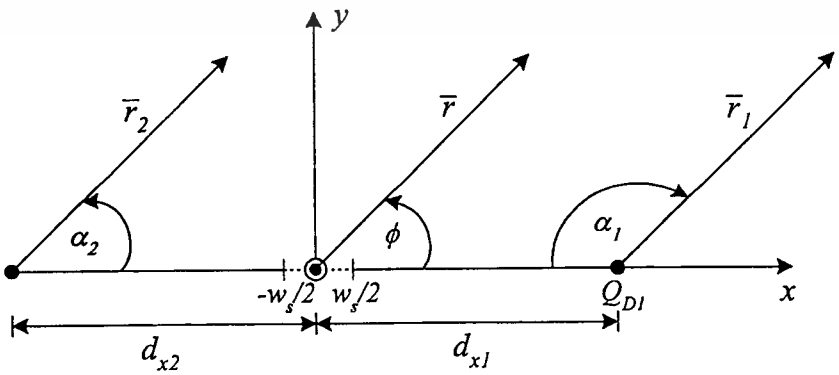

Fig. 5.10 *xy* plane diffracted ray in case of slot located along *z*-direction

This material is reserved for educational use only, not allowed for commercial use.
Forbidden to modify the content, and cite the document when use.

In another slot direction, which is z-direction as shown in Fig.5.10, the radiation patterns of zy plane and xy plane are similarly obtained but the only E_ϕ from (5.18) is used instead. The diffracted fields in xy plane can be illustrated as

$$E^d_{Q_{D1}}(\phi) = E^i_\theta(Q_{D1})\frac{D_h(Q_{D1})}{2}A(s)e^{-jkr_1} \tag{5.44}$$

where

$$E^i_\theta(Q_{D1}) = \frac{\sin\left(\frac{kw_s}{2}\cos\phi\right)}{\frac{kw_s}{2}\cos\phi}\frac{e^{-jkd_{x1}}}{d_{x1}} \quad ; \theta = \frac{\pi}{2}$$

$$\alpha - \alpha' = \pi - \phi$$

and

$$E^d_{Q_{D2}}(\phi) = E^i_\theta(Q_{D2})\frac{D_h(Q_{D2})}{2}A(s)e^{-jkr_2} \tag{5.45}$$

where

$$E^i_\theta(Q_{D2}) = \frac{\sin\left(\frac{kw_s}{2}\cos\phi\right)}{\frac{kw_s}{2}\cos\phi}\frac{e^{-jkd_{x2}}}{d_{x2}} \quad ; \theta = \frac{\pi}{2}$$

$$\alpha - \alpha' = \phi$$

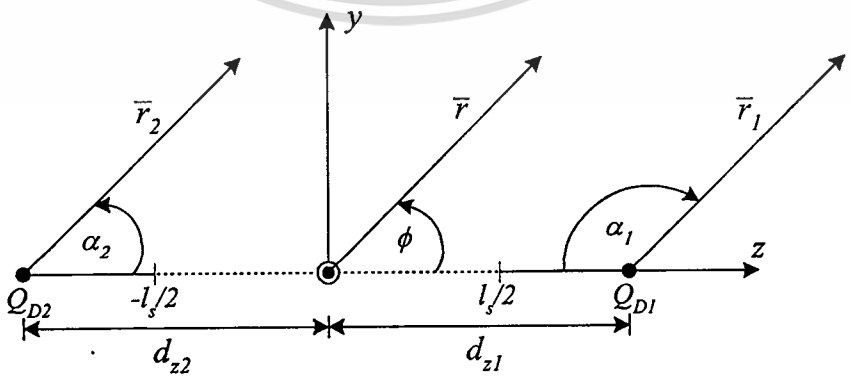

Fig. 5.11 yz plane diffracted ray in case of slot located along z-direction

This material is reserved for educational use only, not allowed for commercial use.
Forbidden to modify the content, and cite the document when use.

Next, the slope diffraction in *yz* plane are

$$E_{Q_{D3}}^{sd}(\theta) = \frac{1}{jkd_{z3}} \frac{\partial E_{\theta}^{i}(Q_{D3})}{\partial \phi} \frac{\partial D_{h}(Q_{D3})}{\partial \alpha'} A(s) e^{-jkr_3} \tag{5.46}$$

and

$$E_{Q_{D4}}^{sd}(\theta) = \frac{1}{jkdz_4} \frac{\partial E_{\theta}^{i}(Q_{D4})}{\partial \phi} \frac{\partial D_{h}(Q_{D4})}{\partial \alpha'} A(s) e^{-jkr_4} \tag{5.47}$$

5.4 Directivity Estimations

One of the significant antenna characteristics is the directivity. The directivity is an evaluation of the ability of an antenna to concentrate the radiated power in a given direction. It occurs in the direction of the main-lobe maximum. The antenna directivity is equal to 4π times the ratio of the antenna maximum radiation intensity over the total radiated power. It can be written in mathematical fashion as

$$D = \frac{4\pi U_{\max}}{P_{rad}} \tag{5.48}$$

where D is directivity. U_{max} represents the maximum radiation intensity. P_{rad} is the total radiated power. The radiation intensity is expressed as

$$U(\theta,\phi) = \frac{1}{2\eta}\left[\left|E_{\theta}(\theta,\phi)\right|^2 + \left|E_{\phi}(\theta,\phi)\right|^2\right] \tag{5.49}$$

where

η = intrinsic impedance of the medium

E_{θ}, E_{ϕ} = far-zone electric field components of the antenna

In case of slot located along z direction, the radiation intensity and total radiated power can be written as

$$U(\theta,\phi) = \frac{1}{2\eta}\left[\left|E_{\phi}(\theta,\phi)\right|^2\right] \qquad ; E_{\theta} = 0 \tag{5.50}$$

This material is reserved for educational use only, not allowed for commercial use.
Forbidden to modify the content, and cite the document when use.

$$U(\theta,\phi)=\frac{1}{2\eta}\left[\left|j\frac{k}{2l_s}\sin\theta\frac{\cos\left(\frac{kl_s}{2}\cos\theta\right)}{\left(\frac{\pi}{l_s}\right)^2-(k\cos\theta)^2}\frac{\sin\left(\frac{kw_s}{2}\sin\theta\cos\phi\right)}{\frac{kw_s}{2}\sin\theta\cos\phi}\right|^2\right] \tag{5.51}$$

$$P_{rad}=\int_0^{\pi}\int_0^{\pi}U(\theta,\phi)\sin\theta d\theta d\phi \tag{5.52}$$

On the other hand, along y direction, they are

$$U(\theta,\phi)=\frac{1}{2\eta}\left[|E_\theta(\theta,\phi)|^2+|E_\phi(\theta,\phi)|^2\right] \tag{5.53}$$

$$U(\theta,\phi)=\frac{1}{2\eta}\left[\left|-j\frac{kl_s}{4}\cos\phi\frac{\cos\left(\frac{kl_s}{2}\sin\theta\sin\phi\right)}{\left(\frac{kl_s}{2}\sin\theta\sin\phi\right)^2-\left(\frac{\pi}{2}\right)^2}\frac{\sin\left(\frac{kw_s}{2}\sin\theta\cos\phi\right)}{\frac{kw_s}{2}\sin\theta\cos\phi}\right|^2+\left|-j\frac{kl_s}{4}\cos\theta\sin\phi\frac{\cos\left(\frac{kl_s}{2}\sin\theta\sin\phi\right)}{\left(\frac{kl_s}{2}\sin\theta\sin\phi\right)^2-\left(\frac{\pi}{2}\right)^2}\frac{\sin\left(\frac{kw_s}{2}\sin\theta\cos\phi\right)}{\frac{kw_s}{2}\sin\theta\cos\phi}\right|^2\right] \tag{5.54}$$

and

$$P_{rad}=\int_0^{2\pi}\int_0^{\frac{\pi}{2}}U(\theta,\phi)\sin\theta d\theta d\phi \tag{5.55}$$

5.5 Numerical Results

The numerical results of radiation patterns of the cavity-backed slot antenna fed by probe are carried out. There are two cases to demonstrate; that are the slot aligned on y and z direction. The dimensions are tabulated in Table 5.1. The numerical results of radiation pattern for various sizes of the ground plane are shown in Fig. 5.12 and 5.13.

This thesis is allowed for educational use only, not allowed for commercial use.
Forbidden to modify the content, and cite the document when use.

Table 5.1 Dimension of cavity-backed slot with finite size ground plane in the model

Antenna Parameter		
Cavity Width: a	0.75λ	*11.84* cm
Cavity Height: b	0.375λ	*5.92* cm
Cavity Length: c	0.75λ	*11.84* cm
Slot Length: l_s	0.50λ	*7.89* cm
Slot Width: w_s	0.048λ	*0.757* cm
Slot Offset: x_s	0.25λ	*3.94* cm
Slot Offset: z_s	0.303λ	*4.78* cm
Probe Length: l_p	0.25λ	*3.94* cm
Probe Location: z_p	0.375λ	*5.92* cm
Probe Location: y_p	0.187λ	*2.96* cm

From Fig. 5.12 and 5.13, the radiation pattern in E plane and H plane of the slot aligned on y and z direction are carried out. The pattern with various sizes of the ground plane viz., 3λ, 10λ, 100λ and 1000λ are compared with the infinite ground plane. The patterns of all cases are similar except for the ripples and the back lobes occur in case of finite size ground plane. For the large ground plane the ripple is small and becomes pronounce when the ground plane is smaller. For the back lobe in both E plane and H plane, it is observed that the back lobe is lower when the ground plane larger and there is no back lobe for infinite ground plane.

This material is reserved for educational use only, not allowed for commercial use.
Forbidden to modify the content, and cite the document when use.

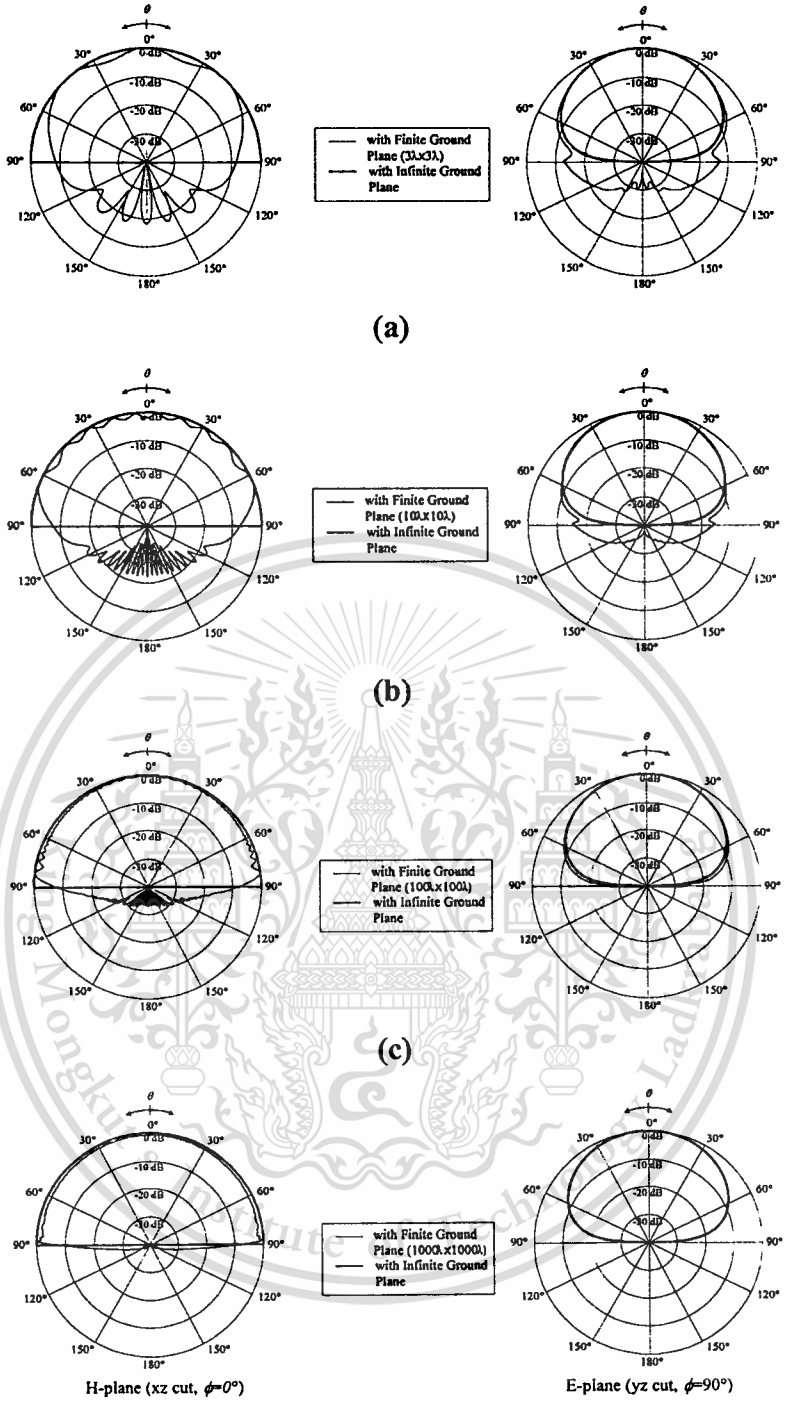

Fig. 5.12 Radiation pattern of *y* direction slot with various size of ground plane and with infinite ground plane

(a) ground plane 3λ

(b) ground plane 10λ

(c) ground plane 100λ

(d) ground plane 1000λ

This material is protected by copyright and is for educational use only, not allowed for commercial use.
Forbidden to modify the content, and cite the document when use.

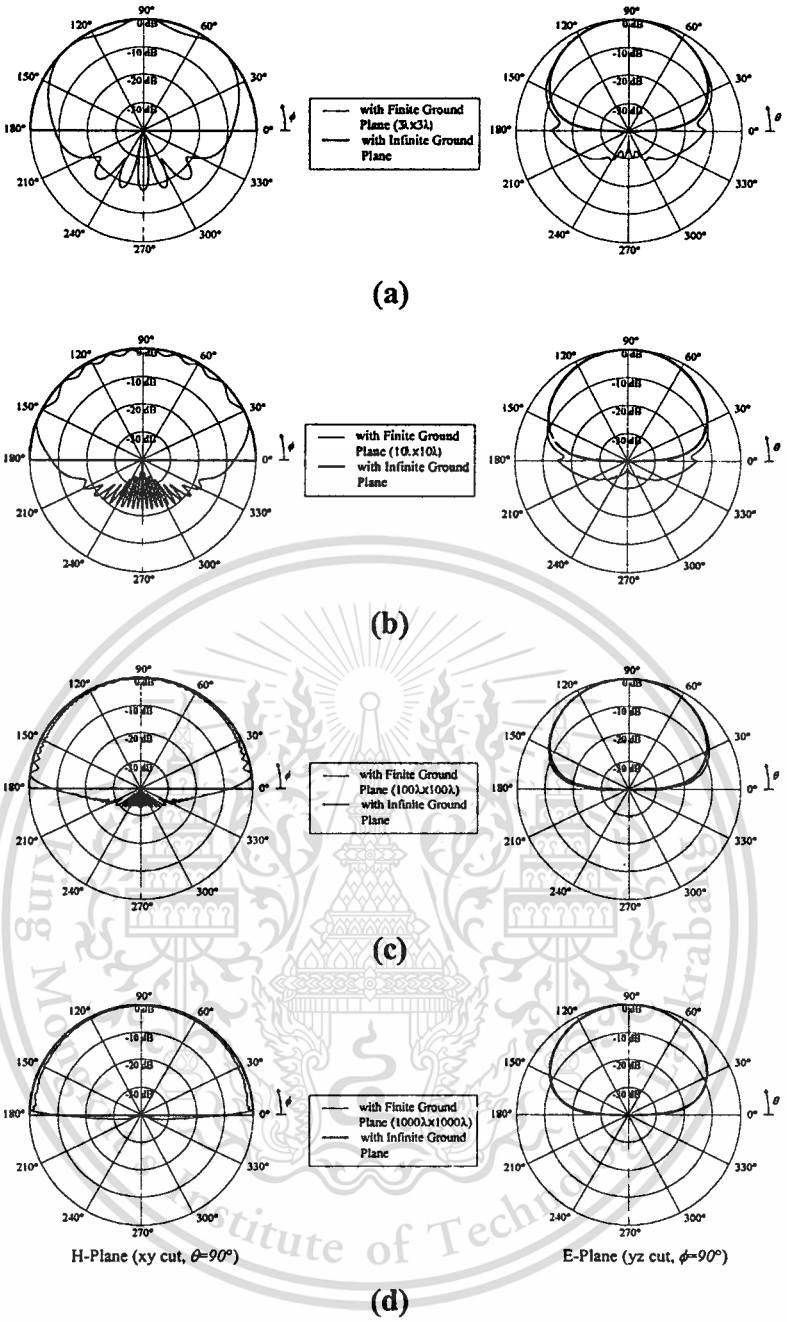

Fig. 5.13 Radiation pattern of *z* direction slot with various sizes of ground plane and with infinite ground plane

(a) ground plane 3λ

(b) ground plane 10λ

(c) ground plane 100λ

(d) ground plane 1000λ

This material is reserved for educational use only, not allowed for commercial use.
Forbidden to modify the content, and cite the document when use.

The numerical of the directivity as the function of the frequency is shown in Fig.5.14. It is apparent that the directivity is increased as the frequency because the slot length is fixed whereas the frequency is increased. This makes the electrical size of the slot to be larger for certain frequency. Accordingly, the directivity is increased as expected.

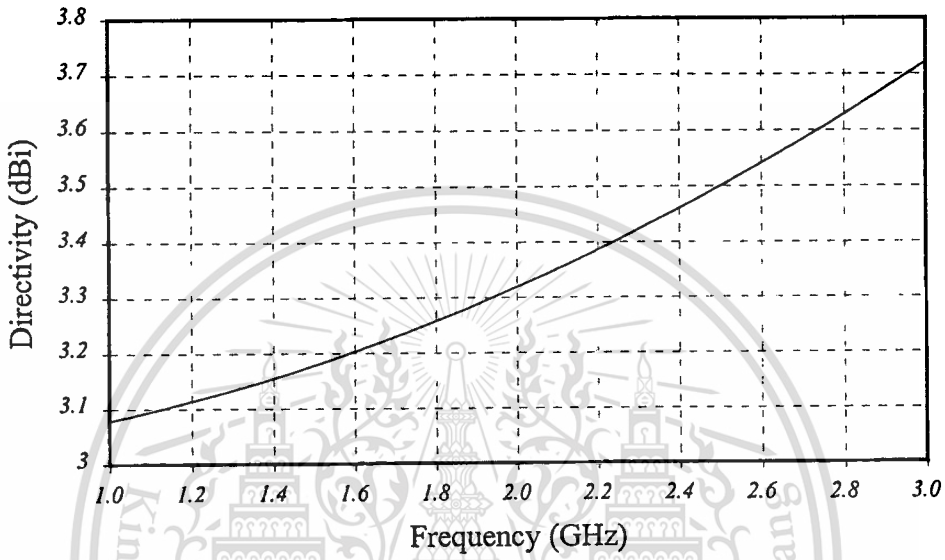

Fig. 5.14 Directivity of slot on infinite ground plane

This material is reserved for educational use only, not allowed for commercial use.
Forbidden to modify the content, and cite the document when use.

5.6 Experimental Results

The fabricated antenna with the dimensions tabulated in Table 5.2 is depicted in Fig. 5.15. The antenna measurements of the radiation pattern are performed at the operating frequency of *12.5* GHz. The antenna under test is the cavity-backed slot antenna fed by probe. The transmitting antenna is the corrugated horn antenna. The pattern measurement is done in the in-house anechoic chamber. The transmitting antenna was connected to the HP8750C network analyzer to transmit the electromagnetic wave. The antenna under test was rotated to receive the signal from the transmitting antenna and connected to HP8750C network analyzer. The experimental results of the radiation pattern are plotted and compared with numerical results as shown in Fig. 5.16 (a) and (b). The far field of the measurement is *90* cm.

Table 5.2 Dimension of cavity-backed slot with finite size ground plane in the experiment

Antenna Parameter		
Cavity Width: a	0.792λ	*1.90* cm
Cavity Height: b	0.396λ	*0.95* cm
Cavity Length: c	0.792λ	*1.90* cm
Slot Length: l_s	0.50λ	*1.20* cm
Slot Width: w_s	0.048λ	*0.115* cm
Slot Offset: x_s	0.25λ	*0.60* cm
Slot Offset: z_s	0.303λ	*0.73* cm
Probe Length: l_p	0.25λ	*0.60* cm
Probe Location: z_p	0.396λ	*0.95* cm
Probe Location: y_p	0.198λ	*0.40* cm
Ground Plane Size: d_g	2.375λ	*5.70* cm

This material is reserved for educational use only, not allowed for commercial use.
Forbidden to modify the content, and cite the document when use.

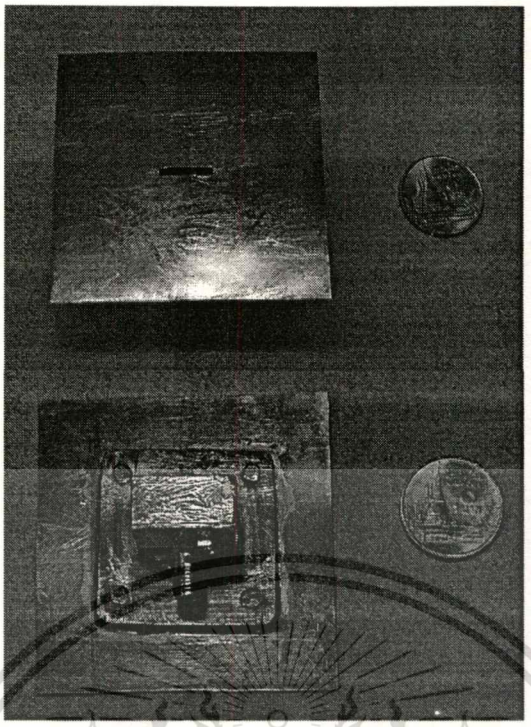

Fig.5.15 Photograph of the cavity backed-slot antenna excited by probe with finite size ground plane (2.375λ)

From the compared results of the radiation pattern as shown in Fig. 5.16, it is obvious that the results are agree reasonably in H plane the beamwidth and the back lobe of the calculated and numerical results are similar. Alternatively, the beamwidth of experimental result is narrower than the calculated one. The reason is from neglecting the effect at the vertex of the ground plane. However, it is evident that this effect has much influence to the pattern. The calculation to improve the result is still necessary and left for further studies

This material is reserved for educational use only, not allowed for commercial use.
Forbidden to modify the content, and cite the document when use.

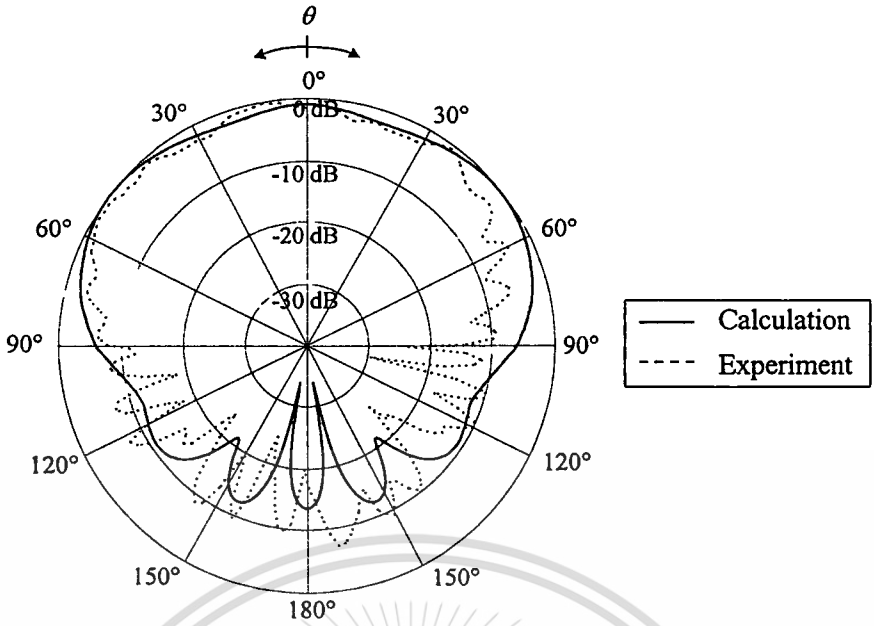

H-Plane (xz cut, ϕ=0°)

(a)

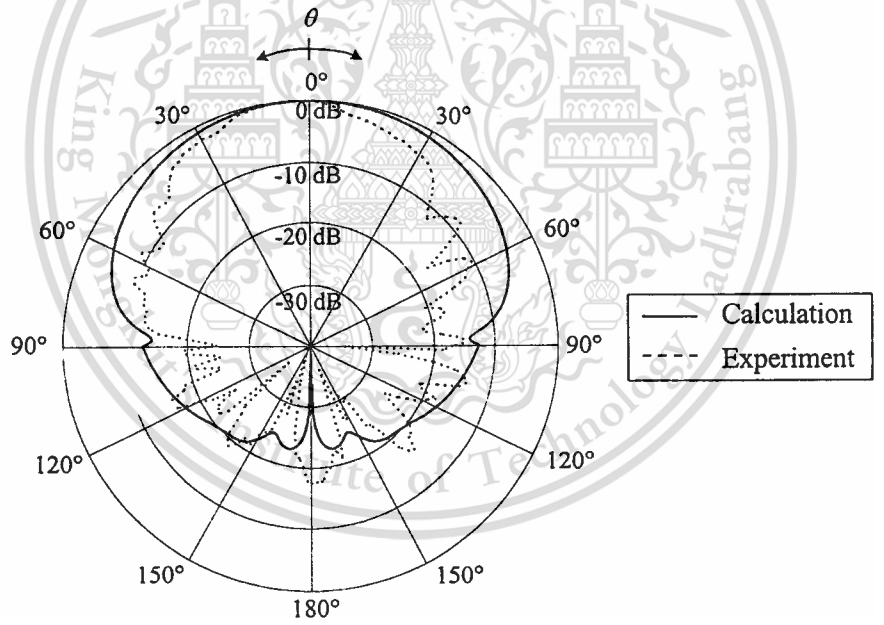

E-Plane (yz cut, ϕ=90°)

(b)

Fig.5.16 Radiation pattern of the cavity-backed slot antenna on finite size ground plane 2.375λ
(a) H plane
(b) E plane

This material is reserved for educational use only, not allowed for commercial use.
Forbidden to modify the content, and cite the document when use.

5.7 Application of the Second Kind Tschebyscheff Array to Synthesize Linear Slotted-Waveguide Array Antenna

5.7.1 Mathematical characteristics of the second kind Tschebyscheff polynomial

The second kind Tschebyscheff polynomial is one type of orthogonal polynomials that can be used for synthesizing the antenna array pattern, which provides the tapered minor lobe. The basic features of the second kind Tschebyscheff polynomial will be described in this section.

The second kind Tschebyscheff polynomial *U(x)* is defined on the interval $a \leq x \leq b$ with respect to the weight function $\sqrt{1-x^2}$, as

$$\int_a^b \sqrt{1-x^2}\, U_n(x) U_m(x) dx = 0 \tag{5.56}$$

where $U_n(x)$ and $U_m(x)$ are the second kind Tscheyscheff polynomials of degree *n* and *m*, respectively. Alternatively, another form, referred to as *standardization*, can be written as

$$\int_a^b \sqrt{1-x^2}\, U_n^2(x) dx = \frac{\pi}{2} \tag{5.57}$$

In order to use the second kind Tschebyscheff polynomial to synthesize the array pattern, the differential equation, the recurrence relation and Rodrigues' formula must be studied.

5.7.1.1 Differential equation

The relationship of the second kind Tschebyscheff polynomial and its derivative is very useful when the coefficient is determined. That relationship can be written in closed form as

$$(1-x^2)\frac{d^2U_n(x)}{dx^2} - 3x\frac{dU_n(x)}{dx} + n(n+2)U_n(x) = 0 \ . \tag{5.58}$$

This material is reserved for educational use only, not allowed for commercial use.
Forbidden to modify the content, and cite the document when use.

5.7.1.2 Recurrence relation

To find the second kind Tschebyscheff polynomial of any order from the polynomial in which order is given, the recurrence relation is used to realize. Normally, the polynomial of higher order would be determined from the polynomial of lower order. The general form of recurrence relation is

$$U_{n+1}(x) = 2xU_n(x) - U_{n-1}(x) . \tag{5.59}$$

5.7.1.3 Rodrigues' formula

Rodrigues' formula is the alternative form of the second kind Tschebyscheff polynomial in which the polynomial of order n is in the form of derivative of weight and coefficient functions as

$$U_n(x) = \frac{(n+1)\sqrt{\pi}}{2^{n+1}\Gamma(n+\frac{3}{2})} \frac{d^n(x^2-1)^n}{dx^n} . \tag{5.60}$$

5.7.2 Array pattern synthesis and design

From the mathematical characteristics of the second kind Tschebyscheff polynomial as described in the previous section, the method to use this polynomial to synthesize the array pattern will be summarized in this section. Let us consider a linear discrete array in which the elements are aligned symmetry with the center of the array and have equal spacing between elements. The isotropic element is used, to simplify in calculations. The array factors in case of the number of elements are even and odd can be expressed, respectively, as [41]

- Even numbers of elements

$$AF_{2N}(\theta) = \sum_{n=1}^{N} I_n \cos[(2n-1)\frac{\pi d}{\lambda}\cos\theta] \tag{5.61a}$$

- Odd numbers of elements

$$AF_{2N+1}(\theta) = \sum_{n=1}^{N+1} I_n \cos[(2n-1)\frac{\pi d}{\lambda}\cos\theta] , \tag{5.61b}$$

This material is reserved for educational use only, not allowed for commercial use.
Forbidden to modify the content, and cite the document when use.

where I_n is the amplitude current excitation coefficients, *2N* and *2N+1* are the number of even and odd elements, respectively, d is the equal spacing between each elements, λ is the wavelength of the operating frequency and θ is the angle between the field direction and the observation point.

Next, the summation of cosine terms for the case of even and odd numbers of elements will be expanded. The order of harmonic cosine term is equal to the total number of elements minus one and the argument of cosine term is the positive integer times of the fundamental frequency that can be written in the form

$$\begin{aligned}\cos(ku) = \cos^k(u) - \binom{k}{2}\cos^{k-2}(u)\sin^2(u) + \binom{k}{4}\cos^{k-4}(u) \\ x\sin^4(u) - \ldots - \binom{k}{k-2}\cos^2(u)\sin^{k-2}(u) + \sin^k(u)\end{aligned} \tag{5.62}$$

where $\binom{k}{n} = \dfrac{k!}{n!(k-n)!}$ and $\sin^2(u) = 1 - \cos^2(u)$.

To design the second kind Tschebyscheff array, the cosine term after expanding as described and the second kind Tschebyscheff polynomial will be equated as

$$\cos(ku) = U_k(x) \tag{5.63}$$

In the design procedure, the number of elements, spacing between the elements in wavelength form, the major to the first minor lobe intensity ratio must be first known. After that the following step can be applied to obtain the array factor expression.

1) From the known number of elements, we can select the array factor from (5.61a) or (5.61b), subjected to the even or odd number of elements.

2) Select the appropriated cosine term function from (5.62) and substitute in the expanded array factor.

3) Find the order of the second kind Tschebyscheff polynomial by subtracting the total number of elements by one. Equating this second kind Tschebyscheff polynomial with the multiplication of the major to the first minor intensity ratio (R_n) and the height of the first ripple (y_n), then solve the root of this polynomial $x = x_m$

This material is reserved for educational use only, not allowed for commercial use.

Forbidden to modify the content, and cite the document when use.

To synthesize the linear slotted-waveguide second kind Tschebyscheff array antenna [42], the element pattern of a slotted-waveguide antenna will be expressed in this section. Consider a slot of the length l and width w cut on the broad wall of the waveguide antenna aligned on z-axis as shown in Fig.5.18. The width and height of the waveguide are a and b, respectively. At one end of the waveguide ($z=0$), it is feed by the aperture excitation, and the another end is terminated by the shorted plate at the distance $n\lambda_g/2+\lambda_g/4$ from the last slot, and λ_g is the guided wavelength. The locations of the slot orientation are offsets, the distance s_n from the center of the broad wall, such that it can interrupt the current along the waveguide to radiate the power. The equivalent circuit of a slotted waveguide antenna was investigated in literature [15] and found to be the shunt conductance, g_n, as revealed in Fig.5.18. The radiation pattern of a single slot cut on the broad wall of the waveguide by neglecting the edge effect and the waveguide thickness can be expressed as

$$E_n = \frac{\cos(\frac{kl}{2}\cos\theta)}{\sin\theta} \tag{5.64}$$

The radiation pattern subjected to (5.64) of the half guided wavelength length is plotted as shown in Fig.5.19.

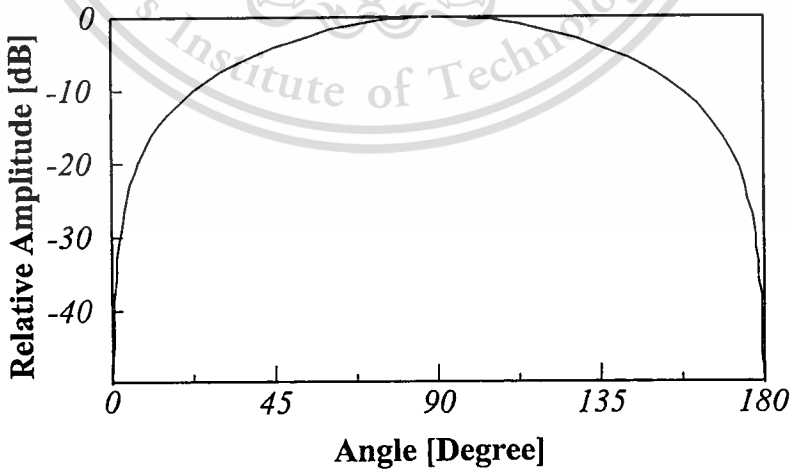

Fig.5.19 Element pattern of a slotted-waveguide antenna

This material is reserved for educational use only, not allowed for commercial use.
Forbidden to modify the content, and cite the document when use.

5.7.4 Design of a linear slotted-waveguide array antenna

To design the broad wall slotted-waveguide array antenna, the relationship between the slot length and slot offsets and normalized conductance of the specified waveguide dimension must be first expressed as [15]

$$s_n = \frac{a}{\lambda}\sin^{-1}\sqrt{0.85g_n} \tag{5.65}$$

and

$$l = \frac{\lambda}{\pi}(1.517 + \frac{s_n^2}{354}). \tag{5.66}$$

In addition, in order to success the input matching of the antenna, the summation of the total normalized conductance should be unity. Conclusively, from the amplitude current excitation determined from section 5.7.2 and input matching condition as described above, the conductance of each slot element can be determined proportional to the amplitude current. The slot length and slot offsets can be obtained, subsequently.

In the practice, when the actual antenna such as a slotted-waveguide is used to synthesize the array pattern in stead of the isotropic radiator, the pattern multiplication is a significant tool to realize the all radiation patterns from the antenna. The total fields are the products of the array factor and the element pattern.

5.7.5 Numerical Results

An isotropic radiator of the *10* elements with the half guided wavelength spacing at the side lobe level *20* dB is utilized as a demonstration to find the array factor at the operating frequency of *9* GHz. By using the procedure as described in the previous section, the amplitude current excitations and radiation pattern of the array factor are found as shown in Figs.5.30 (a) and (b), respectively.

Next, the slot is cut on the WRJ-10 standard waveguide of the width and the height of *22.9* mm and *10.2* mm. The slot length and slot offsets are found by using the procedure in section 5.7.4 and can be tabulated as

This material is reserved for educational use only, not allowed for commercial use.
Forbidden to modify the content, and cite the document when use.

Table 5.3 Slot length and slot offsets of the antenna

n	g_n	l (mm)	s_n (mm)
1	*0.0307*	*16.667*	*-1.0342*
2	*0.0638*	*16.667*	*1.4963*
3	*0.1037*	*16.667*	*-1.9163*
4	*0.1400*	*16.667*	*2.2359*
5	*0.1618*	*16.667*	*-2.4098*
6	*0.1618*	*16.667*	*2.4098*
7	*0.1400*	*16.667*	*-2.2359*
8	*0.1037*	*16.667*	*1.9163*
9	*0.0638*	*16.667*	*-1.4963*
10	*0.0307*	*16.667*	*1.0342*

where the plus and minus sign designates the offsets to one side and opposite side (measured from the center line of the broad wall surface).

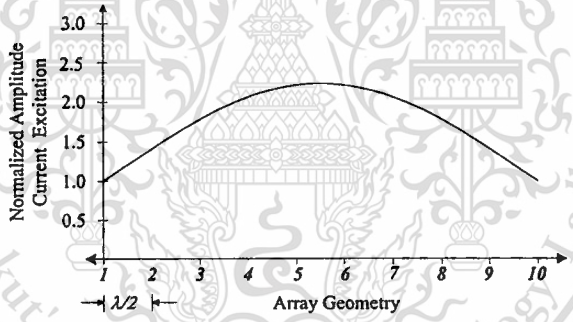

(a)

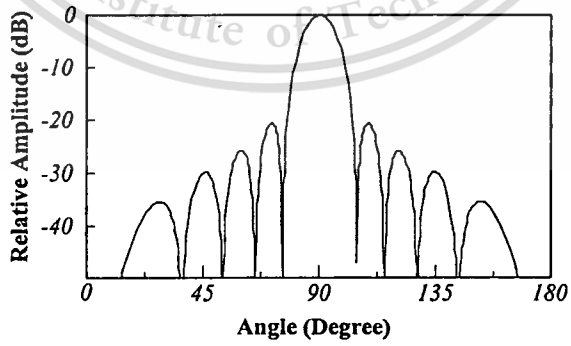

(b)

Fig.5.20 Amplitude current distribution and array pattern for the second kind Tschebyscheff array of *10* elements at SLL *20* dB with half guided wavelength spacing

(a) Amplitude current distribution (b) Array factor

This material is reserved for educational use only, not allowed for commercial use.
Forbidden to modify the content, and cite the document when use.

The total radiation of the antenna is yielded by multiplying the array pattern as shown in Fig.5.20(b) and the element pattern as shown in Fig.5.19. The resultant pattern is shown in Fig.5.21 by the dotted line. It is obvious that the antenna provides the tapered minor lobe especially far-out minor lobes. The furthest minor lobe level of the multiplied pattern is very low compared with the array pattern due to the behavior of the element pattern. It can be summarized that the linear slotted-waveguide array antenna possesses the very low side lobe level because both of the array pattern and element pattern yields the low side lobe.

5.7.4 Experimental Results

The prototype of a linear slotted-waveguide second kind Tschebycheff array antenna was fabricated at the operating frequency of *9* GHz. The available brass waveguide with the same dimension as WRJ10, of the waveguide thickness *1.25* mm is used. The ten elements of slots were cut by CNC milling machine. The shorted plate made of metallic conductor was terminated at one end of the waveguide whereas the another end was connected to the signal generator via the flange as shown in Fig.5.22.

The far-field test site was set up at the distance of *23* m (fourfold of far-field range). A signal generator transmitted microwave signal through a flare horn at the transmitting side. The antenna under test (a linear slotted-waveguide array antenna) was connected to HP8566B Spectrum Analyzer via a low noise block down converter. The measured field strength from the spectrum analyzer was interfaced to the personal computer by using the HPIB interface to plot the radiation pattern. The experimental result is compared with the prediction as shown in Fig.5.21. It is obvious that those two results are in good agreement especially in the main lobe. However, there are some errors in the minor lobe region, expected to result from the effect of multipath environment of the test range that makes the wave front at receiving antenna is not plane wave as ideal. The effect of the finite ground plane of the antenna and some imperfect fabrications are the alternative reasons. The field strength at the backside of the antenna is also measured. The maximum minor lobe level of -17 dB is confirmed.

This material is reserved for educational use only, not allowed for commercial use.
Forbidden to modify the content, and cite the document when use.

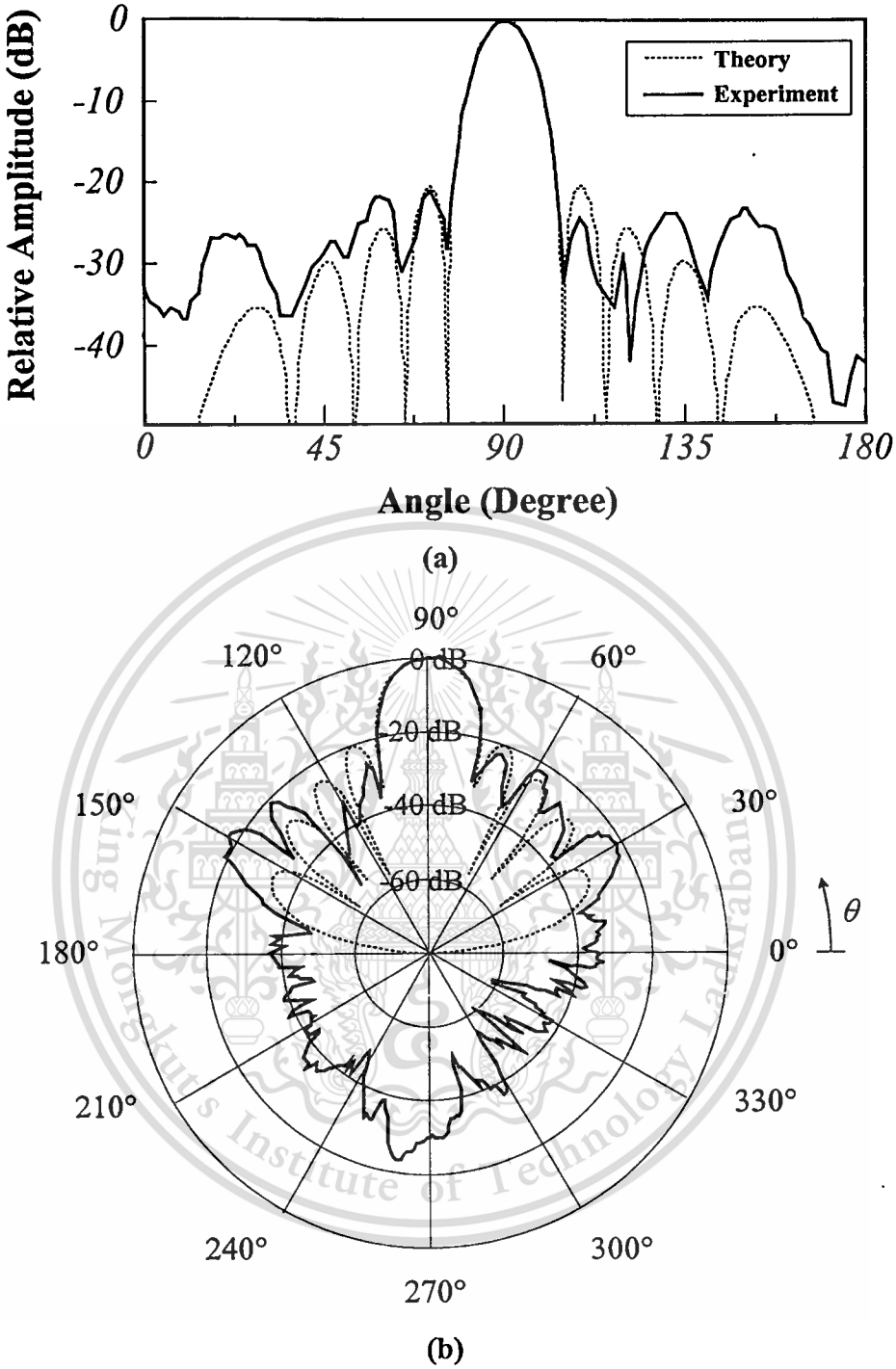

Fig.5.21 Radiation pattern of a linear slotted-waveguide second kind Tschebycheff array antenna

(a) Rectangular plot

(b) Polar plot

This material is reserved for educational use only, not allowed for commercial use.
Forbidden to modify the content, and cite the document when use.

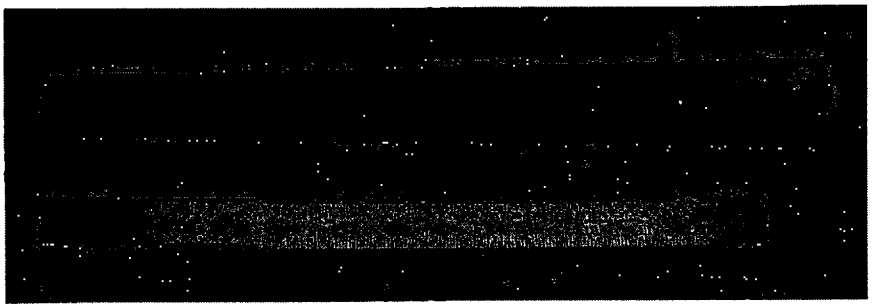

Fig.5.22 Photograph of the prototype fabricated antenna

The application of the second kind Tschebyscheff polynomial to synthesize the pattern of linear slotted-waveguide array antenna is presented in this paper. The pattern multiplication plays a significant role in determining the total radiation by multiplying the array factor with the element pattern. The constructed antenna was measured the radiation pattern and it was found that the experimental results are in good agreement with the theoretical ones. Accordingly, it can verify that the synthesis principle can be used in practical application efficiently.

5.8 Conclusions

From the theoretical aspects as derived in the preceding chapter, this chapter demonstrates the numerical results. This chapter concentrates on the numerical results of the current distribution together with the radiation pattern. The uniform geometrical theory of diffraction plays an important tool to estimate the radiation pattern including the effect of the finite size ground plane. The radiation pattern for various sizes of the ground plane is illustrated. It is evident that the back lobe ratio is very high for the small size of the ground plane and it is lower as the size of the ground plane is larger and become no back lobe for the ground plane is infinite extent. Experimental results are set up to verify the theoretical principle. The application to synthesis the slotted waveguide array antenna using the second kind Tschebyscheff polynomials are demonstrated.

This material is reserved for educational use only, not allowed for commercial use.
Forbidden to modify the content, and cite the document when use.

CHAPTER 6
IMPEDANCE CHARACTERISTICS OF THE ANTENNA

In order to transfer power from a transmitter to the antenna or from the antenna to a receiver efficiently, impedance of the antenna must be characterized so that appropriate matching is achieved. In this chapter, input impedance of the antenna is calculated from the unknown coefficient of electric current along the probe. In addition, SWR (Standing Wave Ratio) and reflection coefficient are investigated. The comparisons between numerical and experimental results are illustrated to confirm the theoretical principle.

6.1 Input Impedance Characterizations

One of the significant parameters to judge the merit of an antenna is input impedance. To find the input impedance of a linear electric probe, the well-known relation is defined as

$$Z_{in} = \frac{V_{in}}{I_{in}} \tag{6.1}$$

where V_{in} denotes input voltage. I_{in} is input current, and Z_{in} is input impedance.
From chapter 2, the input voltage source is the delta gap source modeling. The amplitude of the delta gap source is assumed to be unity. The input current is the unknown electric current along the probe, J. Therefore, (6.1) can be expressed as

$$\begin{aligned} Z_{in} &= \frac{1}{I_{in}} \\ &= \frac{1}{J_p(y'=0)} \end{aligned} \tag{6.2}$$

where $$J_p(R') = \sum_{g=1}^{N_g} B_g j_g(R')$$

$$j_g(y') = \frac{1}{2}\left(1 + \sin\frac{g\pi}{2l_p}(y' + l_p)\right)$$

This material is reserved for educational use only, not allowed for commercial use.
Forbidden to modify the content, and cite the document when use.

The solutions of unknown electric current along the linear electric probe, solved by Method of Moments, are applied by following this relation

6.2 Reflection Coefficient and Standing Wave Ratio (SWR) Evaluations

The reflection coefficient and SWR are a quantity that is generally appeared in the antenna specification. It presents the resonance situation and the bandwidth of antenna. From input impedance in previous section, they are

$$\Gamma = \left| \frac{Z_o - Z_{in}}{Z_o + Z_{in}} \right| \tag{6.3}$$

$$SWR = \frac{1+\Gamma}{1-\Gamma} \tag{6.4}$$

6.3 Numerical Results

From the formulation to characterize the input impedance, the numerical results of input impedance (resistance and reactance) and SWR for various antenna parameters such as the cavity size, the location and the length of the probe, and location and length of slot are demonstrated. The dimensions of the antenna in the model are shown in Table 6.1 and 6.2. The operating frequency of *1.9* GHz is used throughout this section.

Table 6.1 Dimension of cavity backed-slot antenna: $a = 0.75\lambda$ or *11.94* cm

Antenna Parameter		
Cavity Height: b	0.375λ	*5.92* cm
Cavity Length: c	0.75λ	*11.84* cm
Slot Length: l_s	0.46λ	*7.26* cm
Slot Width: w_s	0.048λ	*0.76* cm
Slot Offset: x_s	0.56λ	*8.88* cm
Slot Offset: z_s	0.303λ	*4.78* cm
Probe Length: l_p	0.25λ	*3.94* cm
Probe Location: z_p	0.375λ	*5.92* cm
Probe Location: x_p	0.375λ	*5.92* cm
Probe Location: y_p	0.187λ	*2.96* cm

This material is reserved for educational use only, not allowed for commercial use.
Forbidden to modify the content, and cite the document when use.

Table 6.2 Dimension of cavity backed-slot antenna: $a = 0.69\lambda$ or *10.89* cm

Antenna Parameter		
Cavity Height: b	0.345λ	*5.44* cm
Cavity Length: c	0.69λ	*10.89* cm
Slot Length: l_s	0.46λ	*7.26* cm
Slot Width: w_s	0.048λ	*0.76* cm
Slot Offset: x_s	0.517λ	*8.17* cm
Slot Offset: z_s	0.303λ	*4.78* cm
Probe Length: l_p	0.25λ	*3.94* cm
Probe Location: z_p	0.345λ	*5.45* cm
Probe Location: x_p	0.345λ	*5.45* cm
Probe Location: y_p	0.173λ	*2.73* cm

6.3.1 Cavity Size

In this subsection, the input impedance and SWR for various sizes of a cavity are revealed. The frequency is varied to operate from *1.0* GHz to *2.6* GHz. There are four cavity sizes to be varied i.e. 0.55λ, 0.69λ, 0.75λ and 0.80λ. It is pointed that the ratio of each dimension of the cavity is still same as previous demonstration (a: b: c = *1*:*0.5*:*1*). Fig.6.1 (a), (b) and (c) show the resistance, reactance and SWR of the probe in x direction for various cavity sizes, respectively. It is apparent that when the cavity size becomes larger, both resistance and reactance exhibit lower values. In addition, the resonance frequency (zero reactance) is inverse proportional to the cavity sizes. The larger the cavity sizes the lower the resonance frequency. For the matching situation, these four cavity sizes posses the value of lowest SWR almost identical but the optimum matching frequency is increased as the smaller cavity sizes.

In the similar fashion, the impedance characteristic for the probe aligned on y direction are illustrated in Fig. 6.2 (a) through (c). It is found that the larger cavity sizes provide the higher both the resistance and reactance. However, the relation between the resonance frequency and the cavity sizes is the same as the case of probe in x direction. The optimum matching frequencies for these four cavity sizes are almost the same manner. It is mentioned that comparing with two cases of the probe excitation the value of both the resistance and reactance of y directed probe is much higher than those of the x directed probe.

reserved for educational use only, not allowed for commercial use.
Forbidden to modify the content, and cite the document when use.

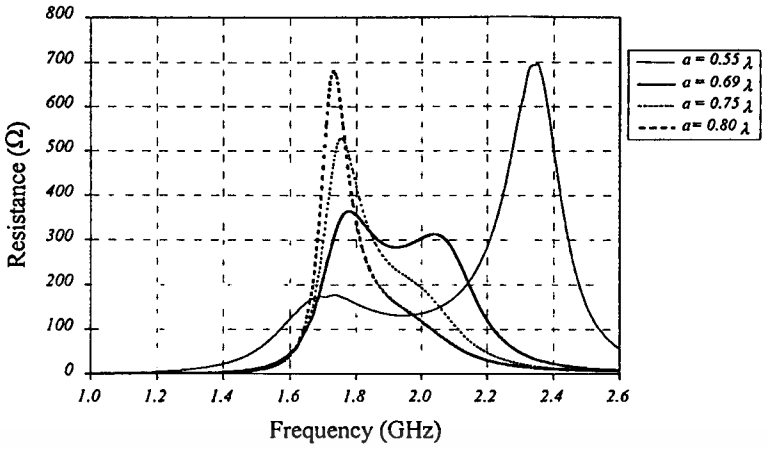

(a)

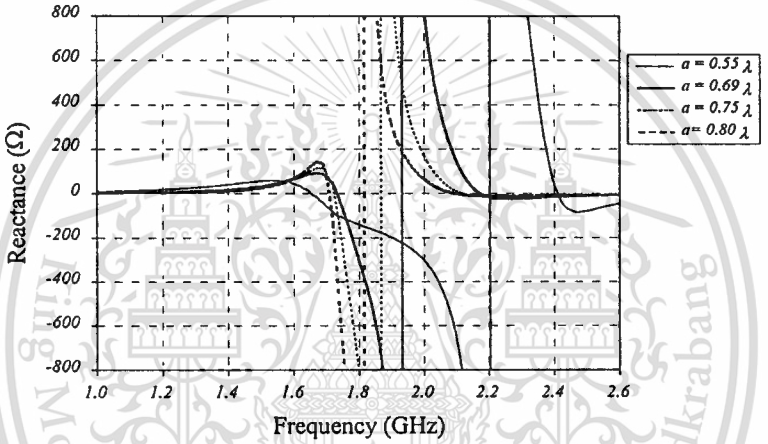

(b)

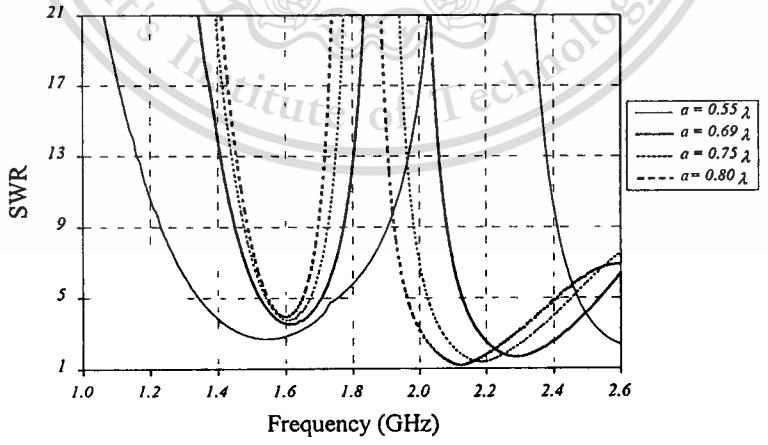

(c)

Fig.6.2 Input Impedance of *y* direction probe for various cavity widths: *a*

(a) Resistance

(b) Reactance

(c) SWR

This material is reserved for educational use only, not allowed for commercial use.
Forbidden to modify the content, and cite the document when use.

6.3.2 Probe Location

In order to improve the resonance and matching condition, the positions of the probe can be adjusted. Firstly, the probe is aligned on x-axis. The positions in y and z-axis can be varied. Figs.6.3 and 6.4 illustrate the resistance, reactance and SWR for different locations of the probe y_p and z_p, respectively. Secondly, the probe is oriented on y direction. Therefore, the location x_p and z_p can be varied as shown in Figs. 6.5 and 6.6, respectively. From these figures, we can summarize the relation between the resonance and matching events and the locations of the probe.

For probe in x direction

- Different y_p

From Fig. 6.3 (a)-(c), it is evident that when the location of the probe is varied in y direction from y_p equal *0.25b, 0.50b* and *0.75b*, respectively both the resistance and reactance have the same trend. When the probe is moved further from the origin the nominal resistance and reactance become higher. Additionally, the resonance frequencies of these locations occur at the same frequency. Moreover, the well-matched condition can be achieved when y_p is equal to *0.75b*. The SWR becomes worse as the probe locations are closed to the origin.

- Different z_p

The impedance characteristic for different z_p is depicted in Figs. 6.4 (a)-(c). It is apparent that the resistance and reactance for z_p equal *0.50c* is the highest due to the strongest effect from the slot. Furthermore, they convert to smaller value as the distance from the slot. Also, the optimum matching condition can be accomplished when the probe is oriented near the slot.

Fig. 6.5 shows the impedance characteristic for different x_p. It can be observed that the maximum resistance and reactance occur at x_p equal *0.5a* and they are decreased as the displacement far from the center of cavity. It is noted that the coupling between the slot and the probe in this case is slight. The resonance frequency for any probe locations is still the same. The matching condition is better as the distance is further from the cavity center.

- Different z_p

In Fig. 6.6, it is obvious that the resistance, reactance and SWR have the same tendency, as the different x_p except for the symmetry of them can not be completely obtained.

This material is reserved for educational use only, not allowed for commercial use.
Forbidden to modify the content, and cite the document when use.

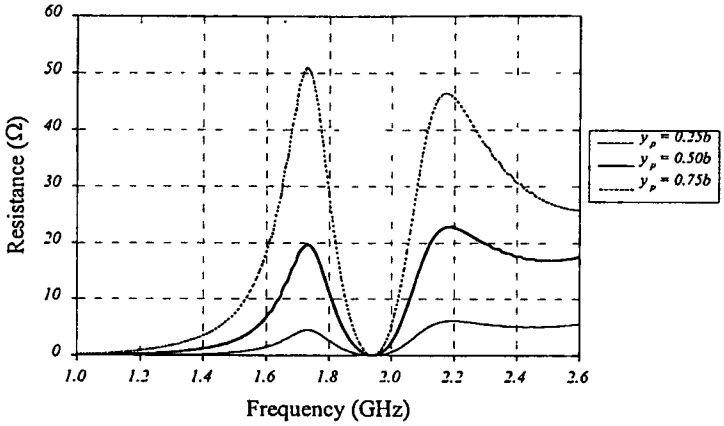

(a)

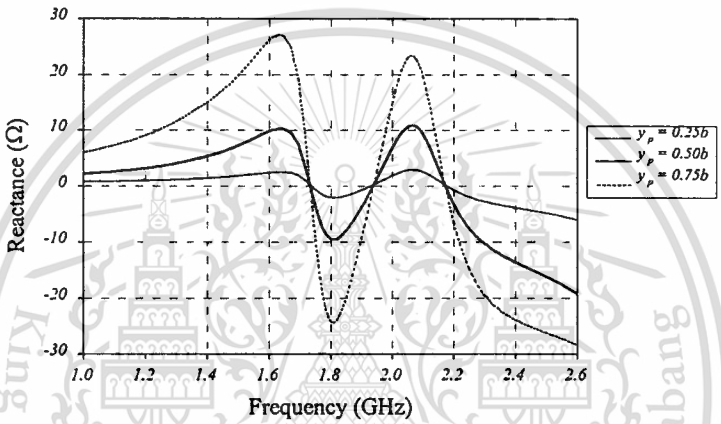

(b)

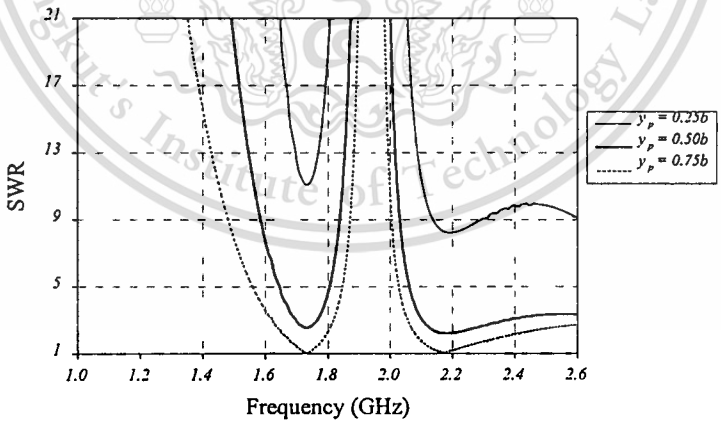

(c)

Fig.6.3 Input Impedance for various x direction probe locations: y_p

(a) Resistance (b) Reactance (c) SWR

This material is reserved for educational use only, not allowed for commercial use.
Forbidden to modify the content, and cite the document when use.

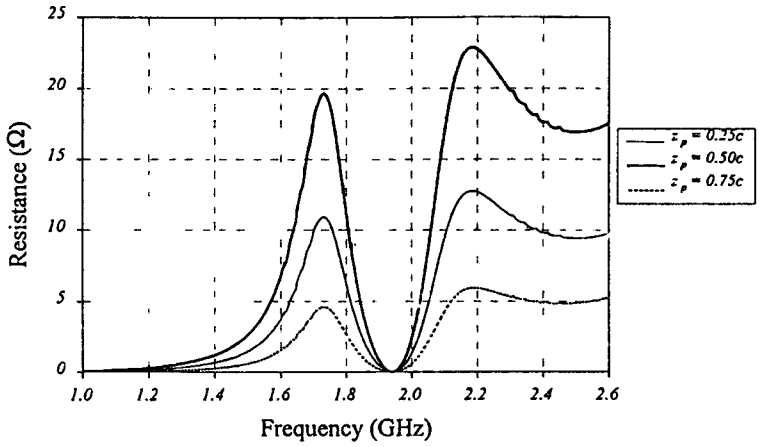

(a)

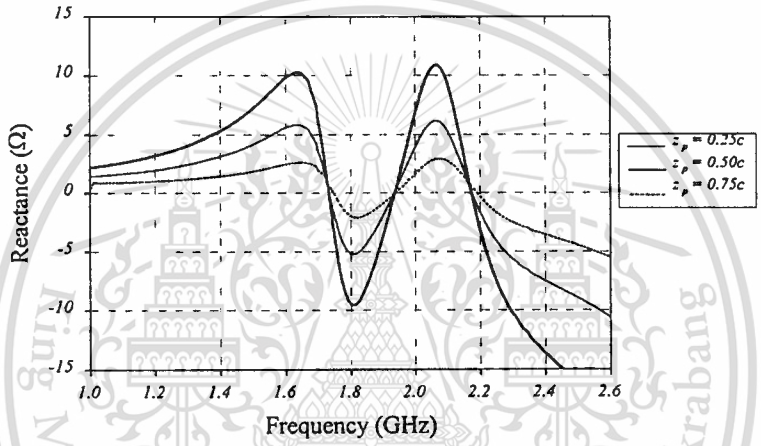

(b)

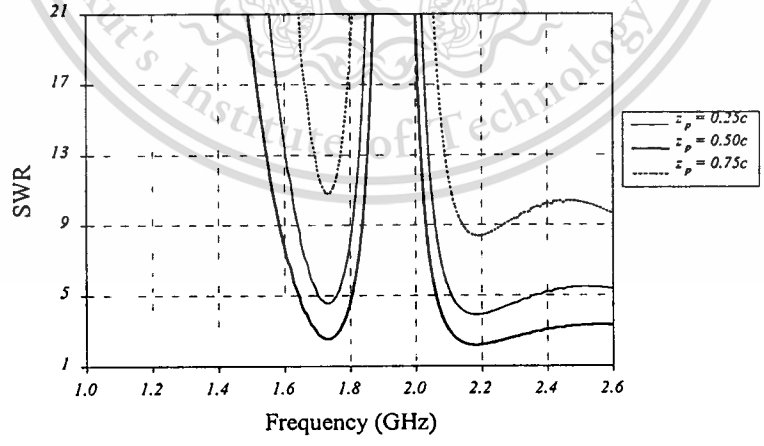

(c)

Fig.6.4 Input Impedance of x direction probe for various probe locations: z_p

(a) Resistance

(b) Reactance

(c) SWR

This material is reserved for educational use only, not allowed for commercial use.
Forbidden to modify the content, and cite the document when use.

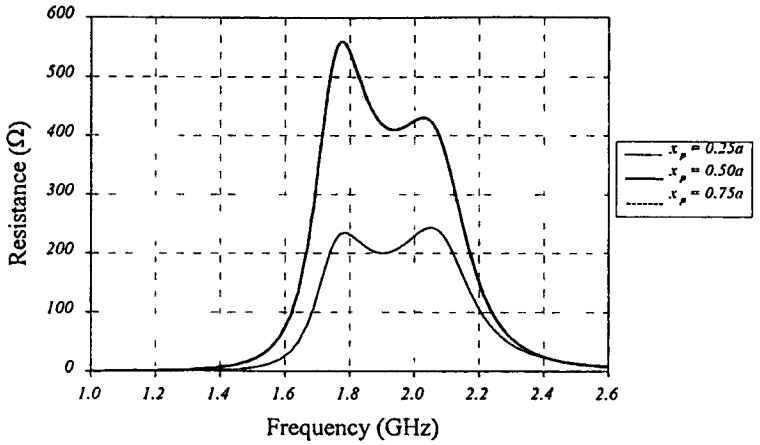

(a)

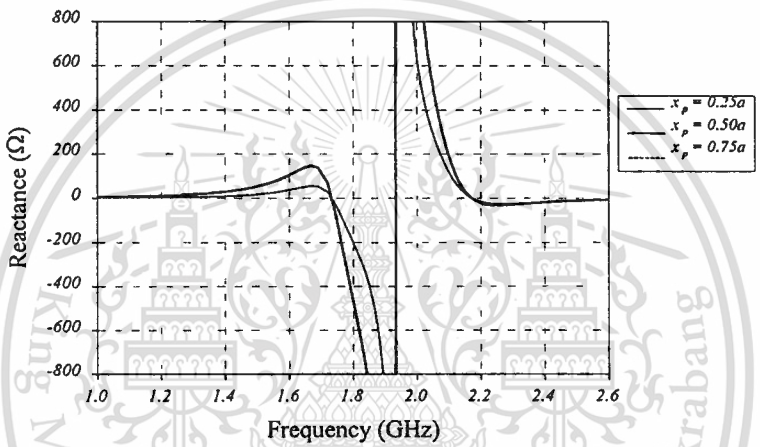

(b)

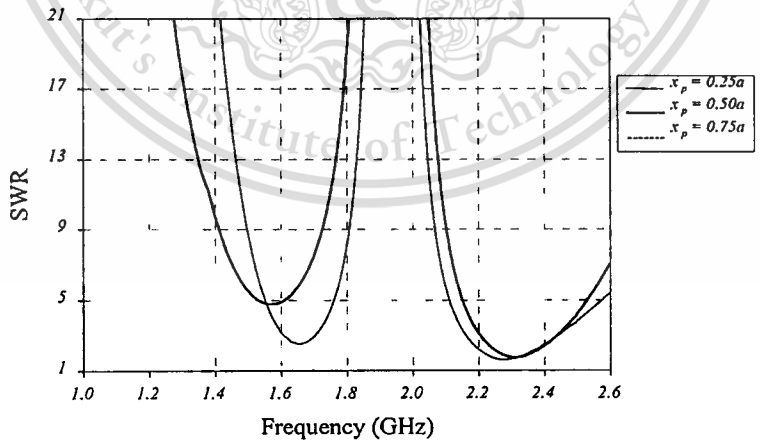

(c)

Fig.6.5 Input Impedance for various *y* direction probe locations: x_p

(a) Resistance

(b) Reactance

(c) SWR

This material is reserved for educational use only, not allowed for commercial use.
Forbidden to modify the content, and cite the document when use.

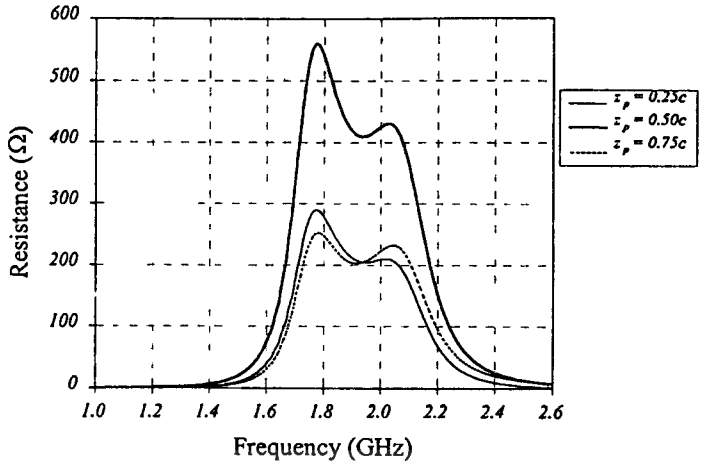

(a)

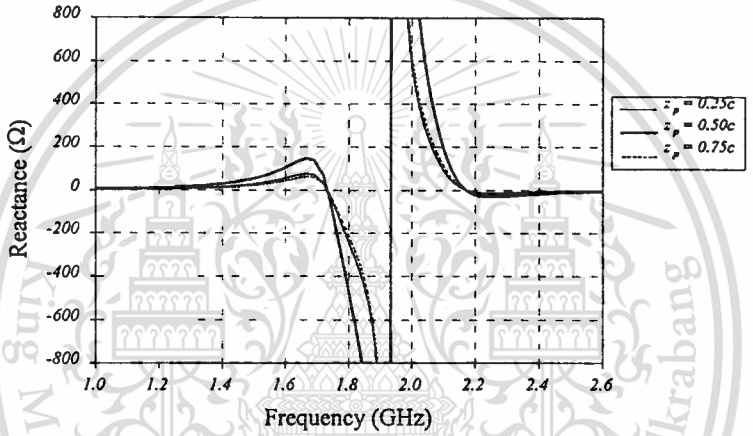

(b)

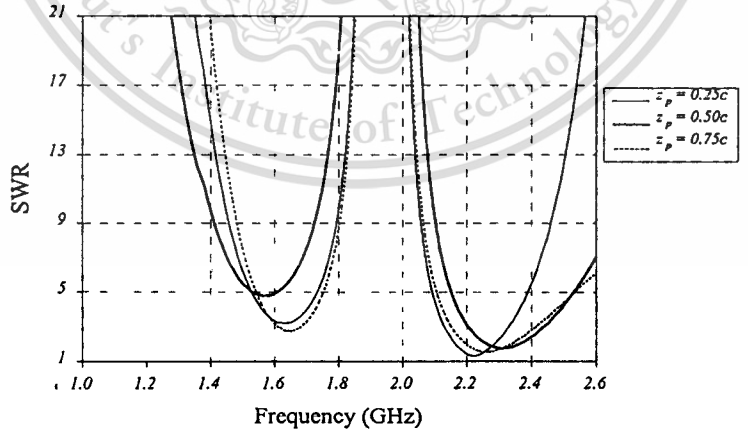

(c)

Fig.6.6 Input Impedance of *y* direction probe for various probe locations: z_p

(a) Resistance

(b) Reactance

(c) SWR

This material is restricted for educational use only, not allowed for commercial use.
Forbidden to modify the content, and cite the document when use.

6.3.3 Probe Length

One easy way to optimize the matching condition is to trim the probe to be lengthen or shorten. The relation between the impedance and SWR, and the probe length is revealed in Fig.6.7 and 6.8 for the probe in x and y direction, respectively. It is clarified that the nominal resistance and reactance for two cases of excitation are higher as the length of the probe. The resonance frequencies for any probe length are identical.

For the SWR, it is found that the matching situation is opposite to each other between the probe in x and y direction. If the probe is excited along the x-axis the longer probe yield better SWR than that the shorter one. In contrary, for y direct probe the shorter probe length exhibit better SWR than that the longer counterpart.

This material is reserved for educational use only, not allowed for commercial use.
Forbidden to modify the content, and cite the document when use.

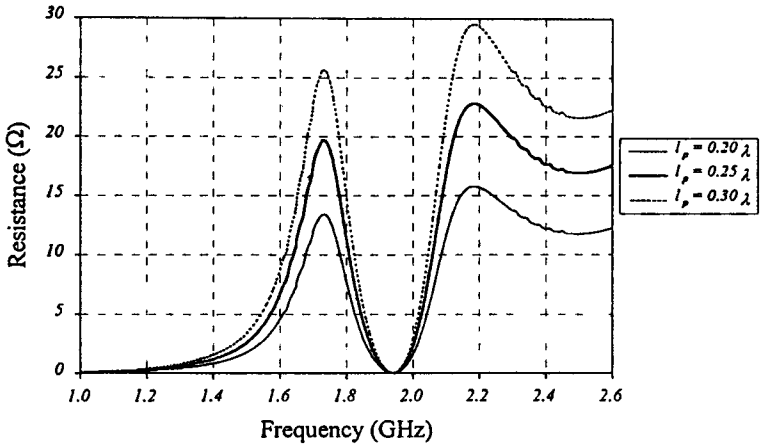

(a)

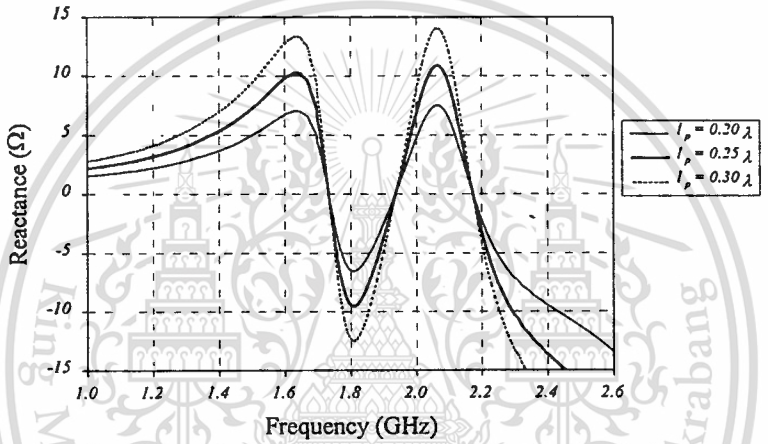

(b)

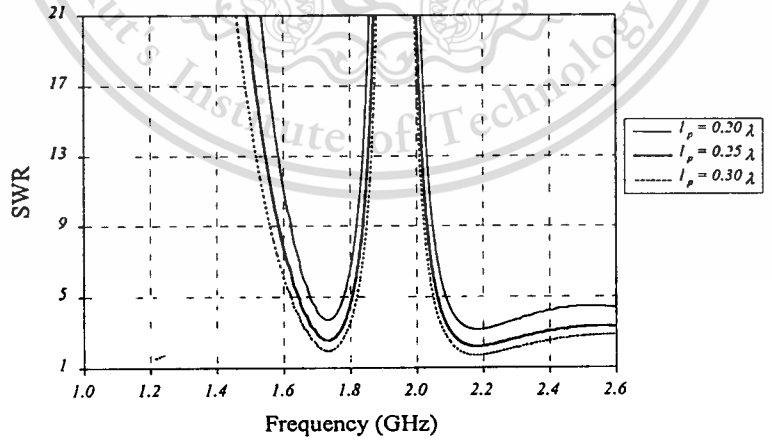

(c)

Fig.6.7 Input Impedance of x direction probe for various probe lengths: l_p

(a) Resistance

(b) Reactance

(c) SWR

This material is reserved for educational use only, not allowed for commercial use.
Forbidden to modify the content, and cite the document when use.

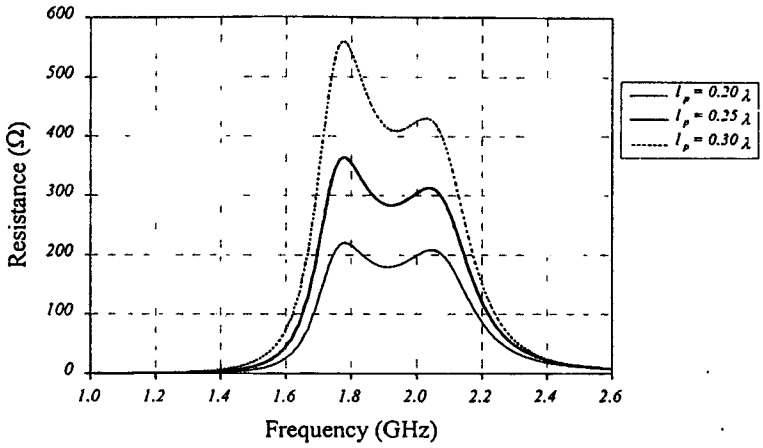

(a)

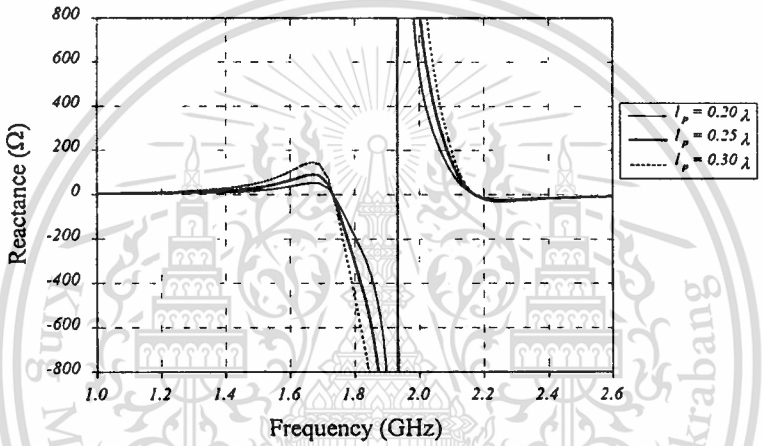

(b)

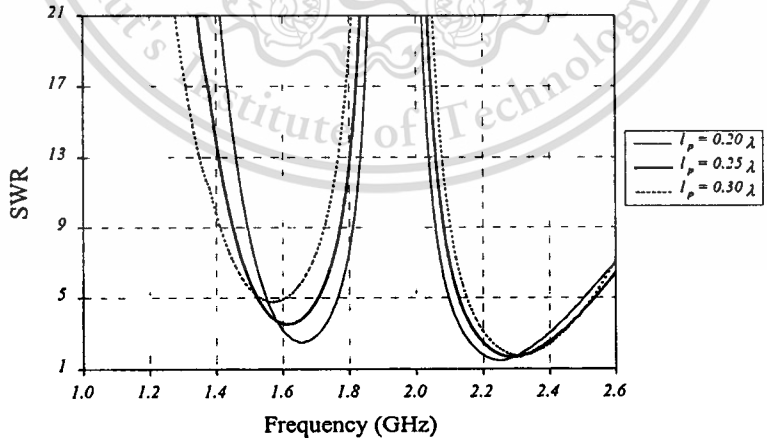

(c)

Fig.6.8 Input Impedance of y direction probe for various probe lengths: l_p

(a) Resistance

(b) Reactance

(c) SWR

This material is protected for educational use only, not allowed for commercial use.
Forbidden to modify the content, and cite the document when use.

6.3.4 Slot Offset

The positions of the slot orientation in x and z directions referred to as the slot offset are of interest variables. They are varied to modify the nominal impedance of the antenna. The impedance of various slot offsets x_s and z_s for the probe excited in x and y direction are shown in Fig.6.9 through Fig.6.12, respectively. The following abridgements are observed.

For probe in x direction

- Different x_s

From Fig. 6.9, the resistance and reactance when the slot is located at the center of the cavity as very small value (no greater than *3* Ω) and it increases as the slot offset is higher. The good matching condition for the slot with x_s equal *0.5a* can not be realized because the SWR is very high (more than *15:1*).

- Different z_s

The resistance, reactance and SWR for various z_s in case of the probe is excited in x direction almost identical as shown in Fig. 6.10. Hence, the variation of the slot in z direction is not affected to the impedance characteristic. The impedance characteristic can be improved by this way.

For probe in y direction

- Different x_s

It is evident from Fig. 6.11 that the impedance for the slot located near the center of the cavity is relatively high. This impedance will be decreased as the offset of the slot. In addition, the near optimum matching situation can be obtained.

- Different z_s

The resistance, reactance and SWR of the antenna excited by the probe in y direction for various z_s are revealed in Fig. 6.12. The resistance and reactance are drastically increased as the distance away from the origin. The resonance frequency for the further distance is higher than the closer case. Similarly, the best matching condition can be completed at the higher frequency for the further distance from the origin.

This material is reserved for educational use only, not allowed for commercial use.
Forbidden to modify the content, and cite the document when use.

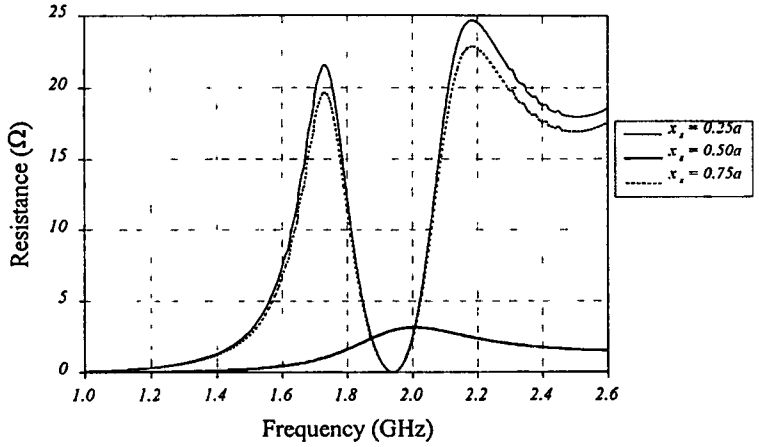

(a)

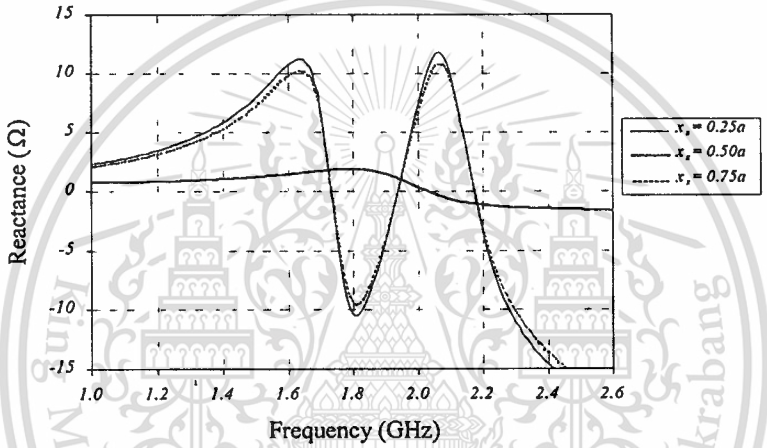

(b)

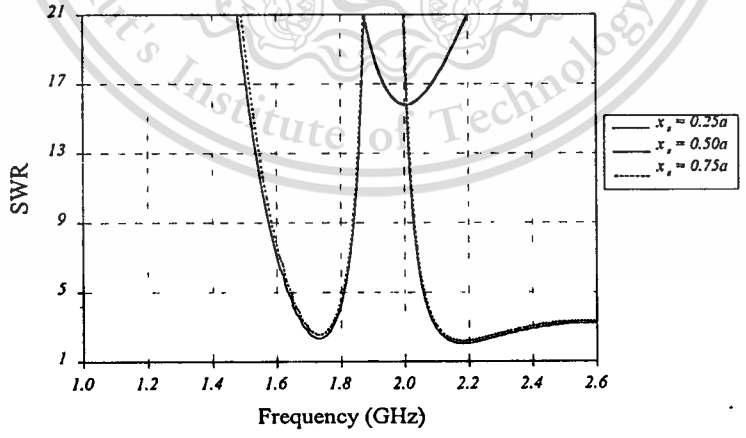

(c)

Fig.6.9 Input Impedance of x direction probe for various slot offsets: x_s

(a) Resistance

(b) Reactance

(c) SWR

This material is reserved for educational use only, not allowed for commercial use.
Forbidden to modify the content, and cite the document when use.

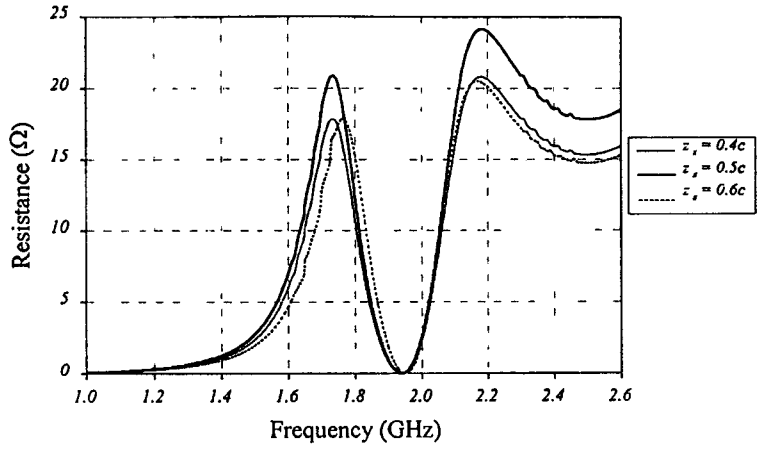

(a)

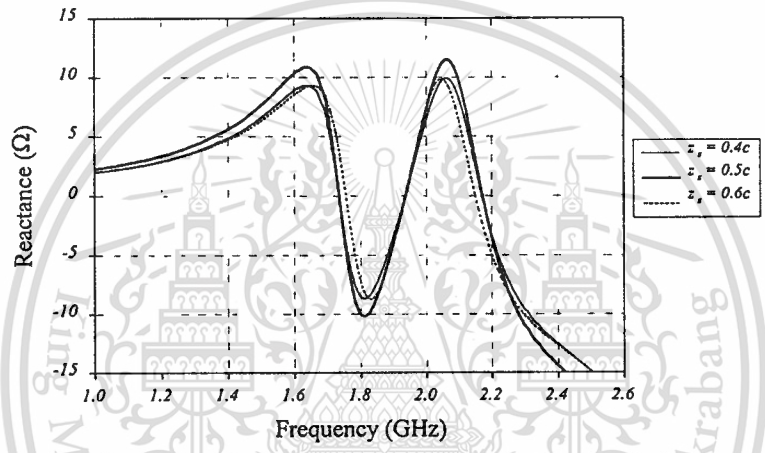

(b)

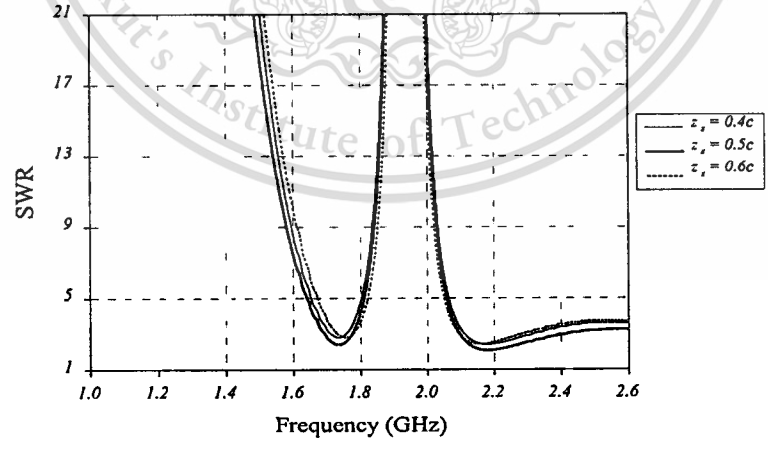

(c)

Fig.6.10 Input Impedance of x direction probe for various slot offsets: z_s

(a) Resistance

(b) Reactance

(c) SWR

This material is for educational use only, not allowed for commercial use.
Forbidden to modify the content, and cite the document when use.

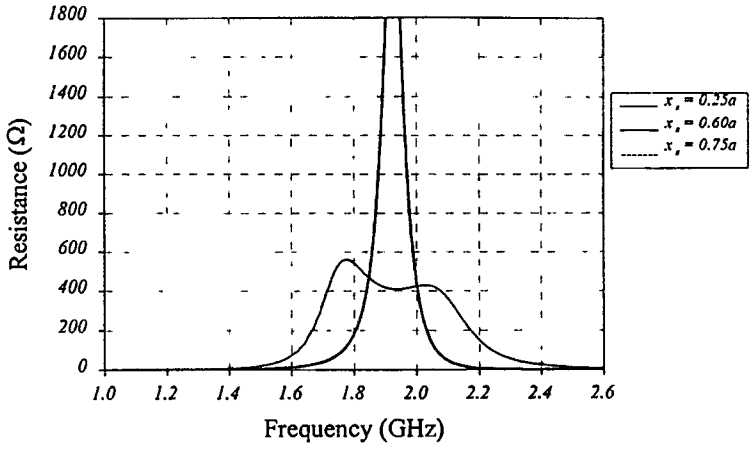

(a)

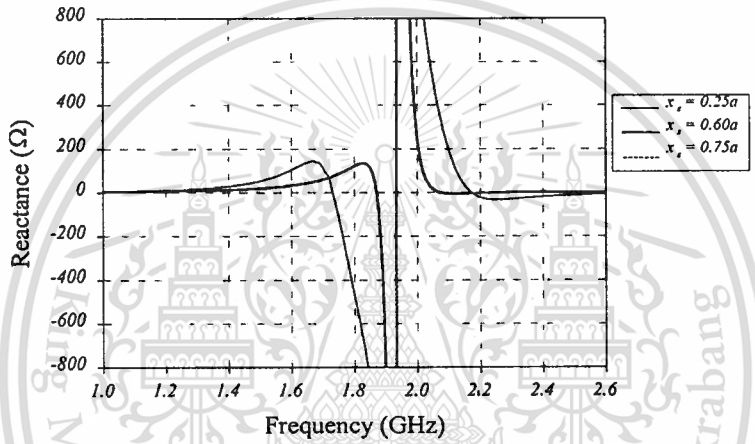

(b)

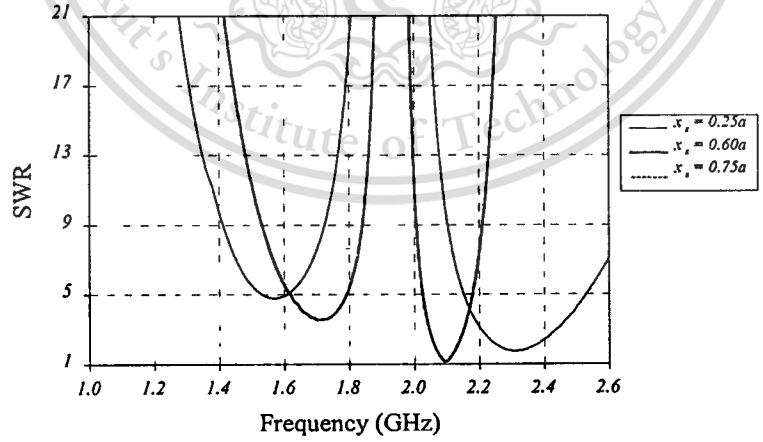

(c)

Fig.6.11 Input Impedance of *y* direction probe for various slot offsets: x_s

(a) Resistance

(b) Reactance

(c) SWR

This material is reserved for educational use only, not allowed for commercial use.
Forbidden to modify the content, and cite the document when use.

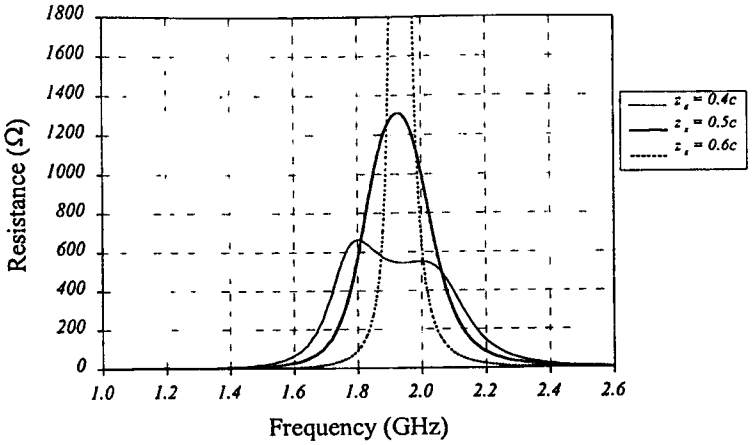

(a)

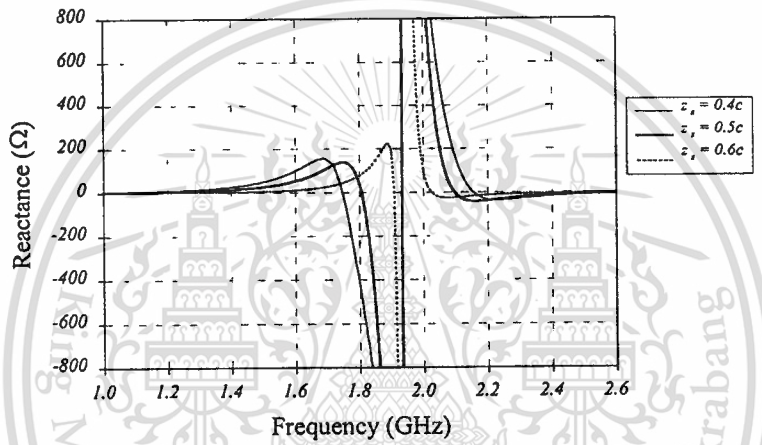

(b)

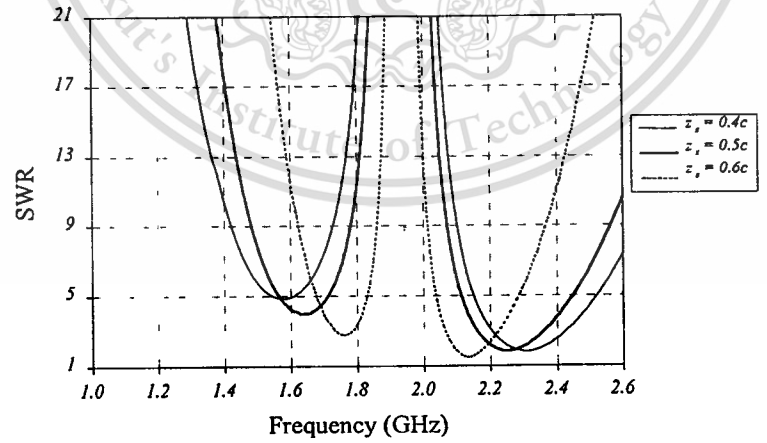

(c)

Fig.6.12 Input Impedance of *y* direction probe for various slot offsets: z_s

(a) Resistance

(b) Reactance

(c) SWR

This material is reserved for educational use only, not allowed for commercial use.
Forbidden to modify the content, and cite the document when use.

6.3.5 Slot Length

The variation of the slot length is an alternative way to find the resonance and optimum-matching situation. It can be seen from Fig.6.13 and 6.14 (for the probe excited in x and y direction, respectively) that for the case of demonstration, the resonance phenomenon is significantly changed as the slot length. Both the probe located in x and y direction, the value of the resistance and reactance are slightly different. The resonance frequency for the shorter slot length is higher than the longer ones. The frequencies yielding the optimum matching condition also have the same tendency. The difference is that SWR for various probe lengths of x directed probe gives the same value whereas that of y directed probe performs the different one. The longer the slot the lower the SWR and vice versa.

King Mongkut's Institute of Technology Ladkrabang

This material is reserved for educational use only, not allowed for commercial use.
Forbidden to modify the content, and cite the document when use.

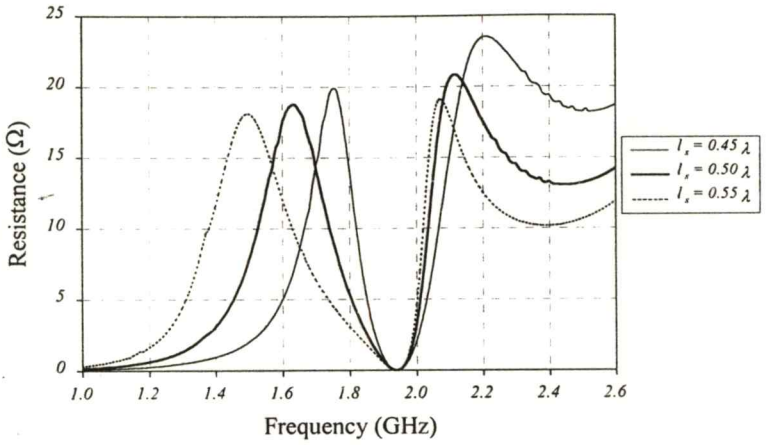

(a)

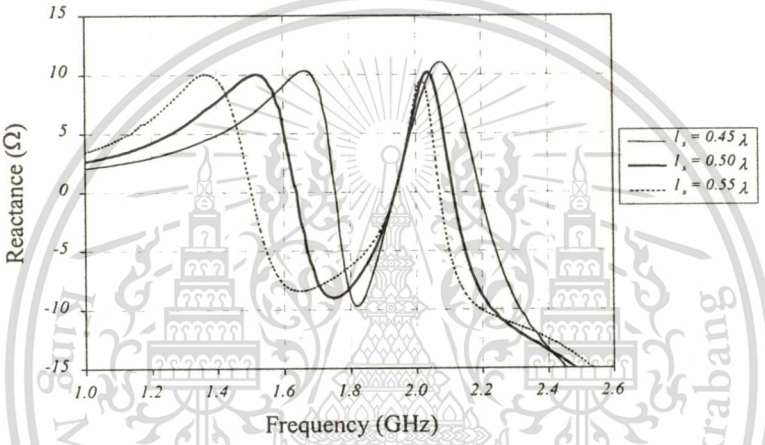

(b)

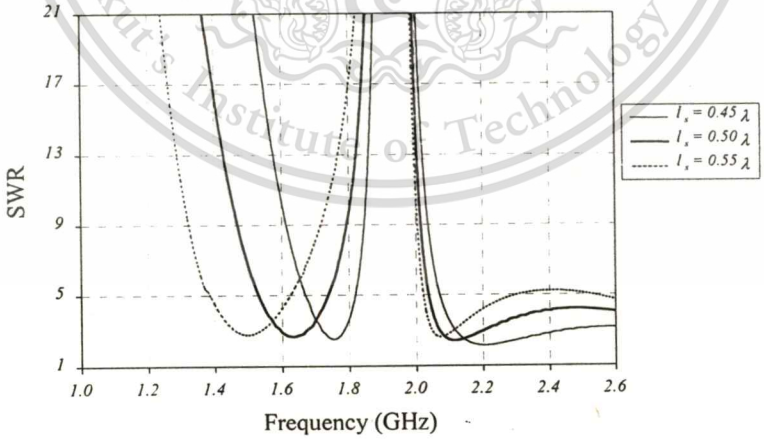

(c)

Fig.6.13 Input Impedance of x direction probe for various slot lengths: l_s

(a) Resistance

(b) Reactance

(c) SWR

This material is reserved for educational use only, not allowed for commercial use.
Forbidden to modify the content, and cite the document when use.

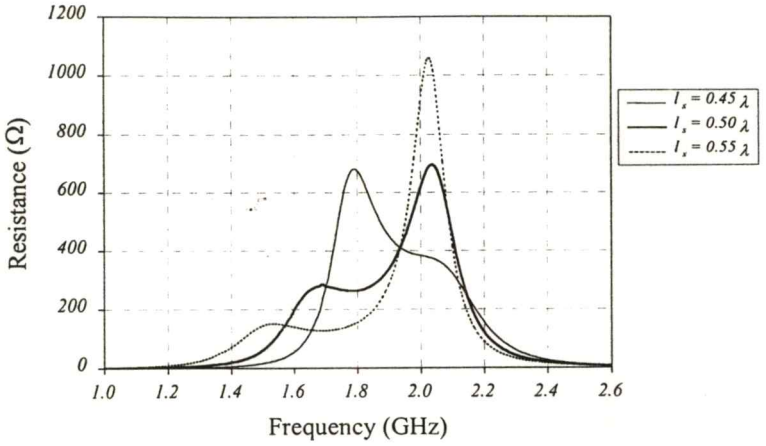

(a)

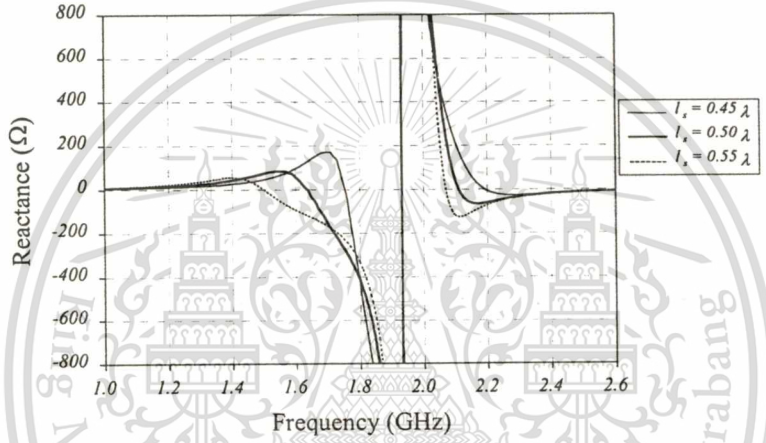

(b)

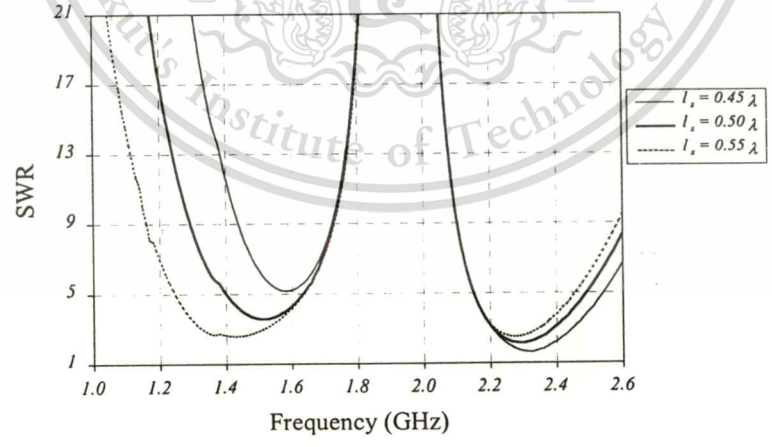

(c)

Fig.6.14 Input Impedance of *y* direction probe various slot lengths: l_s

(a) Resistance

(b) Reactance

(c) SWR

This material is reserved for educational use only, not allowed for commercial use.
Forbidden to modify the content, and cite the document when use.

6.4 Experimental Results

To verify the calculated results, the impedance characteristic measurements are set up to operate at the frequency of *1.9* GHz. The prototype of the cavity-backed slot antenna fed by linear electric probe at which the dimensions are tabulated in Table IV. The photographs of the fabricated antenna are depicted in Fig. 6.15. Fig. 6.15 (a) reveals the perspective view of the cavity-backed slot antenna without ground plane. Fig. 6.15 (b) illustrates the rear of the antenna with the ground plane of 3λ. Fig. 6.15 (c) shows the front view of the slot on the ground plane.

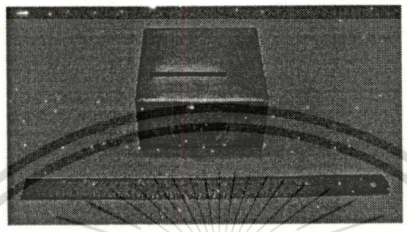

(a)

(b)

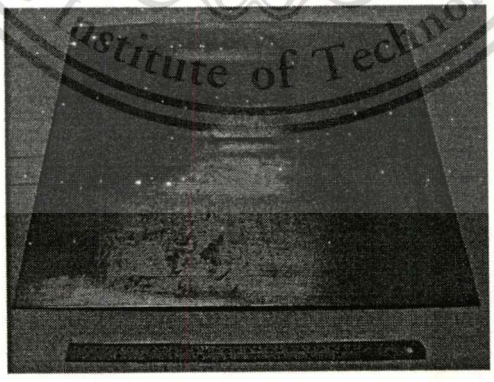

(c)

Fig.6.15 Photograph of prototype antenna cavity width 0.75λ

(a) without ground plane

(b) back view of antenna with ground plane 3λ

(c) front view of antenna with ground plane 3λ

This material is reserved for educational use only, not allowed for commercial use.
Forbidden to modify the content, and cite the document when use.

The fabricated antenna is connected to the HP8150C network analyzer via *50* Ω transmission line to measure the reflection and SWR. The resultants of the measurement are plotted and compared with theoretical prediction as shown in Fig. 6.16. It is obvious that the results are in good agreement. The frequency shift is *3.46* %. This error is due to the assumption that the ground plane is infinite extent but the finite ground plane is used in actual experiments.

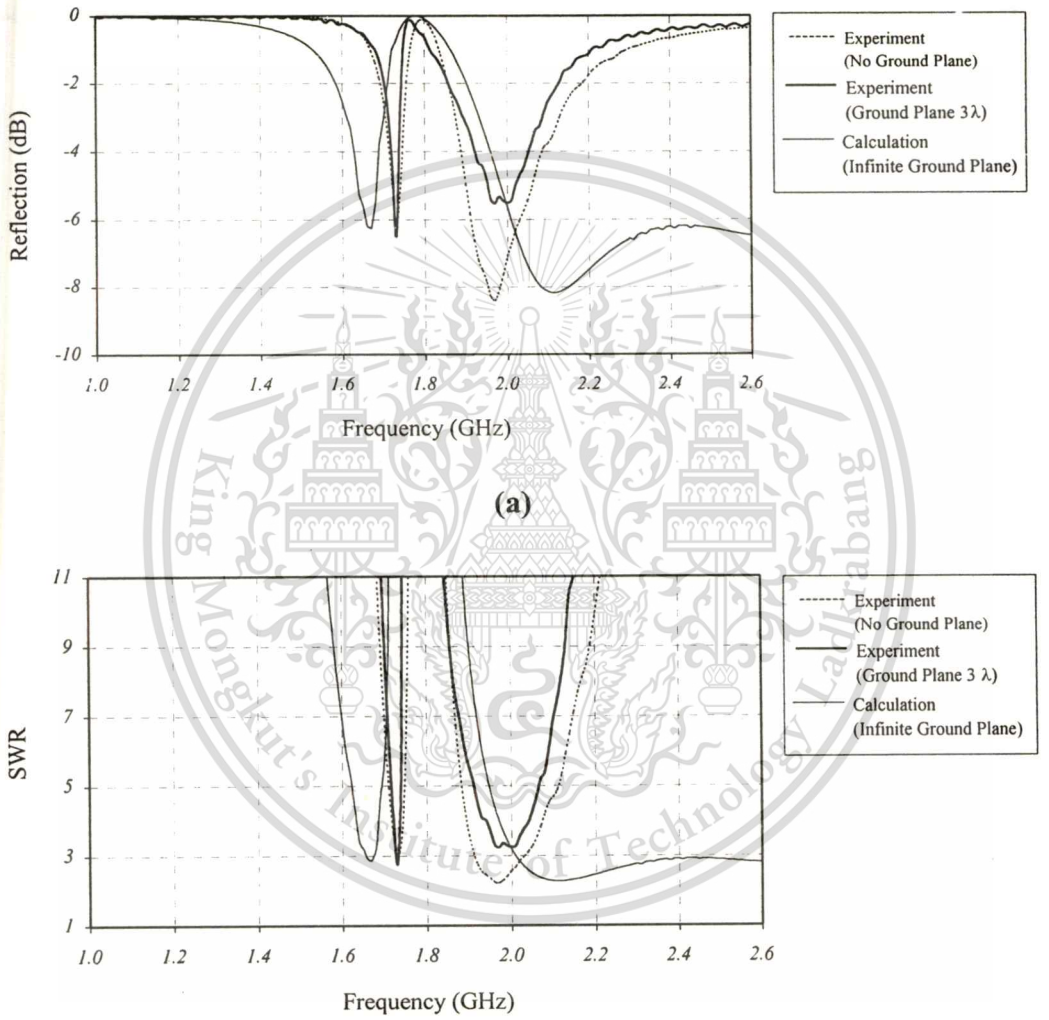

Fig.6.16 Impedance characteristic of antenna for probe in *x* direction and 0.75λ cavity width

(a) Reflection (dB)

(b) SWR

This material is reserved for educational use only, not allowed for commercial use.
Forbidden to modify the content, and cite the document when use.

$$Z_D = -R_D + jX_D$$

$$Z_L = R_L + jX_L$$

At the steady-state oscillating frequency (f_o), the conditions for oscillation can be expressed as:

$$R_L(f_o) = R_D(f_o)$$

$$X_L(f_o) = -X_D(f_o)$$

As aforementioned, the important parameter for oscillation condition is impedance of antenna. Therefore, the characteristic input impedance predictions of antenna from previous section are applied to set up the oscillation situation for active antenna.

Fig.6.19 Experiment of active antenna

In order to obtain the radiated power of active antenna, Friis Transmission Equation are used. It can be written as

$$P_r(\text{dBm}) - P_t(\text{dBm}) = 20\log\left(\frac{\lambda}{4\pi R}\right) + G_r(\text{dBi}) + G_t(\text{dBi}) \qquad (6.5)$$

where P_r is receiving power, collected by standard horn antenna. P_t denotes the output power of active antenna. G_r and G_t are gain of standard horn antenna and slot antenna, respectively. R represents distance between the standard horn antenna and slot antenna.

This material is reserved for educational use only, not allowed for commercial use.
Forbidden to modify the content, and cite the document when use.

From experimental situation in Fig.6.19, the gains of horn antenna and slot on ground plane are *18.13* and *5.17* dBi, respectively. *R* is *1* m. The measurement power from *IFR* AN930A Spectrum Analyzer is *–52.5* dBm as shown in Fig.6.20. Hence the radiated power from slot active antenna is *7.21* μW.

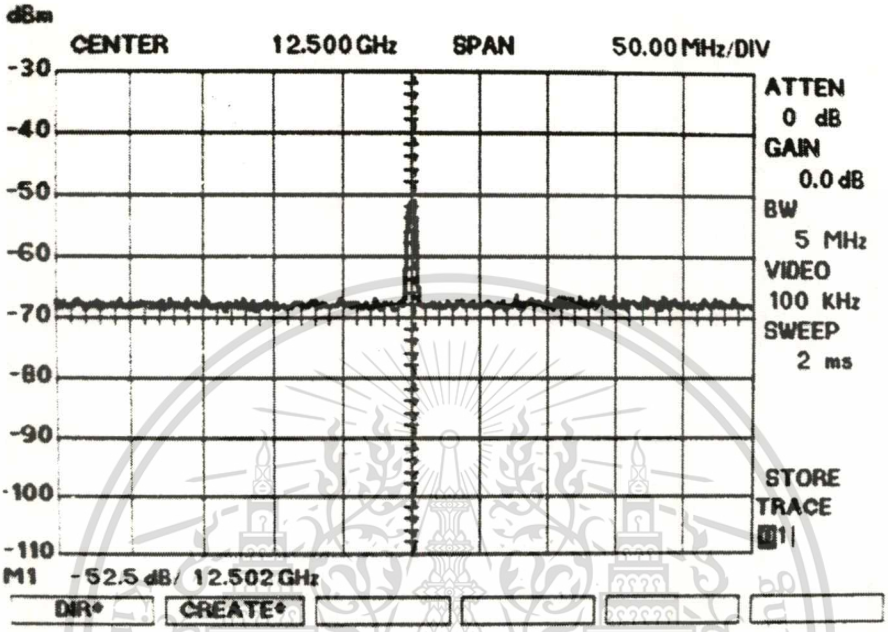

Fig.6.20 Experimental result from spectrum analyzer

6.6 Conclusions

The impedance characteristics of the rectangular cavity-backed slot antenna are analyzed in this chapter. The antenna parameters are varied to find the resonance and optimum matching condition. The experimental results are confirmed the theoretical predictions. The further application of the impedance characteristics can be used in the design of the active antenna.

This material is reserved for educational use only, not allowed for commercial use.
Forbidden to modify the content, and cite the document when use.

CHAPTER 7
DISCUSSIONS AND CONCLUSIONS

Summary of the gist in this thesis and the remark for future researches in this field are performed in this chapter.

7.1 Summary of Preceding Chapters

This thesis is concerned with the analysis of the antenna using the slot on the rectangular cavity excited by the probe at which the geometry of the problems is depicted in Chapter 2. The analysis model is divided into two canonical regions corresponding to the discontinuity in structure. The integral equations of the unknown currents are formulated at the excited probe and the slot aperture. The integral equations are written in terms of the integration of the products of the unknown currents and the dyadic Green's functions. The details of derivation of dyadic Green's function are shown in Chapter 3. The method of magnetic dyadic Green's function is used since it is straightforward and requires only two solenoidal vector wave functions. The eigenfunction expansion technique together with the scattering superposition approach is applied to determine various kinds of dyadic Green's functions. Then, these integral equations are solved by using Method of Moments as describes in Chapter 4. The entire domain sinusoidal basis function with the Galerkin's method is selected to determine the unknown current distributions.

From the theoretical feature as mentioned above, the numerical results of the current distribution and radiation characteristics are revealed in Chapter 5. By combing the uniform geometrical theory of diffraction with the Method of Moments, the radiation pattern with the finite size ground plane is carried out. The radiation patterns of the antenna for various sizes of the ground plane are shown. In addition, in order to validate the theoretical radiation pattern, the experiments are performed. Subsequently, the impedance characteristics for various antenna parameters are demonstrated to find the resonance and optimum matching conditions as in Chapter 6. Experimental results for some cases are set up to verify the theoretical predictions.

Finally, the summary of the material in the thesis and the discussion for the future studies of the researches in this field is included in Chapter 7, the last chapter. Appendices are composed of the trigonometric and exponential functions, scalar,

This material is reserved for educational use only, not allowed for commercial use.
Forbidden to modify the content, and cite the document when use.

vector and dyadic analyses, derivation of dyadic Green's function in three-based directions, some orthogonal relationships of the vector wave functions and integration of reaction expressions for external region.

7.2 Remark for future researches in this field

According to preceding chapters, there are four schemes for further investigations.

(a) In view of input impedance, the size of ground plane is strongly affected to accuracy of input impedance. Therefore, the external dyadic Green's function should be considered edge effect from ground plane by using hybrid method of GTD and Method of Moments [43].

(b) The enhancement of input impedance accuracy relies upon type of source model. The delta gap is the simplest way but it is neglected the radius of linear electric probe, which may be much low accuracy in some cases. The multifilament method is attractive procedure because it can be considered radius of linear electric probe. Moreover, to obtain more accuracy results it can be increased the number of filament along probe and on coaxial aperture.

(c) Radiation pattern of slot on finite size ground plane should be analyzed not only the edge effect but vertex or corner effects as well. The small size of ground plane is substantially impact from vertex diffraction fields.

(d) The wall thickness of cavity must be taken into account because the mutual coupling between slot and probe are considerably changed. The radiation pattern and input impedance would be analyzed more correctly.

This material is reserved for educational use only, not allowed for commercial use.
Forbidden to modify the content, and cite the document when use.

REFERENCES

[1] Stevenson A.F. "Theory of slots in rectangular wave-guides." J. Appl. Phys., vol. 19, no. 1, Jan.1948. pp. 24-38.

[2] Galejs J. "Admittance of rectangular slot which is backed by a rectangular cavity." IEEE Trans. Antennas Propagat., vol. 11, no. 3, Mar.1963. pp. 119-126.

[3] Ando M., Sakurai K., Goto N., Arimura K., and Ito Y. "A radial line slot antenna for 12 GHz satellite TV reception." IEEE Trans. Antennas Propagat., vol. 33, no. 12, Dec.1985. pp. 1347-1353.

[4] Oliner A.A. "The impedance properties of narrow radiating slots in the broad face of the rectangular waveguide, Part I and Part II." IRE Trans. Antennas Propagat., vol. AP-5, Jan. 1957. pp. 4-20.

[5] Long S.A. "Experimental study of the impedance of cavity-backed slot antenna." IEEE Trans. Antennas Propagat., vol. AP-23, no.1, Jan 1975. pp. 1-7.

[6] Khac T.V. and Carson C.T. "Impedance properties of a longitudinal slot antenna in the broad face of a rectangular wavguide." IEEE Trans. Antennas Propagat., vol. 21, no. 9, Sep. 1973. pp. 708-710.

[7] Lyon R.W. and Sangster A.J. "Efficient moment method analysis of radiating slots in a thick-walled rectangular waveguide." Proc. IEEE, vol. 128, Aug. 1981. pp. 197-205.

[8] Elliott R.S. "An improved design procedure for small arrays of shunt slots." IEEE Trans. Antennas Propagat., vol. AP-31, no. 1, Jan 1983. pp. 48-53.

[9] Josefsson L.G. "Analysis of longitudinal slots in rectangular waveguide." IEEE Trans. Antennas Propagat., vol. AP-35, no.12, Dec. 1987. pp. 1351-1357.

[10] Harrington R. "Origin and development of the Method of Moments for field computation." IEEE Antennas Propagat. Soc. Mag., June. 1990. pp. 31-35.

[11] Hirokawa J., Ando M., and Goto N. "Waveguide-fed parallel plate slot array antenna." IEEE Trans. Antennas Propagat., vol. 40, no.2, Feb.1992. pp. 218-223.

[12] Hashemi-Yaganeh S. and Birtcher C. "Theoretical and experimental studies of cavity-backed slot antenna excited by a narrow strip." IEEE Trans. Antennas Propagat., vol. 41, no. 2, Feb. 1993. pp. 236-241.

[13] Takada J., Araoka N. and Tanisho A. "Method of moments analysis of small aperture radial line slot slot antenna using the rectangular cavity Green's

This material is reserved for educational use only, not allowed for commercial use.

Forbidden to modify the content, and cite the document when use.

function." IEE Proc.-Microw. Antennas Propag., vol. 144, no. 6, Dec 1997. pp. 498-500.

[14] Lertwiriyaprapa T., Phongcharoenpanich C. and Krairiksh M. "Method of moments analysis of rectangular slotted-cavity excited by probe." to be presented in PIERS'2000.

[15] Elliott R.S. **Antenna Theory and Design.** India: Prentice Hall, 1985.

[16] Ito K. "Planar antenna for satellite reception." IEEE Trans. Broadcasting, vol. 34, no. 4, Dec. 1988. pp. 457-464.

[17] Yamamoto T., Hirokawa J. and Ando M. "A full-wave analysis of a complete model for a radial line slot antenna." IEICE Trans. Commun., vol. E82-B., Jan. 1999.

[18] James J.R. and Hall P.S. **Handbook of Microstrip Antenna.** vols.1 and 2, London : Peter Peregrinus, 1989.

[19] Balanis C.A. **Advanced Engineering Electromagnetics.** New York : Wiley and Sons. 1989.

[20] Tai C.T. **Dyadic Green Function in Electromagnetic Theory.** 2nd Ed. New York : IEEE Press., 1993.

[21] Stratton J.A. **Electromagnetic Theory.** New York : McGraw-Hill Book Co. 1941.

[22] Collin R.E. **Field Theory of Guided Wave.** 2nd ed., Piscataway, New Jersey : IEEE Press. 1991.

[23] Tai C.T. "Different representations of dyadic Green's functions for a rectangular cavity." IEEE Trans. Microwave Theory Tech., vol. MTT-24, no.9, Sept. 1976. pp. 597-601.

[24] Leong M.S., Li L.W., Kooi P.S., Yeo T.S. and Ho S.L. "Input impedance of a coaxial probe located inside a rectangular cavity: theory and experiment." IEEE Trans. Microwave Theory Tech., vol. 44, no. 7, July. 1996. pp. 1161-1164.

[25] Harrington R.F. **Field Computation by Moment Methods.** Rebert E. Krieger Publishing Company, INC., Florida, 1968.

[26] Miller E.K., Medgyesi-Mitschang L. and Newman E. H. **Computational Electromagnetics Frequency-Domain Method of Moments.** New York : IEEE Press, 1992. pp. 43-47.

[27] Djordjevic A.R. and Sarkar T.K. "A theorem on the Moment Methods.", IEEE Trans. Antennas Propagat., vol. AP-35, no. 3, Mar. 1987. pp. 353-355.

This material is reserved for educational use only, not allowed for commercial use.
Forbidden to modify the content, and cite the document when use.

[28] Richmond J.H. "On the variational aspects of the Moment Method.", IEEE Trans. Antennas Propagat., vol. 39, no. 4, Apr. 1991. pp. 473-479.

[29] Sarkar T.K. "A note on the choice of weighting functions in the Method of Moments." IEEE Trans. Antennas Propagat., vol. AP-33, no. 4, Apr. 1985. pp. 436-441.

[30] Peterson A.F., Wilton D.R. and Jorgenson R.E. "Variational nature of Galerkin and non-Galerkin Moment Methods solutions." IEEE Trans. Antennas Propagat., vol. 44, no. 4, Apr. 1996. pp. 500-503.

[31] Sarkar T.K., Djordjevic A.R. and Arvas E. "On the choice of expansion and weighting functions in the numerical solution of operator equations." IEEE Trans. Antennas Propagat., vol. AP-33, no. 9, Sep. 1985. pp. 988-996.

[32] Chapra S.C. and Canale R. P. **Numerical Methods for Engineers.** Singapore : McGraw-Hill Book Co. 1990.

[33] Press W.H., Teukolsky S.A., Vetterling W.T. and Flannery B.P. **Numerical Recipes in Fortran.** 2nd ed. New York : Cambridge University Press. 1992.

[34] Bucci O.M. and Pelosi G. "From wave theory to ray optics." IEEE Antennas Propagat. Mag., vol. 36, no. 4, Aug. 1994. pp. 35-42.

[35] Cecchini R. and Pelosi G. "Diffraction: The first recorded observation." IEEE Antennas Propagat. Soc. Mag., Apr. 1990. pp. 27-30.

[36] Keller J.B. "One hundred years of diffraction theory." IEEE Trans. Antennas Propagat., vol. AP-33, no. 2, Feb. 1985. pp. 123-126.

[37] Keller J.B. "Diffraction by an aperture." J. Appl. Phys., vol. 28, no. 4, Apr.1957. pp. 426-444.

[38] Kouyoumjian R.G. and Pathak P.H. "A uniform geometrical theory of diffraction for an edge in a perfectly conducting surface." Proc. IEEE, vol.62, no.11, Nov.1974. pp. 1448-1461.

[39] Kouyoumjian R.G. "The geometrical theory of diffraction and its application." in Numerical and Asymptotic Techniques in Electromagnetics, R.Mittra (Ed.), Springer, New York, 1975. pp. 165-215.

[40] McNamara D.A., Pistorius C.W.I. and Malherbe J.A.G. **Introduction to the Uniform Geometrical Theory of Diffraction.** Boston London : Artech House. 1990.

[41] Balanis C.A. **Antenna Theory Analysis and Design.** 2nd ed., New York : Wiley and Sons. 1997.

This material is reserved for educational use only, not allowed for commercial use.
Forbidden to modify the content, and cite the document when use.

[42] Phongcharoenpanich C., Lertwiriyaprapa T. and Krairiksh M. "Synthesis of linear slotted-waveguide array antenna using the second kind Tschebyscheff polynomial." Proceeding of the 22nd Electrical Engineering Conference, Dec. 1999. pp. 91-94.

[43] Stutzman W.L. and Thiele G.A. **Antenna Theory and Design.** 2nd ed. New York : John Wiley & Sons. 1998.

[44] Lertwiriyaprapa T., Phongcharoenpanich C. and Krairiksh M. "Analysis of pattern characteristics of a slot on finite ground plane fed by linear electric probe inside rectangular cavity." to be presented in APS'2000.

King Mongkut's Institute of Technology Ladkrabang

This material is reserved for educational use only, not allowed for commercial use.
Forbidden to modify the content, and cite the document when use.

APPENDICES

This material is reserved for educational use only, not allowed for commercial use.
Forbidden to modify the content, and cite the document when use.

Appendix A
Trigonometric and Exponential Functions

A.1 Trigonometric Relations

$$\sin(\alpha+\beta)=\sin\alpha\cos\beta+\cos\alpha\sin\beta \tag{A.1}$$

$$\sin(\alpha-\beta)=\sin\alpha\cos\beta-\cos\alpha\sin\beta \tag{A.2}$$

$$\cos(\alpha+\beta)=\cos\alpha\cos\beta-\sin\alpha\sin\beta \tag{A.3}$$

$$\cos(\alpha-\beta)=\cos\alpha\cos\beta+\sin\alpha\sin\beta \tag{A.4}$$

$$\tan(\alpha+\beta)=\frac{\tan\alpha+\tan\beta}{1-\tan\alpha\tan\beta} \tag{A.5}$$

$$\tan(\alpha-\beta)=\frac{\tan\alpha-\tan\beta}{1+\tan\alpha\tan\beta} \tag{A.6}$$

$$\sin\left(\frac{\pi}{2}+\alpha\right)=\cos\alpha \tag{A.7}$$

$$\sin\left(\frac{\pi}{2}-\alpha\right)=\cos\alpha \tag{A.8}$$

$$\cos\left(\frac{\pi}{2}+\alpha\right)=-\sin\alpha \tag{A.9}$$

$$\cos\left(\frac{\pi}{2}-\alpha\right)=\sin\alpha \tag{A.10}$$

$$\sin\alpha+\sin\beta=2\sin\frac{1}{2}(\alpha+\beta)\cos\frac{1}{2}(\alpha-\beta) \tag{A.11}$$

$$\sin\alpha-\sin\beta=2\cos\frac{1}{2}(\alpha+\beta)\sin\frac{1}{2}(\alpha-\beta) \tag{A.12}$$

$$\cos\alpha+\cos\beta=2\cos\frac{1}{2}(\alpha+\beta)\cos\frac{1}{2}(\alpha-\beta) \tag{A.13}$$

$$\cos\alpha-\cos\beta=-2\sin\frac{1}{2}(\alpha+\beta)\sin\frac{1}{2}(\alpha-\beta) \tag{A.14}$$

$$\sin\alpha\cos\beta=\frac{1}{2}[\sin(\alpha+\beta)+\sin(\alpha-\beta)] \tag{A.15}$$

This material is reserved for educational use only, not allowed for commercial use.
Forbidden to modify the content, and cite the document when use.

$$\cos\alpha\sin\beta=\frac{1}{2}[\sin(\alpha+\beta)-\sin(\alpha-\beta)] \quad (A.16)$$

$$\cos\alpha\cos\beta=\frac{1}{2}[\cos(\alpha+\beta)+\cos(\alpha-\beta)] \quad (A.17)$$

$$\sin\alpha\sin\beta=-\frac{1}{2}[\cos(\alpha+\beta)-\cos(\alpha-\beta)] \quad (A.18)$$

$$\sin^2\alpha+\cos^2\alpha=1 \quad (A.19)$$

$$\sin\alpha=2\sin\frac{\alpha}{2}\cos\frac{\alpha}{2} \quad (A.20)$$

$$\sin 2\alpha=2\sin\alpha\cos\alpha \quad (A.21)$$

$$\cos\alpha=2\cos^2\frac{\alpha}{2}-1=1-2\sin^2\frac{\alpha}{2} \quad (A.22)$$

$$\cos 2\alpha=2\cos^2\alpha-1=\cos^2\alpha-\sin^2\alpha=1-2\sin^2\alpha \quad (A.23)$$

$$\cos 3\alpha=4\cos^3\alpha-3\cos\alpha \quad (A.24)$$

$$\cos 4\alpha=8\cos^4\alpha-8\cos^2\alpha+1 \quad (A.25)$$

A.2 Exponential Relations

$$e^{j\alpha}=\cos\alpha+j\sin\alpha \quad (A.26)$$

$$e^{-j\alpha}=\cos\alpha-j\sin\alpha \quad (A.27)$$

$$\sin\alpha=\frac{e^{j\alpha}-e^{-j\alpha}}{2j} \quad (A.28)$$

$$\cos\alpha=\frac{e^{j\alpha}+e^{-j\alpha}}{2} \quad (A.29)$$

$$\tan\alpha=\frac{e^{j\alpha}-e^{-j\alpha}}{j\left(e^{j\alpha}+e^{-j\alpha}\right)} \quad (A.30)$$

$$\sinh(\alpha)=\frac{e^{\alpha}-e^{-\alpha}}{2} \quad (A.31)$$

This material is reserved for educational use only, not allowed for commercial use.
Forbidden to modify the content, and cite the document when use.

$$\cosh(\alpha) = \frac{e^{\alpha} + e^{-\alpha}}{2} \tag{A.32}$$

$$\sinh(j\alpha) = \frac{e^{j\alpha} - e^{-j\alpha}}{2} \tag{A.33}$$

$$\cosh(j\alpha) = \cos\alpha = \frac{e^{j\alpha} + e^{-j\alpha}}{2} \tag{A.34}$$

This material is reserved for educational use only, not allowed for commercial use.
Forbidden to modify the content, and cite the document when use.

Appendix B
Vector and Dyadic Analysis

B.1 Vector Analysis

B.1.1 Vector Identities

$$\bar{a}\cdot\bar{a}=|\bar{a}|^2 \tag{B.1}$$

$$\bar{a}\cdot\bar{a}^*=|\bar{a}|^2 \tag{B.2}$$

$$\bar{a}+\bar{b}=\bar{b}+\bar{a} \tag{B.3}$$

$$\bar{a}\cdot\bar{b}=\bar{b}\cdot\bar{a} \tag{B.4}$$

$$\bar{a}\times\bar{b}=-\bar{b}\times\bar{a} \tag{B.5}$$

$$(\bar{a}+\bar{b})\cdot\bar{c}=\bar{a}\cdot\bar{c}+\bar{b}\cdot\bar{c} \tag{B.6}$$

$$(\bar{a}+\bar{b})\times\bar{c}=\bar{a}\times\bar{c}+\bar{b}\times\bar{c} \tag{B.7}$$

$$\bar{a}\cdot(\bar{b}\times\bar{c})=\bar{b}\cdot\bar{c}\times\bar{a}=\bar{c}\cdot\bar{a}\times\bar{b} \tag{B.8}$$

$$\bar{a}\times(\bar{b}\times\bar{c})=(\bar{a}\cdot\bar{c})\bar{b}-(\bar{a}\cdot\bar{b})\bar{c} \tag{B.9}$$

$$\begin{aligned}(\bar{a}\times\bar{b})\cdot(\bar{c}\times\bar{d}) &= \bar{a}\cdot\bar{b}\times(\bar{c}\times\bar{d})\\ &= \bar{a}\cdot(\bar{b}\cdot\bar{d}\bar{c}-\bar{b}\cdot\bar{c}\bar{d})\\ &= (\bar{a}\cdot\bar{c})(\bar{b}\cdot\bar{d})-(\bar{a}\cdot\bar{d})(\bar{b}\cdot\bar{c})\end{aligned} \tag{B.10}$$

$$(\bar{a}\times\bar{b})\times(\bar{c}\times\bar{d})=(\bar{a}\times\bar{b}\cdot\bar{d})\bar{c}-(\bar{a}\times\bar{b}\cdot\bar{c})\bar{d} \tag{B.11}$$

$$\nabla(ab)=a\nabla b+b\nabla a \tag{B.12}$$

$$\nabla\cdot(a\bar{b})=a\nabla\cdot\bar{b}+\bar{b}\cdot\nabla a \tag{B.13}$$

$$\nabla\times(a\bar{b})=a\nabla\times\bar{b}-\bar{b}\times\nabla a=a\nabla\times\bar{b}+\nabla a\times\bar{b} \tag{B.14}$$

$$\nabla\cdot(\bar{a}\times\bar{b})=\bar{b}\cdot\nabla\times\bar{a}-\bar{a}\cdot\nabla\times\bar{b} \tag{B.15}$$

$$\nabla(\bar{a}\cdot\bar{b})=\bar{a}\times\nabla\times\bar{b}+\bar{b}\times\nabla\times\bar{a}+(\bar{a}\cdot\nabla)\bar{b}+(\bar{b}\cdot\nabla)\bar{a} \tag{B.16}$$

$$\nabla\times(\bar{a}\times\bar{b})=\bar{a}\nabla\cdot\bar{b}-\bar{b}\nabla\cdot\bar{a}-(\bar{a}\cdot\nabla)\bar{b}+(\bar{b}\cdot\nabla)\bar{a} \tag{B.17}$$

This material is reserved for educational use only, not allowed for commercial use.
Forbidden to modify the content, and cite the document when use.

$$\nabla \cdot (\nabla a) = \nabla^2 a \tag{B.18}$$

$$\nabla \times (\nabla \times \bar{a}) = \nabla(\nabla \cdot \bar{a}) - \nabla^2 \bar{a} \tag{B.19}$$

$$\nabla \times (\nabla a) = 0 \tag{B.20}$$

$$\nabla \cdot (\nabla \times \bar{a}) = 0 \tag{B.21}$$

B.1.2 Vector Differential Operators in Rectangular Coordinates.

$$\nabla a = \hat{x}\frac{\partial a}{\partial x} + \hat{y}\frac{\partial a}{\partial y} + \hat{z}\frac{\partial a}{\partial z} \tag{B.22}$$

$$\nabla \cdot \bar{a} = \frac{\partial a_x}{\partial x} + \frac{\partial a_y}{\partial y} + \frac{\partial a_z}{\partial z} \tag{B.23}$$

$$\begin{aligned} \nabla \times \bar{a} &= \hat{x}\left(\frac{\partial a_z}{\partial y} - \frac{\partial a_y}{\partial z}\right) + \hat{y}\left(\frac{\partial a_x}{\partial z} - \frac{\partial a_z}{\partial x}\right) + \hat{z}\left(\frac{\partial a_y}{\partial x} - \frac{\partial a_x}{\partial y}\right) \\ &= \begin{vmatrix} \hat{x} & \hat{y} & \hat{z} \\ \frac{\partial}{\partial x} & \frac{\partial}{\partial y} & \frac{\partial}{\partial z} \\ a_x & a_y & a_z \end{vmatrix} \end{aligned} \tag{B.24}$$

where a is scalar function, $\bar{a}$, $\bar{b}$, $\bar{c}$ and $\bar{d}$ are vector functions. ∇a represents gradient of a scalar function. $\nabla \cdot \bar{a}$ denotes divergence of a vector function. $\nabla \times \bar{a}$ is curl of a vector function. $\nabla^2 a$ and $\nabla^2 \bar{a}$ are Laplacian of a scalar and vector, respectively.

B.2 Dyadic Analysis

B.2.1 Dyadic Identities

$$\bar{a} \cdot (\bar{b} \times \bar{\bar{c}}) = -\bar{b} \cdot (\bar{a} \times \bar{\bar{c}}) = (\bar{a} \times \bar{b}) \cdot \bar{\bar{c}} \tag{B.25}$$

$$\bar{a} \times (\bar{b} \times \bar{\bar{c}}) = \bar{b}(\bar{a} \cdot \bar{\bar{c}}) - (\bar{a} \cdot \bar{b})\bar{\bar{c}} \tag{B.26}$$

$$\nabla \cdot (a\bar{\bar{b}}) = a\nabla \cdot \bar{\bar{b}} + (\nabla a) \cdot \bar{\bar{b}} \tag{B.27}$$

$$\nabla \times (a\bar{\bar{b}}) = a\nabla \times \bar{\bar{b}} + (\nabla a) \times \bar{\bar{b}} \tag{B.28}$$

$$\nabla \cdot (\bar{a} \times \bar{\bar{b}}) = (\nabla \times \bar{a}) \cdot \bar{\bar{b}} - \bar{a} \cdot (\nabla \times \bar{\bar{b}}) \tag{B.29}$$

$$\nabla \times (\nabla \times \bar{\bar{a}}) = \nabla(\nabla \cdot \bar{\bar{a}}) - \nabla^2 \bar{\bar{a}} \tag{B.30}$$

This material is reserved for educational use only, not allowed for commercial use.
Forbidden to modify the content, and cite the document when use.

$$\nabla \cdot (\nabla \times \overline{\overline{a}}) = 0 \tag{B.31}$$

$$\overline{a} \cdot \overline{\overline{b}} = [\overline{\overline{b}}]^T \cdot a \tag{B.32}$$

$$\overline{a} \times \overline{\overline{b}} = \left\{ -[\overline{\overline{b}}]^T \times \overline{a} \right\}^T \tag{B.33}$$

$$[\overline{\overline{c}}]^T \cdot (a \times \overline{\overline{b}}) = -[\overline{a} \times \overline{\overline{c}}]^T \cdot \overline{\overline{b}} \tag{B.34}$$

where $\overline{\overline{a}}$, $\overline{\overline{b}}$, and $\overline{\overline{c}}$ are a dyadic function. $[\cdot]^T$ is transpose of dyadic function.

B.2.2 Integral Theorems.

- Gauss or divergence theorem

$$\iiint \nabla \cdot \overline{a} dv = \oiint (\hat{n} \cdot \overline{a}) ds \tag{B.35}$$

- Curl theorem

$$\iiint \nabla \times \overline{a} dv = \oiint (\hat{n} \times \overline{a}) ds \tag{B.36}$$

- Gradient theorem

$$\iiint \nabla a dv = \oiint \hat{n} a ds \tag{B.37}$$

where $\hat{n}$ denotes the outward unit normal vector for closed surface.

This material is reserved for educational use only, not allowed for commercial use.
Forbidden to modify the content, and cite the document when use.

Appendix C
Derivation of Dyadic Green's Function in Three-Based Directions

C.1 In x direction

$$\overline{\overline{G}}_{EJ}^{in}(\bar{R},\bar{R}') = -\frac{1}{k^2}\hat{x}\hat{x}\delta(\bar{R}-\bar{R}') + \frac{2}{bc}\sum_{m,n}\frac{(2-\delta_0)}{k_{gx}k_{cx}^2\sin k_{gx}a}\begin{cases} \bar{M}_{eo}^{x}(a-x)\bar{M}_{eo}^{\prime x}(x') - \bar{N}_{oe}^{x}(a-x)\bar{N}_{oe}^{\prime x}(x'), x>x' \\ \bar{M}_{eo}^{x}(x)\bar{M}_{eo}^{\prime x}(a-x') - \bar{N}_{oe}^{x}(x)\bar{N}_{oe}^{\prime x}(a-x'), x<x' \end{cases} \tag{C.1}$$

$$\overline{\overline{G}}_{HJ}^{in}(\bar{R},\bar{R}') = \frac{2k}{bc}\sum_{m,n}\frac{(2-\delta_0)}{k_{gx}k_{cx}^2\sin k_{gx}a}\begin{cases} \bar{N}_{eo}^{x}(a-x)\bar{M}_{eo}^{\prime x}(x') - \bar{M}_{oe}^{x}(a-x)\bar{N}_{oe}^{\prime y}(x'), x>x' \\ \bar{N}_{eo}^{x}(x)\bar{M}_{eo}^{\prime x}(a-x') - \bar{M}_{oe}^{x}(x)\bar{N}_{oe}^{\prime x}(a-x'), x<x' \end{cases} \tag{C.2}$$

$$\overline{\overline{G}}_{HM}^{in}(\bar{R},\bar{R}') = -\frac{1}{k^2}\hat{x}\hat{x}\delta(\bar{R}-\bar{R}') + \frac{2}{bc}\sum_{m,n}\frac{(2-\delta_0)}{k_{gx}k_{cx}^2\sin k_{gx}a}\begin{cases} \bar{N}_{eo}^{x}(a-x)\bar{N}_{eo}^{\prime x}(x') - \bar{M}_{oe}^{x}(a-x)\bar{M}_{oe}^{\prime x}(x'), x>x' \\ \bar{N}_{eo}^{x}(x)\bar{N}_{eo}^{\prime x}(a-x') - \bar{M}_{oe}^{x}(x)\bar{M}_{oe}^{\prime x}(a-x'), x<x' \end{cases} \tag{C.3}$$

$$\overline{\overline{G}}_{EM}^{in}(\bar{R},\bar{R}') = \frac{2k}{bc}\sum_{m,n}\frac{(2-\delta_0)}{k_{gx}k_{cx}^2\sin k_{gx}a}\begin{cases} \bar{M}_{eo}^{x}(a-x)\bar{N}_{eo}^{\prime x}(x') - \bar{N}_{oe}^{x}(a-x)\bar{M}_{oe}^{\prime x}(x'), x>x' \\ \bar{M}_{eo}^{x}(x)\bar{N}_{eo}^{\prime x}(a-x') - \bar{N}_{oe}^{x}(x)\bar{M}_{oe}^{\prime x}(a-x'), x<x' \end{cases} \tag{C.4}$$

where $\bar{M}_{eo}^{x}(x)$, $\bar{M}_{oe}^{x}(x)$, $\bar{N}_{eo}^{x}(x)$ and $\bar{N}_{oe}^{x}(x)$ the eigenvalues are given by

$$\underset{oe}{\bar{M}_{eo}^{x}}(x) = \nabla\times\left[\underset{oe}{\psi_{eo}}(x,y,z)\hat{x}\right]$$

$$\underset{eo}{\bar{N}_{oe}^{x}}(x) = \frac{1}{k}\nabla\times\nabla\times\left[\underset{eo}{\psi_{oe}}(x,y,z)\hat{x}\right]$$

and

$$\underset{oe}{\psi_{eo}}(x,y,z) = \begin{bmatrix}\cos\\ \sin\end{bmatrix}(k_{gx}x)\begin{matrix}\cos\\ \sin\end{matrix}(k_y y)\begin{matrix}\sin\\ \cos\end{matrix}(k_z z)$$

$$k_z = \frac{m\pi}{c} \qquad k_y = \frac{n\pi}{b}$$

$$k_{cx}^2 = k_y^2 + k_z^2 \qquad k_{gx}^2 = k^2 - k_{cx}^2$$

This material is reserved for educational use only, not allowed for commercial use.
Forbidden to modify the content, and cite the document when use.

C.2 In *y* direction

$$\overline{\overline{G}}_{EJ}^{in}(\overline{R},\overline{R}') = -\frac{1}{k^2}\hat{y}\hat{y}\delta(\overline{R}-\overline{R}') + \frac{2}{ac}\sum_{m,n}\frac{(2-\delta_0)}{k_{gy}k_{cy}^2\sin k_{gy}b}\begin{cases}\overline{M}_{eo}^{y}(b-y)\overline{M}_{eo}^{'y}(y') - \overline{N}_{oe}^{y}(b-y)\overline{N}_{oe}^{'y}(y'), y>y'\\ \overline{M}_{eo}^{y}(y)\overline{M}_{eo}^{'y}(b-y') - \overline{N}_{oe}^{y}(y)\overline{N}_{oe}^{'y}(b-y'), y<y'\end{cases} \quad \text{(C.5)}$$

$$\overline{\overline{G}}_{HJ}^{in}(\overline{R},\overline{R}') = \frac{2k}{ac}\sum_{m,n}\frac{(2-\delta_0)}{k_{gy}k_{cy}^2\sin k_{gy}b}\begin{cases}\overline{N}_{eo}^{y}(b-y)\overline{M}_{eo}^{'y}(y') - \overline{M}_{oe}^{y}(b-y)\overline{N}_{oe}^{'y}(y'), y>y'\\ \overline{N}_{eo}^{y}(y)\overline{M}_{eo}^{'y}(b-y') - \overline{M}_{oe}^{y}(y)\overline{N}_{oe}^{'y}(b-y'), y<y'\end{cases} \quad \text{(C.6)}$$

$$\overline{\overline{G}}_{HM}^{in}(\overline{R},\overline{R}') = -\frac{1}{k^2}\hat{y}\hat{y}\delta(\overline{R}-\overline{R}') + \frac{2}{ac}\sum_{m,n}\frac{(2-\delta_0)}{k_{gy}k_{cy}^2\sin k_{gy}b}\begin{cases}\overline{N}_{eo}^{y}(b-y)\overline{N}_{eo}^{'y}(y') - \overline{M}_{oe}^{y}(b-y)\overline{M}_{oe}^{'y}(y'), y>y'\\ \overline{N}_{eo}^{y}(y)\overline{N}_{eo}^{'y}(b-y') - \overline{M}_{oe}^{y}(y)\overline{M}_{oe}^{'y}(b-y'), y<y'\end{cases} \quad \text{(C.7)}$$

$$\overline{\overline{G}}_{EM}^{in}(\overline{R},\overline{R}') = \frac{2k}{ac}\sum_{m,n}\frac{(2-\delta_0)}{k_{gy}k_{cy}^2\sin k_{gy}b}\begin{cases}\overline{M}_{eo}^{y}(b-y)\overline{N}_{eo}^{'y}(y') - \overline{N}_{oe}^{y}(b-y)\overline{M}_{oe}^{'y}(y'), y>y'\\ \overline{M}_{eo}^{y}(y)\overline{N}_{eo}^{'y}(b-y') - \overline{N}_{oe}^{y}(y)\overline{M}_{oe}^{'y}(b-y'), y<y'\end{cases} \quad \text{(C.8)}$$

where $\overline{M}_{eo}^{y}(y)$, $\overline{M}_{oe}^{y}(y)$, $\overline{N}_{eo}^{y}(y)$ and $\overline{N}_{oe}^{y}(y)$ the eigenvalues are given by

$$\underset{oe}{\overline{M}_{eo}^{y}}(y) = \nabla\times\left[\underset{oe}{\psi_{eo}}(x,y,z)\hat{y}\right]$$

$$\underset{eo}{\overline{N}_{oe}^{y}}(y) = \frac{1}{k}\nabla\times\nabla\times\left[\underset{eo}{\psi_{oe}}(x,y,z)\hat{y}\right]$$

and

$$\underset{oe}{\psi_{eo}}(x,y,z) = \begin{bmatrix}\cos\\ \sin\end{bmatrix}(k_x x)\begin{matrix}\cos\\ \sin\end{matrix}(k_{gy}y)\begin{matrix}\sin\\ \cos\end{matrix}(k_z z)$$

$$k_x = \frac{m\pi}{a} \qquad k_z = \frac{n\pi}{c}$$

$$k_{cy}^2 = k_x^2 + k_z^2 \qquad k_{gy}^2 = k^2 - k_{cy}^2$$

This material is reserved for educational use only, not allowed for commercial use.
Forbidden to modify the content, and cite the document when use.

C.3 In z direction

$$\overline{\overline{G}}_{EJ}^{in}(\bar{R},\bar{R}') = -\frac{1}{k^2}\hat{z}\hat{z}\delta(\bar{R}-\bar{R}') + \frac{2}{ab}\sum_{m,n}\frac{(2-\delta_0)}{k_{gz}k_{cz}^2\sin k_{gz}c}\begin{cases} \bar{M}_{eo}^{z}(c-z)\bar{M}_{eo}^{\prime z}(z') - \bar{N}_{oe}^{z}(c-z)\bar{N}_{oe}^{\prime z}(z'), z>z' \\ \bar{M}_{eo}^{z}(z)\bar{M}_{eo}^{\prime z}(c-z') - \bar{N}_{oe}^{z}(z)\bar{N}_{oe}^{\prime z}(c-z'), z<z' \end{cases} \quad \text{(C.9)}$$

$$\overline{\overline{G}}_{HJ}^{in}(\bar{R},\bar{R}') = \frac{2k}{ab}\sum_{m,n}\frac{(2-\delta_0)}{k_{gz}k_{cz}^2\sin k_{gz}c}\begin{cases} \bar{N}_{eo}^{z}(c-z)\bar{M}_{eo}^{\prime z}(z') - \bar{M}_{oe}^{z}(c-z)\bar{N}_{oe}^{\prime z}(z'), z>z' \\ \bar{N}_{eo}^{z}(z)\bar{M}_{eo}^{\prime z}(c-z') - \bar{M}_{oe}^{z}(z)\bar{N}_{oe}^{\prime z}(c-z'), z<z' \end{cases} \quad \text{(C.10)}$$

$$\overline{\overline{G}}_{HM}^{in}(\bar{R},\bar{R}') = -\frac{1}{k^2}\hat{z}\hat{z}\delta(\bar{R}-\bar{R}') + \frac{2}{ab}\sum_{m,n}\frac{(2-\delta_0)}{k_{gz}k_{cz}^2\sin k_{gz}c}\begin{cases} \bar{N}_{eo}^{z}(c-z)\bar{N}_{eo}^{\prime z}(z') - \bar{M}_{oe}^{z}(c-z)\bar{M}_{oe}^{\prime z}(z'), z>z' \\ \bar{N}_{eo}^{z}(z)\bar{N}_{eo}^{\prime z}(c-z') - \bar{M}_{oe}^{z}(z)\bar{M}_{oe}^{\prime z}(c-z'), z<z' \end{cases} \quad \text{(C.11)}$$

$$\overline{\overline{G}}_{EM}^{in}(\bar{R},\bar{R}') = \frac{2k}{ab}\sum_{m,n}\frac{(2-\delta_0)}{k_{gz}k_{cz}^2\sin k_{gz}c}\begin{cases} \bar{M}_{eo}^{z}(c-z)\bar{N}_{eo}^{\prime z}(z') - \bar{N}_{oe}^{z}(c-z)\bar{M}_{oe}^{\prime z}(z'), z>z' \\ \bar{M}_{eo}^{z}(z)\bar{N}_{eo}^{\prime z}(c-z') - \bar{N}_{oe}^{z}(z)\bar{M}_{oe}^{\prime z}(c-z'), z<z' \end{cases} \quad \text{(C.12)}$$

where $\bar{M}_{eo}^{z}(z)$, $\bar{M}_{oe}^{z}(z)$, $\bar{N}_{eo}^{z}(z)$ and $\bar{N}_{oe}^{z}(z)$ the eigenvalues are given by

$$\bar{M}_{\substack{eo\\oe}}^{z}(z) = \nabla\times\left[\psi_{\substack{eo\\oe}}(x,y,z)\hat{z}\right]$$

$$\bar{N}_{\substack{oe\\eo}}^{z}(z) = \frac{1}{k}\nabla\times\nabla\times\left[\psi_{\substack{eo\\eo}}(x,y,z)\hat{z}\right]$$

and

$$\psi_{\substack{eo\\oe}}(x,y,z) = \begin{bmatrix}\cos\\\sin\end{bmatrix}(k_x x)\begin{matrix}\cos\\\sin\end{matrix}(k_y y)\begin{matrix}\sin\\\cos\end{matrix}(k_{gz}z)$$

$$k_x = \frac{m\pi}{a} \qquad k_y = \frac{n\pi}{b}$$

$$k_{cz}^2 = k_x^2 + k_y^2 \qquad k_{gz}^2 = k^2 - k_{cz}^2$$

This material is reserved for educational use only, not allowed for commercial use.
Forbidden to modify the content, and cite the document when use.

Appendix D
Some Orthogonal Relationships of the Vector Wave Functions

$$\left.\begin{aligned}\iiint \overline{M}_{\substack{e\\o}mn}(h)\cdot\overline{N}_{\substack{e\\o}m'n'}(-h')dV=0\\ \iiint \overline{M}_{\substack{e\\o}mn}(h)\cdot\overline{N}_{\substack{o\\e}m'n'}(-h')dV=0\end{aligned}\right\} \tag{D.1}$$

$$\left.\begin{aligned}\iiint \overline{M}_{emn}(h)\cdot\overline{M}_{om'n'}(-h')dV=0\\ \iiint \overline{N}_{emn}(h)\cdot\overline{N}_{om'n'}(-h')dV=0\end{aligned}\right\} \tag{D.2}$$

$$\left.\begin{aligned}\iiint \overline{M}_{emn}(h)\cdot\overline{M}_{em'n'}(-h')dV=0\\ \iiint \overline{M}_{omn}(h)\cdot\overline{M}_{om'n'}(-h')dV=0\\ \iiint \overline{N}_{emn}(h)\cdot\overline{N}_{em'n'}(-h')dV=0\\ \iiint \overline{N}_{omn}(h)\cdot\overline{N}_{om'n'}(-h')dV=0\end{aligned}\right\} \tag{D.3}$$

$$\int_0^a\int_0^b\int_{-\infty}^{\infty}\overline{M}_{emn}(h)\cdot\overline{M}_{emn}(-h')dxdydz=(1+\delta_0)\frac{abk_c^2}{4}\int_{-\infty}^{\infty}e^{i(h-h')z}dz$$

$$=(1+\delta_0)\frac{abk_c^2}{2}\delta(h-h') \tag{D.4}$$

$$\int_0^a\int_0^b\int_{-\infty}^{\infty}\overline{M}_{omn}(h)\cdot\overline{M}_{omn}(-h')dxdydz=\frac{\pi abk_c^2}{2}\delta(h-h'),\quad m\neq 0, n\neq 0 \tag{D.5}$$

$$\int_0^a\int_0^b\int_{-\infty}^{\infty}\overline{M}_{omn}(h)\cdot\overline{M}_{omn}(-h')dxdydz=(1+\delta_0)\frac{\pi abk_c^2}{2}\delta(h-h'),\ n\neq 0\ and\ m\neq 0 \tag{D.6}$$

$$\int_0^a\int_0^b\int_{-\infty}^{\infty}\overline{N}_{emn}(h)\cdot\overline{N}_{emn}(-h')dxdydz=(1+\delta_0)\frac{\pi abk_c^2}{2\kappa\kappa'}(k_c^2+hh')\delta(h-h') \tag{D.7}$$

$$\int_0^a\int_0^b\int_{-\infty}^{\infty}\overline{N}_{emn}(h)\cdot\overline{N}_{emn}(-h')dxdydz=(1+\delta_0)\frac{\pi abk_c^2}{2}\delta(h-h') \tag{D.8}$$

$$\int_0^a\int_0^b\int_{-\infty}^{\infty}\overline{N}_{omn}(h)\cdot\overline{N}_{omn}(-h')dxdydz=(1+\delta_0)\frac{\pi abk_c^2}{2}\delta(h-h') \tag{D.9}$$

This material is reserved for educational use only, not allowed for commercial use.
Forbidden to modify the content, and cite the document when use.

Appendix E
Integration of Reaction Expressions for External Region

From external term of system equation Y^{ext}

$$Y^{ext} = j\omega\varepsilon_0 \sum_{i=1}^{N_l} A_i \iint_{s_a} \iint_{s_a} \overline{m}_{n_j} \cdot \overline{\overline{G}}_{HM}^{ext} \cdot \overline{m}_i dS dS' \tag{E.1}$$

Substituting basis, weighting and dyadic Green's function

$$\overline{m}_i = \frac{1}{w_s} \sin\frac{i\pi}{l_s}\left(z + \frac{l_s}{2}\right)\hat{z} \tag{E.2a}$$

$$\overline{m}_{n_j} = \frac{1}{w_s} \sin\frac{n_j\pi}{l_s}\left(z' + \frac{l_s}{2}\right)\hat{z} \tag{E.2b}$$

$$\overline{\overline{G}}_{HM}^{ext} = \left(\overline{\overline{I}} + \frac{\nabla\nabla}{k^2}\right)\frac{e^{-jk|\overline{R}-\overline{R}'|}}{2\pi|\overline{R}-\overline{R}'|} \tag{E.3}$$

$$Y^{ext} = \frac{j\omega\varepsilon_0}{w_s^2} \sum_{i=1}^{N_l} A_i \iint_{s_a} \iint_{s_a} \sin\frac{n_j\pi}{l_s}\left(z + \frac{l_s}{2}\right) G_{HM,zz}^{ext} \sin\frac{i\pi}{l_s}\left(z' + \frac{l_s}{2}\right) dS dS' \tag{E.4}$$

where

$$G_{HM,zz}^{ext} = \left(1 + \frac{1}{k^2}\frac{\partial^2}{\partial z^2}\right)\frac{e^{-jkR}}{2\pi R}$$

$$R = \sqrt{(x+x')^2 + (z-z')^2}$$

$$Y^{ext} = \frac{j\omega\varepsilon_0}{2\pi w_s^2} \sum_{i=1}^{N_l} A_i \int_{-\frac{l_s}{2}}^{\frac{l_s}{2}} \int_{-\frac{w_s}{2}}^{\frac{w_s}{2}} \int_{-\frac{l_s}{2}}^{\frac{l_s}{2}} \int_{-\frac{w_s}{2}}^{\frac{w_s}{2}} \sin\frac{n_j\pi}{l_s}\left(z + \frac{l_s}{2}\right)\left(1 + \frac{1}{k^2}\frac{\partial^2}{\partial z^2}\right)\frac{e^{-jkR}}{R} \sin\frac{i\pi}{l_s}\left(z' + \frac{l_s}{2}\right) dx dz dx' dz' \tag{E.5}$$

Consider only first term of Y^{ext}

This material is reserved for educational use only, not allowed for commercial use.
Forbidden to modify the content, and cite the document when use.

$$Y_l^{ext} = \frac{j\omega\varepsilon_0}{2\pi w_s^2}\sum_{i=1}^{N_l} A_i \int_{-\frac{l_s}{2}}^{\frac{l_s}{2}}\int_{-\frac{w_s}{2}}^{\frac{w_s}{2}}\int_{-\frac{l_s}{2}}^{\frac{l_s}{2}}\int_{-\frac{w_s}{2}}^{\frac{w_s}{2}} \sin\frac{n_j\pi}{l_s}\left(z+\frac{l_s}{2}\right)\frac{e^{-jkR}}{R}\sin\frac{i\pi}{l_s}\left(z'+\frac{l_s}{2}\right)dxdzdx'dz' \quad \text{(E.6)}$$

In order to make it possible to integrate (E.3) is change the limit of its integration as shown in Fig.E.1 (a) and (b)

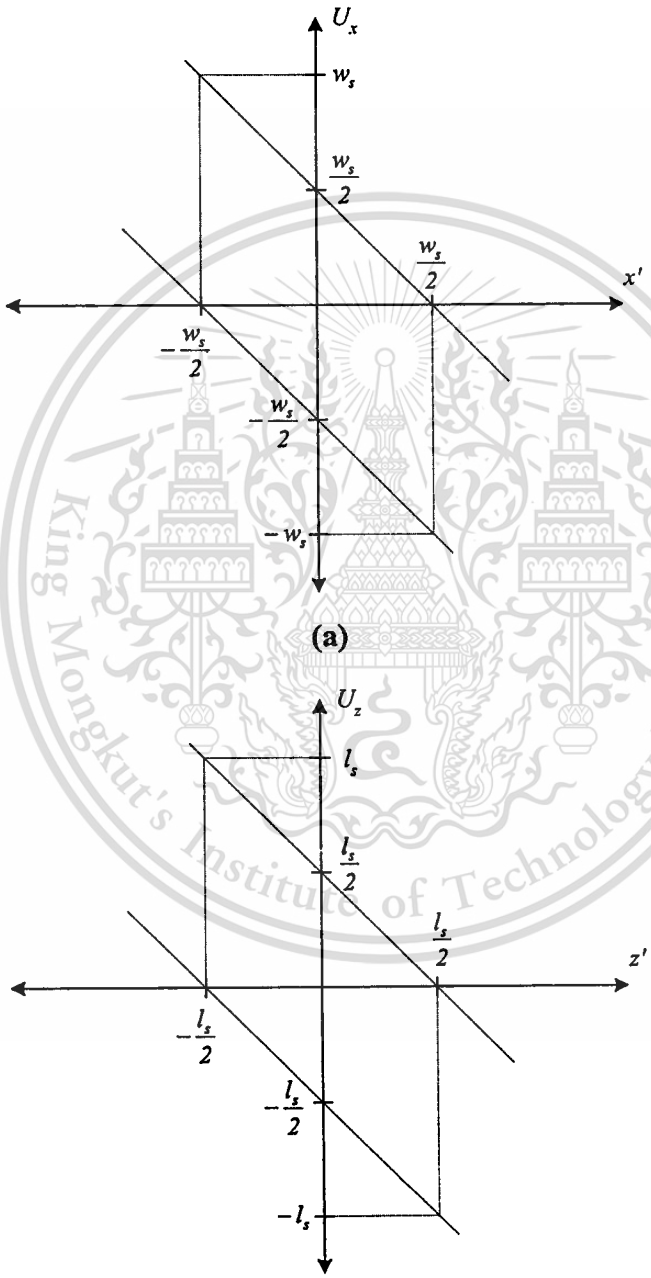

(b)

Fig.E.1 Transformation limit of integration

(a) with respect to x

(b) with respect to z

This material is reserved for educational purposes only, not allowed for commercial use.
Forbidden to modify the content, and cite the document when use.

Let $u_z = z - z'$ and $u_x = x - x'$

$$Y_l^{ext} = \frac{j\omega\varepsilon_0}{2\pi w_s^2}\sum_{i=1}^{N_l} A_i \left[\int_0^{l_s} du_z \int_{-\frac{l_s}{2}}^{\frac{l_s}{2}-u_z} dz' + \int_{-l_s}^{0} du_z \int_{-\frac{l_s}{2}-u_z}^{\frac{l_s}{2}} dz'\right]\left[\int_0^{w_s} du_x \int_{-\frac{w_s}{2}}^{\frac{w_s}{2}-u_x} dx' + \int_{-w_s}^{0} du_x \int_{-\frac{w_s}{2}-u_x}^{\frac{w_s}{2}} dx'\right]$$
$$\sin\frac{n_j\pi}{l_s}\left(u_z + z' + \frac{l_s}{2}\right)\frac{e^{-jk\sqrt{u_x^2+u_z^2}}}{\sqrt{u_x^2+u_z^2}}\sin\frac{i\pi}{l_s}\left(z' + \frac{l_s}{2}\right)$$

$$Y_l^{ext} = \frac{j\omega\varepsilon_0}{2\pi w_s^2}\sum_{i=1}^{N_l} A_i \left[\int_0^{l_s} du_z \int_{-\frac{l_s}{2}}^{\frac{l_s}{2}-u_z} dz' + \int_{-l_s}^{0} du_z \int_{-\frac{l_s}{2}-u_z}^{\frac{l_s}{2}} dz'\right] 2\left[\int_0^{w_s} du_x \int_{-\frac{w_s}{2}}^{\frac{w_s}{2}-u_x} dx'\right]$$
$$\sin\frac{n_j\pi}{l_s}\left(u_z + z' + \frac{l_s}{2}\right)\frac{e^{-jk\sqrt{u_x^2+u_z^2}}}{\sqrt{u_x^2+u_z^2}}\sin\frac{i\pi}{l_s}\left(z' + \frac{l_s}{2}\right)$$

$$Y_l^{ext} = \frac{j\omega\varepsilon_0}{\pi w_s^2}\sum_{i=1}^{N_l} A_i \left[\int_0^{l_s} du_z \int_{-\frac{l_s}{2}}^{\frac{l_s}{2}-u_z} dz' + \int_{-l_s}^{0} du_z \int_{-\frac{l_s}{2}-u_z}^{\frac{l_s}{2}} dz'\right]\int_0^{w_s} du_x (w-u_x)$$
$$\sin\frac{n_j\pi}{l_s}\left(u_z + z' + \frac{l_s}{2}\right)\frac{e^{-jk\sqrt{u_x^2+u_z^2}}}{\sqrt{u_x^2+u_z^2}}\sin\frac{i\pi}{l_s}\left(z' + \frac{l_s}{2}\right)$$

$$Y_l^{ext} = \frac{j\omega\varepsilon_0}{\pi w_s^2}\sum_{i=1}^{N_l} A_i \int_0^{l_s}\int_0^{w_s}(w-u_x) I_l^{ext}\frac{e^{-jk\sqrt{u_x^2+u_z^2}}}{\sqrt{u_x^2+u_z^2}} du_x du_z \qquad \text{(E.7)}$$

when $i = n_j$, $i \neq 0$, $n_j \neq 0$

$$I_l^{ext} = \frac{l_s}{i\pi}\sin\frac{i\pi u_z}{l_s} + (l_s - u_z)\cos\frac{i\pi u_z}{l_s}$$

$i = n_j = 0$, $i + n_j = odd$

$$I_l^{ext} = 0$$

$i \neq 0$, $n_j \neq 0$, $i + n_j = odd$

$$I_l^{ext} = \frac{2l_s}{\pi\left(n_j^{\,2} - i^2\right)}\left(n_j \sin\frac{i\pi u_z}{l_s} - i\sin\frac{n_j\pi u_z}{l_s}\right)$$

This material is reserved for educational use only, not allowed for commercial use.
Forbidden to modify the content, and cite the document when use.

Next the second term of Y^{ext} is regarded as

$$Y_2^{ext} = \frac{j\omega\varepsilon_0}{2\pi w_s^2}\sum_{i=1}^{N_l} A_i \int_{-\frac{l_s}{2}}^{\frac{l_s}{2}}\int_{-\frac{w_s}{2}}^{\frac{w_s}{2}}\int_{-\frac{l_s}{2}}^{\frac{l_s}{2}}\int_{-\frac{w_s}{2}}^{\frac{w_s}{2}} \sin\frac{n_j\pi}{l_s}\left(z+\frac{l_s}{2}\right)\frac{1}{k^2}\frac{\partial^2}{\partial z^2}\frac{e^{-jkR}}{R}\sin\frac{i\pi}{l_s}\left(z'+\frac{l_s}{2}\right)dxdzdx'dz' \tag{E.8}$$

Using the by part integration with respect to z, it can be written as

$$Y_2^{ext} = \frac{-j\omega\varepsilon_0}{\pi k^2 w_s^2}\sum_{i=1}^{N_l} A_i \frac{i\pi}{l_s}\int_{-\frac{l_s}{2}}^{\frac{l_s}{2}}\int_{-\frac{l_s}{2}}^{\frac{l_s}{2}} \sin\frac{n_j\pi}{l_s}\left(z'+\frac{l_s}{2}\right)\cos\frac{i\pi}{l_s}\left(z+\frac{l_s}{2}\right)\frac{\partial}{\partial z}\frac{e^{-jkR}}{R}\int_0^{w_s} du_x(w-u_x) \tag{E.9}$$

since

$$\frac{\partial}{\partial z}\frac{e^{-jkR}}{R} = -\frac{\partial}{\partial z'}\frac{e^{-jkR}}{R}$$

$$Y_2^{ext} = \frac{j\omega\varepsilon_0}{\pi k^2 w_s^2}\sum_{i=1}^{N_l} A_i \frac{i\pi}{l_s}\int_{-\frac{l_s}{2}}^{\frac{l_s}{2}}\int_{-\frac{l_s}{2}}^{\frac{l_s}{2}} \sin\frac{n_j\pi}{l_s}\left(z'+\frac{l_s}{2}\right)\cos\frac{i\pi}{l_s}\left(z'+\frac{l_s}{2}\right)\frac{\partial}{\partial z'}\frac{e^{-jkR}}{R}\int_0^{w_s} du_x(w-u_x) \tag{E.10}$$

Again using by part integration with respect to z', it is

$$Y_2^{ext} = \frac{-j\omega\varepsilon_0}{2\pi k^2 w_s^2}\sum_{i=1}^{N_l} A_i\left(\frac{n_j\pi}{l_s}\right)\left(\frac{i\pi}{l_s}\right)\int_{-\frac{l_s}{2}}^{\frac{l_s}{2}}\int_{-\frac{l_s}{2}}^{\frac{l_s}{2}} \cos\frac{n_j\pi}{l_s}\left(z'+\frac{l_s}{2}\right)\cos\frac{i\pi}{l_s}\left(z'+\frac{l_s}{2}\right)\frac{e^{-jkR}}{R}\int_0^{w_s} du_x(w-u_x) \tag{E.11}$$

In similar manner with Y_1^{ext}, the integration limit of Y_2^{ext} is changed to make integration easy. It yields

$$Y_2^{ext} = \frac{j\omega\varepsilon_0}{\pi k^2 w_s^2}\sum_{i=1}^{N_l} A_i \int_0^{l_s}\int_0^{w_s}(w-u_x)I_2^{ext}\frac{e^{-jk\sqrt{u_x^2+u_z^2}}}{\sqrt{u_x^2+u_z^2}}du_x du_z \tag{E.12}$$

when $i = n_j$, $i \neq 0$, $n_j \neq 0$

This material is reserved for educational use only, not allowed for commercial use.
Forbidden to modify the content, and cite the document when use.

$$I_2^{ext} = -\left(\frac{\pi}{l_s}\right)^2\left[\frac{-l_s}{i\pi}\sin\frac{i\pi u_z}{l_s} + (l_s - u_z)\cos\frac{i\pi u_z}{l_s}\right]$$

when $i = 0$, $n_j = 0$, $i + n_j = odd$

$$I_2^{ext} = 0$$

when $i \neq 0$, $n_j \neq 0$, $i + n_j = odd$

$$I_2^{ext} = -\left(\frac{i\pi}{l_s}\right)\left(\frac{n_j\pi}{l_s}\right)\left[\frac{2l_s}{\pi\left(n_j{}^2 - i^2\right)}\left(i\sin\frac{i\pi u_z}{l_s} - n_j\sin\frac{n_j\pi u_z}{l_s}\right)\right]$$

Therefore, Y^{ext} can be finally expressed as

$$Y^{ext} = \frac{j\omega\varepsilon_0}{\pi w_s^2}\sum_{i=1}^{N_l} A_i \int_0^{l_s}\int_0^{w_s}(w - u_x)\left(I_1^{ext} + \frac{I_2^{ext}}{k^2}\right)\frac{e^{-jk\sqrt{u_x^2+u_z^2}}}{\sqrt{u_x^2+u_z^2}}du_x du_z \qquad \text{(E.13)}$$

King Mongkut's Institute of Technology Ladkrabang

This material is reserved for educational use only, not allowed for commercial use.
Forbidden to modify the content, and cite the document when use.

AUTHOR BIOGRAPHY

Author : Titipong Lertwiriyaprapa

Date of Birth : October 24, 1973

Bachelor Degree : B.S.Tech.Edu. in Electrical Engineering (Hons.)

Institution : Department of Teacher Training in Electrical Engineering
Faculty of Technical Education
King Mongkut's Institute of Technology North Bangkok

Year of Graduation : 1996

Undergraduate Research :
Yagi Antenna Design for Windows (1995)

Scholarship : Graduate Scholarship Loan, Ministry of University Affairs

Experience : Lecturer at King Mongkut's Institute of Technology North Bangkok (From 1996)

Interested Researches : Slot Antenna, Array Antenna, Method of Moments and Geometrical Theory of Diffraction.

This material is reserved for educational use only, not allowed for commercial use.
Forbidden to modify the content, and cite the document when use.